



Terms and Conditions of Use of Digitised Theses from Trinity College Library Dublin

Copyright statement

All material supplied by Trinity College Library is protected by copyright (under the Copyright and Related Rights Act, 2000 as amended) and other relevant Intellectual Property Rights. By accessing and using a Digitised Thesis from Trinity College Library you acknowledge that all Intellectual Property Rights in any Works supplied are the sole and exclusive property of the copyright and/or other IPR holder. Specific copyright holders may not be explicitly identified. Use of materials from other sources within a thesis should not be construed as a claim over them.

A non-exclusive, non-transferable licence is hereby granted to those using or reproducing, in whole or in part, the material for valid purposes, providing the copyright owners are acknowledged using the normal conventions. Where specific permission to use material is required, this is identified and such permission must be sought from the copyright holder or agency cited.

Liability statement

By using a Digitised Thesis, I accept that Trinity College Dublin bears no legal responsibility for the accuracy, legality or comprehensiveness of materials contained within the thesis, and that Trinity College Dublin accepts no liability for indirect, consequential, or incidental, damages or losses arising from use of the thesis for whatever reason. Information located in a thesis may be subject to specific use constraints, details of which may not be explicitly described. It is the responsibility of potential and actual users to be aware of such constraints and to abide by them. By making use of material from a digitised thesis, you accept these copyright and disclaimer provisions. Where it is brought to the attention of Trinity College Library that there may be a breach of copyright or other restraint, it is the policy to withdraw or take down access to a thesis while the issue is being resolved.

Access Agreement

By using a Digitised Thesis from Trinity College Library you are bound by the following Terms & Conditions. Please read them carefully.

I have read and I understand the following statement: All material supplied via a Digitised Thesis from Trinity College Library is protected by copyright and other intellectual property rights, and duplication or sale of all or part of any of a thesis is not permitted, except that material may be duplicated by you for your research use or for educational purposes in electronic or print form providing the copyright owners are acknowledged using the normal conventions. You must obtain permission for any other use. Electronic or print copies may not be offered, whether for sale or otherwise to anyone. This copy has been supplied on the understanding that it is copyright material and that no quotation from the thesis may be published without proper acknowledgement.

Aspects of the fatigue behaviour of acrylic bone cement

by

Bruce Philip Murphy, B.A., B.A.I.

A thesis submitted to the University of Dublin in partial fulfilment of the requirements for the degree of

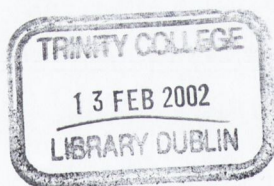
Doctor in Philosophy

Trinity College Dublin
May 2001

Supervisor
Dr. Patrick J. Prendergast

Dr. ir. Nico Verdonschot
External examiner

Prof. David Taylor
Internal examiner



THESIS 6543

Contents

Nomenclature	ii
List of Figures	iii
List of Tables	ix
Declaration	x
Acknowledgments	xi
Abstract	xii
Publications and presentations of the thesis	xiii
Chapter 1 Introduction	1
The problem of <i>in vivo</i> fatigue failure is shown to be the main reason for failure of cemented joint replacements. However many questions remain unanswered regarding the fatigue behaviour of acrylic bone cement.	
Chapter 2 Literature Review	10
Bone cement as a material is introduced and the <i>in vivo</i> failure mechanisms are identified from the literature. Previous research regarding the fatigue properties and porosity of acrylic bone cement are discussed in this chapter.	
Chapter 3 Materials and methods	42
The design and development of the test set-up and testing protocols are described in this chapter.	
Chapter 4 Results	63
The fatigue results are presented in this chapter and are divided into three sections: comparison of mixing techniques, damage accumulation in acrylic bone cement, and the effect of multiaxial stresses on the fatigue life of acrylic bone cement.	
Chapter 5 Discussion	100
The results are discussed in detail, with an emphasis on the development of empirical laws for computer simulations that model the damage accumulation failure scenario. Moreover, the clinical significance of the results is discussed.	
Chapter 6 Conclusions	120
The main conclusions of this thesis are enumerated and future research directions are noted.	
References	123
Appendices	132

Nomenclature

a_i	Crack length
C	Monkman-Grant constant
F	Axial force [N]
N	Number of fatigue cycles
N_a	Characteristic fatigue life
n_c	Number of cracks
N_f	Number of cycles to failure
N_o	Guaranteed fatigue life
n_p	Number of pores
P	Pressure [psi]
P_f	Probability of failure
P_s	Probability of survival
R	Free radical
r	Correlation coefficient
R_i	Inner radius of tubular specimen [mm]
R_o	Outer radius of tubular specimen [mm]
SD	Standard deviation
t_f	Time to failure [s]

Greek Letters

α	Shape parameter of the Weibull distribution
β	Location parameter of the Weibull distribution
$\dot{\epsilon}_{ss}$	Steady state creep rate
ϵ	Strain
γ	Material constant
σ	Stress [MPa]
ω	Damage
ω_f	Damage at failure

List of Figures

Figure 1.1	Schematic of a cemented total hip replacement, from Hardinge (1983).	3
Figure 1.2	Survival results from the Swedish Hip Register for different types of implantation techniques. A clear improvement in cemented implant survival compared to cementless implants can be observed for the latter period (1987-1996) compared to the early period (1979-1986).	4
Figure 2.1	The repeating unit of the monomer, MMA. The initiator is a Benzoyl Peroxide molecule, initiation only occurs when benzoyloxy radicals are produced.	12
Figure 2.2	The process of free radical addition in PMMA. Terminated macromolecule of PMMA composing of n MMA molecules, termination in this case is caused by combination. A macromolecule of PMMA; propagation has been stopped by hydrogen transfer.	13
Figure 2.3	Temperature versus time curve of curing acrylic bone cement	14
Figure 2.4	Schematic of the interaction between the damage accumulation failure scenario and the particulate reaction failure scenario.	16
Figure 2.5	Risk ratio for Cement mixing technique, Vacuum vs. manual mixing. When the line is greater than one vacuum-mixing has an increased risk associated with it compared to hand-mixing.	19
Figure 2.6	Porosity results from Linden and Guillquist (1989) showing that the combination of vacuum and mechanical mixing significantly reduced porosity in acrylic bone cement compared to other mixing methods.	20
Figure 2.7	Centrifugation decreases percentage porosity (a) and the mean pore size (b). However the number of pores/cm ² is increased after centrifugation.	21
Figure 2.8	Weibull distributions from Johnson et al. (1989) showing that the 5 Hz distribution is wildly skewed because of one outlier.	24
Figure 2.9	Fatigue Results from Davies and Harris (1990) showing that vacuum-mixing and centrifugation increased the mean fatigue life.	29
Figure 2.10	Uniaxial fully reversed tension-compression fatigue test results, fitted to an Olgive curve. (Lewis and Austin, 1994).	31

Figure 2.11	Guaranteed fatigue life (estimated from the three-parameter Weibull distribution) plotted against stress amplitude, from Lewis and Austin (1994).	32
Figure 2.12	An estimation of the guaranteed fatigue life for acrylic bone cement, adapted from Lewis and Mladsi (1998).	34
Figure 2.13	A schematic of the suggested model of expansion of the fatigue crack damage zone in the presence of the porosity phase in the vicinity of the crack tip.	37
Figure 2.14	Miner's Law describing damage accumulation is linear and the rate of damage accumulation is equal to one.	38
Figure 2.15	Typical creep strain curves for hand-mixed and vacuum-mixed Palacos R and Zimmer Regular bone cements at 20°C. The vacuum-mixed specimens showed reduced creep compared to hand-mixed specimens. (Norman et al., 1995)	39
Figure 3.1	Working curves for Cemex bone cement for different ambient temperatures (adapted from Kühn, 2000).	44
Figure 3.2	Hand-mixing schematic	45
Figure 3.3	Optivac Vacuum-mixing cartridge	45
Figure 3.4	Dimensioned drawing of moulded specimen. All dimensions are in millimetres.	46
Figure 3.5	Exploded view of the mould, two aluminium plates 8 mm thickness were added for rigidity.	47
Figure 3.6	Schematic of a moulded damage accumulation specimen, with a 16 mm × 16 mm gauge section and a thickness of 3.5 mm.	48
Figure 3.7	The application of an internal pressure on the tubular specimen resulting in the following testing conditions; (a) 1:1 ratio axial v's hoop at 15 MPa axial; (b) 1:1 ratio at 11 MPa axial and (c) 1:1.5 ratio at axial 11 MPa.	49
Figure 3.8	Plot of internal pressure and load cell reading while in position control	50
Figure 3.9	Dimensioned cross section of a moulded multiaxial bone cement specimen. All dimensions are in millimetres.	51
Figure 3.10	(a) Cross section and (b) plan view of the assembled mould. The clear section represents the area filled with cement.	52
Figure 3.11	Uniaxial experimental test rig	54
Figure 3.12	Multiaxial experimental test rig	55

Figure 3.13	Detail of multiaxial specimen gripping arrangement	56
Figure 3.14	Schematic of the pressure set-up.	57
Figure 3.15	Schematic of the data logging scheme.	60
Figure 4.1	Stress versus number of cycles to failure curves for vacuum-mixed and hand-mixed Cemex Rx bone cement. The trend-lines were determined by a least squares fit through all the data points.	66
Figure 4.2	Stress versus number of cycles to failure curves for vacuum-mixed and hand-mixed Cemex Rx bone cement. The S-N curves for both mixing techniques have been fitted through the average $\log_{10}(N_f)$ values for the four stress levels.	66
Figure 4.3	Probability-of-survival diagrams for the vacuum-mixed and hand-mixed fatigue tests. The vertical axis indicates the probability-of-survival and the horizontal axis indicates the number of cycles to failure.	68
Figure 4.4	Fractographs of interacting pores forming stress concentrations in hand-mixed cement. The pattern on the fracture surface is consistent with discontinuous crack growth bands.	69
Figure 4.5	The fracture surface of a hand-mixed bone cement specimen; the area around the large pore was suspected of acting as the crack initiation site and on closer inspection (the white box) a pore of $< 100\mu\text{m}$ interacted with the large pore to form the crack initiation site.	70
Figure 4.6	The crack initiation site in this case was formed by two large pores. A close-up view shows that only a narrow ridge separated the two pores. The fatigue crack can be seen to grow from both ends of this ridge.	70
Figure 4.7	Failure site of a vacuum-mixed specimen, river lines are marked by the arrows radiating out from the pore; the direction of the arrow points in the direction crack growth.	71
Figure 4.8	Fracture surface of a vacuum-mixed specimen devoid of a porosity distribution. The close-up is highlighted by the white box; an irregular pore of approximately $200\mu\text{m}$ acted as the crack initiation site.	72
Figure 4.9	BaSO_4 clump acting as the crack initiation site, river lines are present propagating out from the BaSO_4 clump. Note the secondary crack passing through the BaSO_4 clump.	72
Figure 4.10	A large pore on a vacuum-mixed fracture surface and a considerably large pore acting as the fatigue crack initiation site.	72

Figure 4.11	Microcracks propagating from a pore. The direction of loading is in the horizontal direction.	73
Figure 4.12	Crack angle and crack length distributions for all cracks at failure. (a) the crack angle versus crack number distribution for the 9.76 MPa stress (b) the crack distribution for the 12.11 MPa stress and (c) the crack distribution for the 15MPa stress.	74
Figure 4.13	(a) Damage per cycle versus stress. (b) Damage per cycle normalised for porosity versus stress.	76
Figure 4.14	Plots of the number of cracks per specimen versus the number of pores for each specimen it can be seen that the number of cracks is dependent on the number of pores.	77
Figure 4.15	Crack growth graphs for the specimens tested at 15 MPa. (a) 183 cracks are present (b) 40 cracks (c) 27 cracks (d) 27 cracks and (e) 5 cracks	78
Figure 4.16	Crack growth graphs for the specimens tested at 12.11 MPa. (a) 34 cracks are present (b) 35 cracks (c) 8 cracks (d) 14 cracks and (e) 24 cracks	79
Figure 4.17	Crack growth graphs for the specimens tested at 9.76 MPa. (a) 16 cracks are present (b) 16 cracks (c) 92 cracks (d) 34 cracks and (e) 205 cracks	80
Figure 4.18	The sum of the crack lengths at each measurement point for the specimens tested at 9.76 MPa	82
Figure 4.19	Power law curves fitted to the normalised life and normalised damage for each specimen at 9.76 MPa.	82
Figure 4.20	The sum of the crack lengths at each measurement point for the specimens tested at 12.11 MPa	83
Figure 4.21	Power law curves fitted to the normalised life and normalised damage for each specimen at 12.11 MPa.	83
Figure 4.22	The sum of the crack lengths at each measurement point for the specimens tested at 15 MPa.	84
Figure 4.23	Power law curves fitted to the normalised life and normalised damage for each specimen at 15 MPa	84
Figure 4.24	Most Likely damage evolution curves for the stress levels tested at (a) 9.76 MPa (b) 12.11 MPa (c) 15 MPa	86
Figure 4.25	Relationship between damage evolution power law constant and cyclic stress level	87

Figure 4.26	Cumulative Weibull distributions for the fatigue tests with an axial stress of 11 MPa. The distribution of fatigue strength of the specimens with no hoop stress is almost identical to the distribution of fatigue strength of the specimens which had a hoop and axial stress of 11 MPa.	89
Figure 4.27	Cumulative Weibull distributions for the fatigue tests with an axial stress of 15 MPa. The distribution of fatigue strength of the specimens tested under multiaxial conditions (hoop and axial stress equal to 15 MPa) shows that that the fatigue life at 50% probability of survival is reduced significantly.	89
Figure 4.28	Initial deformation measured in the axial direction showing that the axial extension is a function of the von Mises equivalent stress. The values are taken at the first sampling point.	90
Figure 4.29	The extension of the specimens at the last sampling point before failure of the specimen occurred. The extension does not conform to the von Mises equivalent because of different failure lives and different extension slopes.	91
Figure 4.30	Uniaxial creep data for an axial stress of 11 MPa, graph (a) clearly shows the primary and secondary creep region for each specimen. Regression lines have been fitted to the data on a log-log scale.	92
Figure 4.31	Uniaxial creep data for an axial stress of 15 MPa, graph (a) clearly shows the primary and secondary creep region for each specimen. Regression lines have been fitted to the data on a log-log scale.	93
Figure 4.32	Uniaxial creep data for specimens with an axial stress of 11 MPa and a hoop stress of 11 MPa, graph (a) clearly shows the primary and secondary creep region for each specimen. Regression lines have been fitted to the data on a log-log scale.	94
Figure 4.33	Uniaxial creep data for specimens with an axial stress of 11 MPa and a hoop stress of 16.5 MPa, graph (a) clearly shows the primary and secondary creep region for each specimen. Regression lines have been fitted to the data on a log-log scale.	95
Figure 4.34	The creep curves for the three specimens (axial 11 MPa) with a low fatigue life are plotted in (a) and linear regression lines have been fitted to the creep data from 10,000 cycles to the last sampling point before failure. Similarly the three specimens with a greater fatigue life have been plotted in (b).	96
Figure 4.35	The slope of the steady state creep region of each specimen tested at axial 11 MPa plotted against the inverse of the time to failure.	98

Figure 4.36	The slope of the steady state creep region of each specimen tested at 11 MPa axial and hoop stress plotted against the inverse of the time to failure.	99
Figure 4.37	The slope of the steady state creep region of each specimen tested at 11 MPa axial and 16.5 MPa hoop stress plotted against the inverse of the time to failure.	99
Figure 5.1	Crack initiation process in hand mixed acrylic bone cement. The crack initiates in the lower left-hand corner of the image in the “valley” between two beads on the pore’s interior surface the crack then propagates through the beads.	102
Figure 5.2	A plot of the vacuum-mixed fatigue data, the cross sectional area has been adapted to account for porosity consequently a net section stress could be calculated. The original data has also been plotted for comparison purposes.	105
Figure 5.3	Various patterns of porosity in a 2-D case porosity increases down the page similarly the value of the maximum stress concentration increases as porosity increases (Tsukrov and Kachanov, 1997).	108
Figure 5.4	Predicted damage versus the number of loading cycles	110
Figure 5.5	S-N curves for different specimens tested under near-identical conditions (same cement and mixing technique). The lines plotted are regression lines through the averages at each stress level; the equations of these lines are given in Eqn. 5.1 and 5.2.	111
Figure 5.6	Range of S-N curves for acrylic bone cement based on a size effect, with the lowest fatigue strength associated with the large cement mantle and the greatest fatigue strength associated with a small discrete element.	113
Figure 5.7	The use of one fatigue curve for all cement mantles will weight against a smaller cement mantle by a value of Y'' minus Y' .	114
Figure 5.8	The orientation of pores will effect the orientation of the failure crack (a) σ_1 will cause failure in this case, while in (b) σ_2 will cause failure (if $\sigma_1 = \sigma_2$).	116
Figure 5.9	Comparison of the parameter B, which relates initial creep, with the work of Verdonschot <i>et al.</i> (1994) and the present work, showing that Cemex Rx bone cement exhibits 30% more creep at 11MPa than Simplex P bone cement.	118

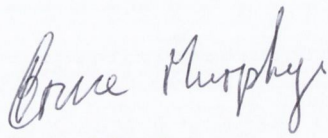
List of Tables

Table 1.1	Second and third generation cementing techniques which have led to an improvement in success rate for cemented joint replacements.	4
Table 2.1	(a) Porosity results for Palacos R [®] bone cement using different vacuum-mixing systems (Wang et al., 1996).	22
Table 2.2	The removal of specimens with large pores is not consistent in the literature.	26
Table 2.3	Fatigue results of Palacos R bone cement from Lewis (1999), vacuum-mixing increases mean fatigue life by over 50%.	30
Table 2.4	Fatigue results for Oteopal bone cement from Lewis (1999a); there is an increase of approximately ten times the hand-mixed value compared to only double the strength for the high viscosity Palacos R cement, see Table 2.3.	30
Table 3.1	Composition of the powder and liquid components of the bone cement used in this study. The monomer component is the same in both cements	44
Table 3.2	Multiaxial loading conditions	50
Table 4.1	Stress to number of cycles to failure data for vacuum-mixed and hand-mixed cement	64
Table 4.2	The results of statistical significance tests comparing the two mixing techniques.	65
Table 4.3	Determined shape parameters (α) and location parameters (β) for the two-parameter Weibull distribution.	67
Table 4.4	Summary of crack results at failure	75
Table 4.5	Empirical power law constants	85
Table 4.6	Summary fatigue results for the tubular specimens. p-values are reported is for the multiaxial stress states versus its corresponding control set.	88
Table 4.7	Fluctuation in hoop stress caused by specimen expansion and resulting R-ratio. (R-ratio is defined as the minimum cyclic stress value divided by the maximum cyclic stress value).	90
Table 4.8	Table of the regression line constants fitted to the log-log creep data presented in figures 4.29 and 4.30.	96
Table 5.1	The slopes of all the fatigue curves determined in this thesis based on two different regression methods. The slopes of the lines fitted to the averages at each stress level are more consistent compared to regression lines fitted to all the data.	103

Declaration

I declare that the present work has not previously been submitted for a degree at any University. It consists entirely of my own work, except where references indicate otherwise.

The library of Trinity College, Dublin may lend or copy this thesis on request.

A handwritten signature in cursive script that reads "Bruce Murphy".

Bruce Murphy

May 2001

Acknowledgements

Sincere thanks are due to Dr. Patrick Prendergast for his guidance, encouragement, grammar corrections, philosophy regarding Irish women, and most of all his never-ending enthusiasm for research. Thanks very much Paddy.

Many thanks go to Dr. Brendan McCormack, who in the early part of this work gave me an excellent introduction to the world of bone cement damage accumulation. I would also like to thank Prof. David Taylor whose mind was always available for probing.

I must express my gratitude to the technicians Tom, Sean, Gabriel and Jerry for a number of practical tips, without which I may still be running around the testing lab. Many thanks go to Peter O'Reilly for manufacturing the testing rigs, Paul Normoyle for photographic assistance. Further gratitude goes to Peter and Ray for adding a few extra thumps to the Instron whenever it decided to go belly-up.

I would like to acknowledge my fellow post-grads and friends for their support Linda (for keeping me smiling), Damien (for laughing at my jokes), Fergal (for many hangovers), Suzanne (nagging), Helen (more nagging), Alex (*in-depth* conversations about damage), Frank, Connor, Magali, Richard, Seosamh, John, Danny, Laoise, Adriele, Mark, Triona and Stephen.

I would also like to express my thanks to Prof. John Monaghan and Joan Gillen for their assistance whenever it was necessary.

Finally, I thank my parents and family for their continuous support.

I would like to acknowledge my funding source: The European Commission under the Standards, Measurements and Testing programme (Contract No. SMT-CT96-2076). I would also like to thank Tecres for the bone cement, Scandimed for the vacuum-mixing system, and The Dept. of Mechanical Engineering, UCD for the use of their optical comparator.

Abstract

Polymethylmethacrylate bone cement is used to fixate many orthopaedic implants. However, it is a brittle material, prone to damage accumulation leading to cement cracking and prosthesis loosening. The damage accumulation failure scenario has been recognised as the predominant mode of cemented implant loosening, and a combination of finite element analysis and continuum damage mechanics can be used to model this failure scenario; however, the empirical laws used to model the fatigue behaviour of acrylic bone cement are incomplete. The objective of this thesis is to develop empirical laws which accurately describe the fatigue behaviour of acrylic bone cement. Furthermore, this thesis addresses a number of aspects of the fatigue behaviour of acrylic bone cement which are relevant to experimental testing and clinical performance.

Three experimental tests were designed to investigate a number of aspects of the fatigue behaviour of acrylic bone cement. Namely: the mismatch between the *in vivo* and *in vitro* performance of vacuum-mixed cement; the relationship between damage accumulation and stress; the effect of an off-axis tensile stress on the fatigue strength of acrylic bone cement.

The results show that the *in vivo* underperformance of vacuum-mixed cement can be explained by the greater variation in fatigue strength of vacuum-mixed cement, which is caused by occasional large pores. Moreover, the practice of removing specimens with these large pores will lead to an overestimation of the fatigue strength, and in addition the *variability* associated with a certain mixing technique/cement will be missed. The rate of damage accumulation in bone cement was found to be non-linear and stress dependent. The effect of an off-axis tensile stress was found to reduce the mean fatigue strength by up to one order of magnitude, showing that the *in vivo* fatigue strength of acrylic bone cement is presently underestimated.

In conclusion the work of this thesis has developed empirical laws to model the fatigue behaviour of acrylic bone cement and it has also determined a number of key aspects of the fatigue behaviour of acrylic bone cement.

Publications and presentations

Journal Publications

Murphy B.P., Prendergast P.J. (1999) Measurement of non-linear damage accumulation in PMMA bone cement under cyclic loading, *Journal of Materials Science: Materials in Medicine*, 10 (12): p779-782

Murphy B.P., Prendergast P.J. (2000) On the magnitude and variability of the fatigue strength of acrylic bone cement, *International Journal of Fatigue*, 22 p855-864

Murphy B.P., Prendergast P.J. (2002) The relationship between stress, porosity, and non-linear damage accumulation in acrylic bone cement, *Journal of Biomedical Materials Research*, 10 (4) p646-654

Conference Abstracts

Murphy B.P., Prendergast, P.J. (2001) Multiaxial fatigue of acrylic bone cement. Presented at the European Society of Engineering in Medicine May 2001. *International Journal of Health Care Engineering* vol 9; p121-123

Murphy, B. P., Prendergast, P. J. (2000) The relationship between stress, porosity, damage accumulation, and fatigue life in acrylic bone cement, *Proceedings of the 12th Conference of the European Society of Biomechanics*, p. 235

Murphy, B.P., Prendergast, P.J. (2000) Quantification of the variability in fatigue life of PMMA bone cement in relation to mixing technique, *Transactions of the 46th Annual Meeting of the Orthopaedic Research Society*, Vol. 25, p.252

Murphy B.P., McCormack B.A.O., Prendergast P.J. (1999) Measurement of Non-Linear Damage Accumulation in PMMA Bone Cement Under Cyclic Loading, *Proceedings of the 15th European Conference on Biomaterials* Sep 8-12 1999

Murphy B.P., McCormack B.A.O., Prendergast P.J. (1999) Fatigue Strength of Vacuum Mixed Cement Is Higher But More Variable Than Hand Mixed Cement, *J Bone Joint Surg [BR]* 81-B:SUPP III p317

Murphy B.P., Prendergast P.J. (1999) Determinants Of The Fatigue Strength Of Cemented Prosthetic Fixations, *Irish Journal of Medical Science*, Vol. 168, Supplement no. 4, p5-6

Murphy B.P., Prendergast P.J., McCormack B.A.O., O'Reilly P. (1999) Non-Linear Damage Accumulation In Orthopaedic Bone Cement. *Irish Journal of Medical Science*. 168, p211

Chapter 1

Introduction

1.1	Implant fixation	2
1.2	The problem of fatigue of bone cement	5
1.3	Predicting failure in joint replacements	6
1.4	Conclusion	8

1.1 Implant fixation

Polymethylmethacrylate (PMMA) is the most common orthopaedic material and is used as a means of fixating orthopaedic implants. When used for biomedical applications, certain additions are made to PMMA and it is given the name *bone cement*. It was introduced to hip surgery in 1951 by Kiaer and Jansen of Copenhagen (Charnley, 1970). It was Charnley who popularised the use of PMMA as the fixation material for total hip replacement in 1958. Presently some 40 different bone cements are available on the market (Kühn, 2000), and they are all based on the same substance, namely methyl methacrylate. The volume of bone cement implanted in humans is very considerable; Stryker-Howmedica-Osteonics (which manufactures Simplex P bone cement) reports that 15 million doses of Simplex P have been implanted to date (www.howmedica.com). This figure represents only 24% of the bone cement market and similar amounts of other bone cements have been implanted, namely bone cements manufactured by the following companies: Johnson & Johnson/DePuy (24% market share), Zimmer (19%), and Biomet (16%) (Biomet Annual Report, 2000).

The function of acrylic bone cement is to smoothly transfer the joint load from the prosthesis to the underlying bone; in some cases (for example, the hip joint, see Fig. 1.1) the loading may be several times body weight (Bergmann *et al.*, 1993). Bone cement is not just confined to use in hip surgery, it is also used as the fixation medium in a number of joint replacements including knee, shoulder, elbow, ankle, and wrist replacements, and in all cases implants are subjected to cyclic loading (Prendergast, 2001).

If a cemented joint replacement is to perform successfully over its expected lifetime, the fixation material (i.e. the bone cement) must be able to withstand the *in vivo* cyclic loading. However, there is a problem with bone cement – its fatigue resistance is inadequate and the predominant mode of cemented implant failure is fatigue damage accumulation (Huiskes, 1993). As a material, bone cement has a similar composition to Perspex; however there is a considerable difference in fatigue strength. Perspex, which is cured at high temperatures and pressures, has a fatigue limit of 35 MPa (Daniels, 1989) whereas acrylic bone cement has a fatigue limit of

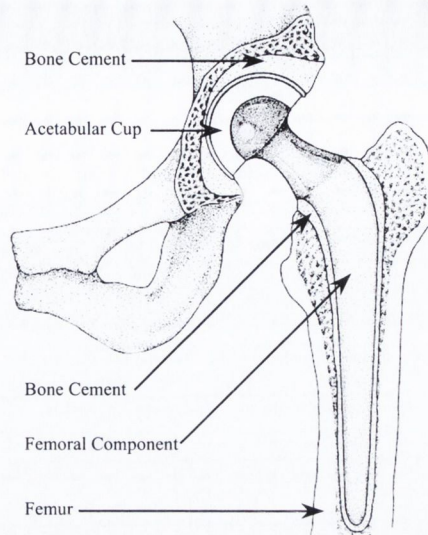


Figure 1.1 *Schematic of a cemented total hip replacement, from Hardinge (1983).*

the order of 7 MPa. This difference in fatigue strength is caused by two factors: firstly, bone cement contains additives in the form of radio-pacifiers and antibiotics, and secondly, bone cement is prepared under surgical conditions. During its preparation air entrapment occurs resulting in a porous heterogeneous material. Porosity is the most prominent inconsistency in acrylic bone cement and has been identified as one of the principal causes of fatigue crack initiation *in vivo* (Topoleski *et al.*, 1990). Because of the poor durability of cemented joint replacements other fixation methods have been tried.

Orthopaedic implants can also be fixated without cement by so-called cementless fixation. This fixation technique relies on bone ingrowth into the surface of an implant. In theory biological fixation should be permanent whereas cemented fixation will demonstrate progressive loosening with time (Gruen *et al.*, 1979). However uncertainty and relatively low survival rates have become the dominant experience with cementless implants. The Swedish hip register confirms this uncertainty—cemented designs are less prone to loosening than cementless designs, see Fig. 1.2 (Malchau and Herberts, 1998). In the latter period, 1987-1996, improvements in cementing technique have increased the probability-of-survival of cemented implants whereas no such improvements to cementless designs/techniques have appeared. According to Malchau *et al.* (2000) there is a trend whereby surgeons are reverting back to cemented fixation.

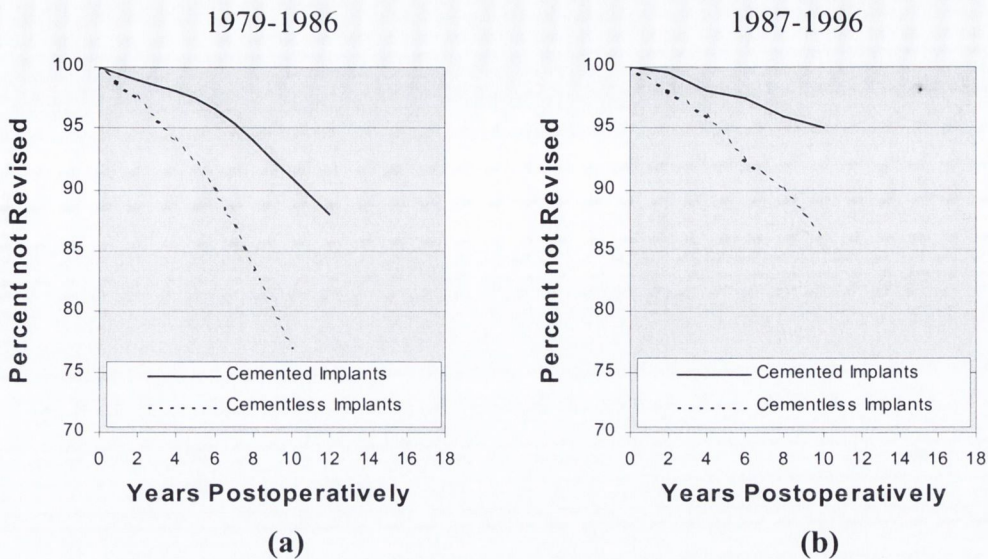


Figure 1.2 *Survival results from the Swedish Hip Register for different types of implantation techniques. A clear improvement in cemented implant survival can be observed for the latter period (1987-1996) compared to the early period (1979-1986), whereas no such improvement is present for cementless designs. (adapted from Malchau and Herberts, 1998).*

Over the years a number of improvements have been introduced to increase the durability of cemented joint replacements; since the inception of cemented joint replacements hand-packing and hand-mixing of the bone cement have been superseded by what are called “modern cementing techniques”, see Table 1.1. These improved cementing techniques (Mulroy and Harris, 1990) and enhanced surgical practices (Herberts and Malchau, 1996) are responsible for a recent increase in success rate of cemented implants. However, aseptic loosening remains the dominant failure mode of cemented hip replacements (Malchau *et al.*, 2000), knee replacements (Lidgren, 2000), and shoulder implants (Writh and Rockwood, 1996). If long-term success is to be achieved, a durable cement mantle is required with ample fatigue strength. This will only be achieved with a deeper understanding than we have at present of the parameters that affect the durability of bone cement.

Table 1.1 *Second and third generation cementing techniques which have led to an improvement in success rate for cemented joint replacements.*

Cementing Technique	Function
Vacuum-mixing	Reduce cement porosity
Centrifugation mixing	Reduce cement porosity
Pressurisation of the bone cement	Increase cement/bone interface strength
Bone Plugs	Maintain pressure in cement
Pulsatile Lavage of the bone cavity	Remove debris from bone cavity
Cement gun	Eliminate cement laminations

1.2 The problem of fatigue of bone cement

Because bone cement is primarily subjected to cyclic loading *in vivo*, its fatigue properties are of great importance. It has been shown that fatigue cracks do occur in a cement mantle under physiological loading (Culleton *et al.*, 1993, Jasty *et al.*, 1991, Topoleski *et al.*, 1990). Bone cement is very susceptible to the problem of fatigue-cracking due to the numerous inconsistencies which exist within the material such as pores caused by air entrapment during mixing, pores from evaporation of the monomer, blood entrapment, clumps of barium sulphate and bone debris. These inconsistencies within the material generate stress risers and fatigue crack initiation sites; moreover they increase the variation in fatigue strength because a consistent material with a regular microstructure is not formed. In conclusion bone cement is not an ideal fixation material and may always be prone to fatigue failure.

The *in vitro* fatigue properties of acrylic bone cement have been improved by the introduction of new mixing methods. Originally hand-mixing was the only option available, but nowadays vacuum-mixing and centrifugation are common with the objective of producing a more consistent material by reducing cement porosity (Table 1.1). Surprisingly, some clinical results indicate that vacuum-mixing is less successful than hand-mixing (Malchau and Herberts, 1998), but the majority of *in vitro* studies show that vacuum-mixing outperforms hand-mixing. *In vitro* studies show that there is an increase in fatigue strength when bone cement is vacuum-mixed, though a large degree of variation in fatigue strength is associated with vacuum-mixing. If the fatigue strength of bone cement determines the survival of cemented joint replacements, why does vacuum-mixing sometimes under-perform *in vivo*? This is one of the issues to be addressed in this thesis.

Jasty *et al.* (1991) showed that *in vivo* failure of cemented femoral components was caused by the accumulation of microcracks. These microcracks have two main consequences: firstly, the mechanical integrity of the cement may be lost causing loosening of the implant; secondly, PMMA particles may be created by the relative movement of fatigue crack surfaces, and these particles may react with the surrounding tissue causing an inflammatory response leading to osteolysis and prosthesis loosening. McCormack and Prendergast (1999) demonstrated that damage accumulation in acrylic bone cement occurred continuously, and could be monitored

over the course of a fatigue test; however, to date, data relating fatigue damage accumulation to stress level has not been obtained. This data is required for the further development of computer simulations of the damage accumulation failure scenario in cemented joint replacements (Verdonschot, 1995).

Finally, the *in vivo* loading situation of acrylic bone cement involves complex multiaxial stresses; however, there is no data in the literature to describe the fatigue behaviour of acrylic bone cement under these stresses. Stresses predicted in the cement mantle have been shown to be below the *fatigue limit* of bone cement by a factor of three (Prendergast *et al.*, 1989, Harrigan *et al.*, 1992), although a number of retrieval studies implicate fatigue failure as the predominant cause of failure in the *in vivo* situation (Jasty *et al.*, 1991, Topoleski *et al.*, 1990). The question therefore arises, “Do multiaxial stresses significantly influence the fatigue life of acrylic bone cement?”

1.3 Predicting failure in joint replacements

The use of pre-clinical testing of cemented joint replacements as described by Prendergast and Maher (2001) can be divided into three categories; computational modelling, laboratory bench tests, and animal experiments. The cost of testing increases as one moves from computational modelling to laboratory bench tests to animal experiments. If poorly performing prostheses can be identified early in the implant innovation process then the use of animal experiments could be avoided. As bone cement is the weak link in the cemented joint replacement construct, and fatigue failure of the cement mantle has been identified as the predominant mode of *in vivo* failure, new prostheses can be evaluated based on the damage they produce in the cement mantle as follows:

(i) Computational Models

—Predict failure based on the damage accumulation failure scenario (Verdonschot, 1995 and Stolk *et al.*, 2000)

(ii) Laboratory Bench Tests

—Predict failure based on implant migration caused by cement damage (Kärrholm *et al.*, 1994 and Maher and Prendergast, 2001)

The use of computational models combining continuum damage mechanics and finite element modelling have been used to predict failure of cemented joint replacements (Verdonschot and Huiskes, 1997) and more recently these models have been applied to differentiate between different prostheses designs (Stolk *et al.*, 2000a). A feature in these models is the use of empirical laws to characterise the fatigue behaviour of acrylic bone cement. However, it is debatable whether or not the fatigue behaviour is being simulated adequately since the models do not account for several attributes of the cement. Firstly, the stressed volume of the cement mantle is not considered, and secondly, the rate at which damage accumulation occurs is assumed to be linear according to the Palmgren-Miner Law (Miner, 1945). This thesis will show that damage accumulation is non-linear and stress dependent. Furthermore, it is not known if the effect of multiaxial stress states needs to be accounted for in the fatigue life of acrylic bone cement.

It has been proposed that the migration of cemented implants can be used as a predictor of failure (Kärrholm *et al.*, 1994). Maher (2000) suggested that a relationship between implant migration and damage accumulation existed, whereby the time-to-failure was related to the steady state creep rate via the Monkman-Grant relationship:

$$\dot{\epsilon}_{ss} = \frac{C}{t_f}, \quad \text{Eqn. 1.1}$$

where $\dot{\epsilon}_{ss}$ is the steady state creep rate, t_f is the time to failure and C is a material dependent constant. The work of Dr. Suzanne Maher (2000) showed that different cemented prostheses, under dynamic loading, have significantly different steady state subsidence rates. The subsidence of these prostheses was assumed to be due to creep and damage accumulation within the cement mantle. Her thesis showed that the prosthesis with the higher subsidence rate corresponded to the prosthesis that fails faster in the clinical situation. However, no experimental data is available that confirms the relationship between creep rate and time to failure for bone cement under cyclic loading. This thesis will investigate whether or not the Monkman-Grant relationship holds for bone cement under uniaxial fatigue and also under more complex multiaxial stresses. If it does, it opens the possibility of analysis of the

damage accumulation failure scenario (a long term process) by testing for implant migration due to creep as measured in the short term.

1.4 Conclusion

The cement mantle is the weak link in a cemented joint replacement; retrieval studies have identified fatigue failure as the predominant mode of *in vivo* failure. Improvements to the cementing technique have increased the success rate of cemented joint replacements and have revived interest in cemented fixation. However, aseptic loosening caused by fatigue failure of the cement mantle presently accounts for over 75% of all failure cases (Malchau *et al.*, 2000).

Several aspects of the fatigue behaviour of acrylic bone cement are not fully understood. Namely:

- How can it be that vacuum-mixed cement may under-perform hand-mixed cement *in vivo*?
- What is the correct relationship between damage and number of cycles, and is it a function of stress?
- What is the interrelationship between stress and porosity on damage accumulation in acrylic bone cement?
- Do multiaxial stresses significantly influence the fatigue life of acrylic bone cement?
- Is the Monkman-Grant relationship applicable to acrylic bone cement under dynamic loading?

Complete knowledge of these aspects of the fatigue behaviour of acrylic bone cement would improve the pre-clinical evaluation of cemented joint replacements by means of improving the basic knowledge required for computational analysis, and for

understanding experimental results. It is the objective of this thesis to determine these aspects of the fatigue behaviour of acrylic bone cement and to present the data in a form in which it can be used to improve the pre-clinical evaluation of cemented joint replacements.

Chapter 2

Literature Review

2.1 Introduction	11
2.1.1 Components of bone cement	11
2.1.2 Preparation of bone cement	11
2.1.3 Setting of bone cement	12
2.2 Failure of cemented joint replacements	14
2.3 Improved cementing techniques	17
2.3.1 Second generation cementing techniques	17
2.3.2 Third generation cementing techniques	18
2.4 Porosity reduction and sources	19
2.5 Fatigue behaviour	23
2.5.1 Fatigue testing conditions	23
2.5.2 Specimen preparation	25
2.5.3 Effect of additives and sterilisation method on fatigue properties	26
2.5.4 Effect of mixing method	28
2.6 Review of the methods for analysis of results	32
2.7 Fatigue damage accumulation in bone cement	34
2.7.1 Fatigue observations <i>in vivo</i>	34
2.7.2 Damage accumulation – experimental	35
2.7.3 Damage accumulation – computational	36
2.8 Multiaxial fatigue	38
2.9 Creep properties	39
2.10 Summary	40

2.1 Introduction

2.1.1 Components of bone cement

Acrylic bone cement is self-polymerising and consists of two components, a liquid monomer (methyl methacrylate, MMA) and a powder component (polymethylmethacrylate, PMMA). The two components are mixed in the appropriate proportions to form bone cement. Other additives are included in these components. The monomer contains:

- (i) hydroquinone, an inhibitor, which prevents the monomer from pre-polymerising spontaneously,
- (ii) N-N dimethyl-p-toluidine (DPT), an accelerator, which speeds up the polymerisation reaction.

The powder component contains:

- (i) an initiator, benzoyl peroxide, which causes the MMA to polymerise at room temperature.
- (ii) a radiopacifier, either barium sulphate (BaSO_4) or zirconium dioxide (ZrO_2), which allows the bone cement to be observed on x-rays.

A number of commercial formulations contain an antibiotic additive; these products are generally employed in revision arthroplasties, in septic or potentially septic cases.

2.1.2 Preparation of bone cement

Bone cement is prepared under operating room conditions. Typical conditions consist of a temperature of 21-24°C and a relative humidity no less than 50% (Sitwell, 1987). When bone cement was first introduced the only mixing method available was hand-mixing; in this case the two components of bone cement are mixed with a spatula in a mixing bowl at atmospheric pressure. However, new mixing techniques have been introduced such as vacuum-mixing and centrifugation. The objective of these so-called “third-generation” cementing techniques is to reduce the porosity of the cement. In vacuum-mixing, the bone cement is mixed while under a vacuum; in theory this should eliminate the voids entrapped during the mixing process. In the second case the cement may be mixed first and then centrifuged for approximately 30-60 s; again the objective of this mixing method is to reduce the porosity of the cement as the air voids are forced out due to the pressure of centrifugal forces. After mixing,

the cement is either manually placed in the cavity by means of “finger packing” or injected into the cavity with a cement gun. The cement may also be pressurised at this time causing increased cement-bone interdigitation and providing a stronger interface (Davies and Harris, 1993).

2.1.3 Setting of bone cement

Once the two components of the cement have been mixed the polymerisation process of the monomer begins. The monomer, which contains small repeating units of the simple molecule MMA shown in Fig. 2.1 (a) reacts to form macromolecules containing a chain of simple molecules. This reaction requires free radicals; this part of the reaction is termed the initiation. Free radicals are generated when benzoyl peroxide (which is contained in the powder component) undergoes cleavage of the peroxy bond generating two free radicals, see Fig. 2.1 (b). Benzoyl peroxide normally undergoes cleavage at elevated temperatures; however since bone cement contains DPT (the accelerator), cleavage occurs at room temperature.

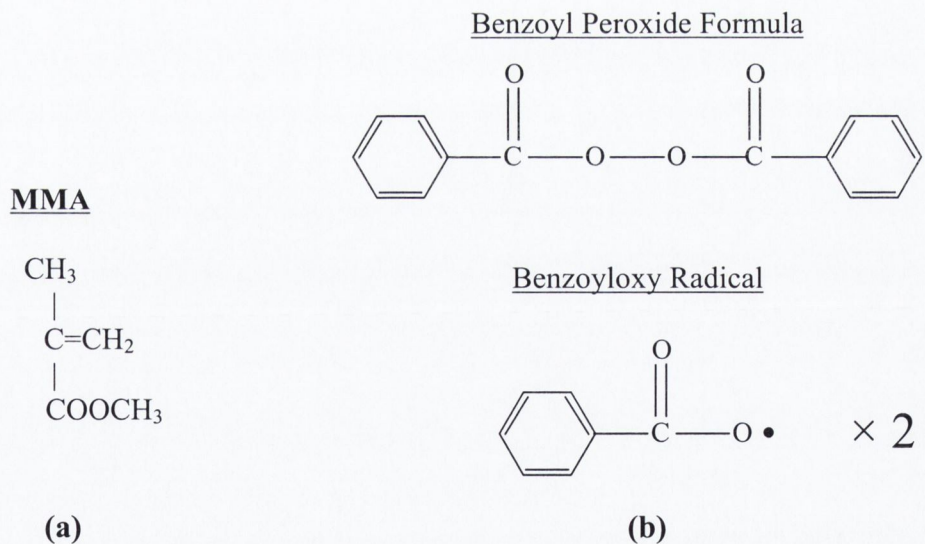
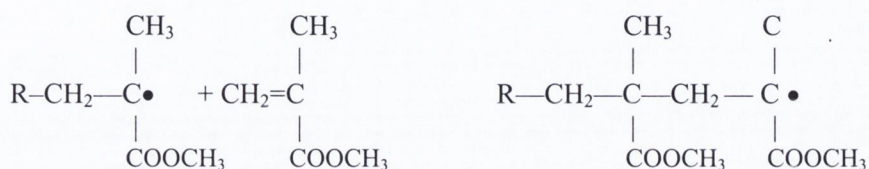


Figure 2.1 (a) The repeating unit of the monomer, MMA. (b) The initiator is a Benzoyl Peroxide molecule, initiation only occurs when benzoyloxy radicals are produced. DPT reacts to break the peroxy bond and forms two free radicals. The free radical will now be referred to as R in successive figures.

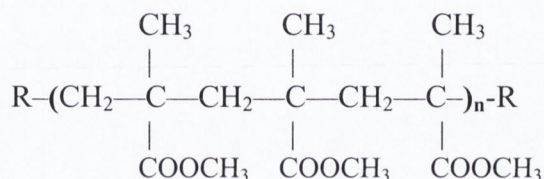
The next step in the reaction is termed the propagation stage. Propagation involves the successive addition of monomer units to the active radicals already produced in the initiation stage. The free radicals cause the double carbon bond of the MMA molecule to break, after this the free radical and the MMA molecule combine

to form one end of a macromolecule resulting in a larger free radical; the polymer chain continues to grow by free radical addition of MMA molecules, see Fig. 2.2 (a).

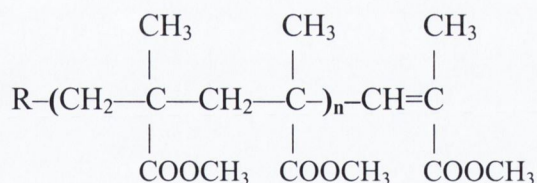
Termination is the final stage of the polymerisation process. The propagation of polymer chains is stopped by either combination or disproportionation (Bovey, 1979). Combination involves the joining together of two chains, see Fig. 2.2 (b). Disproportionation is caused by a hydrogen transfer reaction (Fig. 2.2 (c)).



(a)



(b)



(c)

Figure 2.2 (a) The process of free radical addition in PMMA. (b) A terminated macromolecule of PMMA composing of n MMA molecules, termination in this case is caused by combination. (c) A macromolecule of PMMA; propagation has been stopped by hydrogen transfer.

When polymerisation of the monomer is complete the pre-polymerised PMMA beads that form the powder are embedded into a solid PMMA matrix. The solidification process is an exothermic reaction; heat is generated firstly when the benzoyl peroxide molecule is split, and secondly during the propagation stage of the reaction, a typical polymerisation curve for acrylic bone cement can be seen in Fig. 2.3. The peak curing temperature is proportional to the amount of monomer added.

The peak curing temperature for commercial bone cements ranges between 50-90°C (Kühn, 2000).

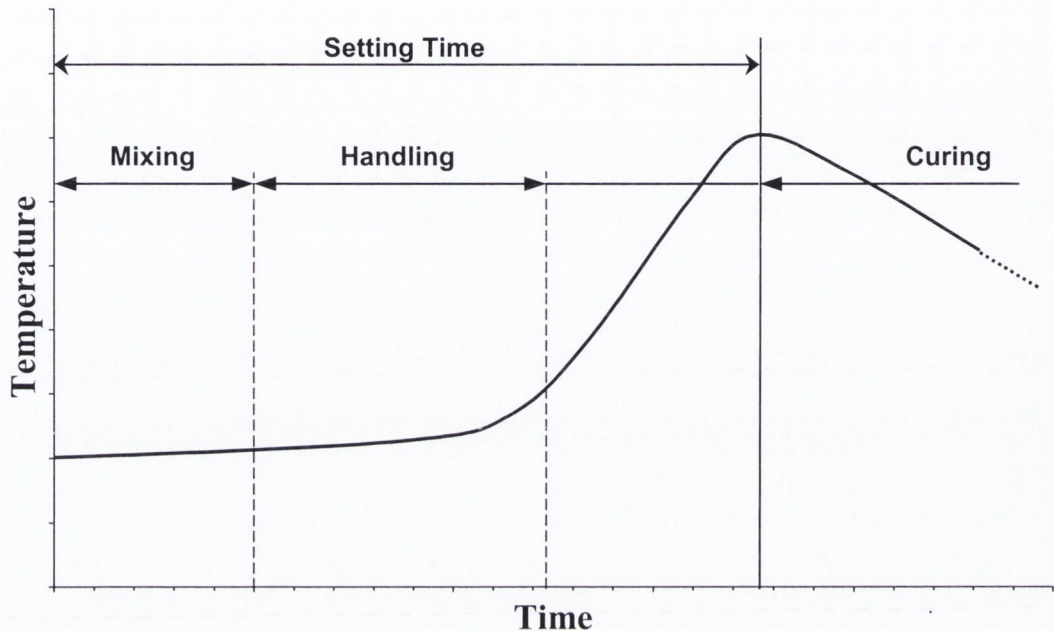


Figure 2.3 *Temperature versus time curve of curing acrylic bone cement*

The solidification process for acrylic bone cement consists of a time period defined as the setting time (see Fig 2.3). This time period is approximately 7-16 min. depending on ambient temperature. The mixing phase comprises of 1-2 min. of the setting time while handling takes up the remaining working time of the cement. Once the cement begins to heat up it becomes unworkable.

2.2 Failure of cemented joint replacements

At the present time, the main cause of failure of cemented hip replacements is aseptic loosening of the implant. Aseptic loosening is responsible for approximately 76% of all revision operations (Malchau *et al.*, 2000). Aseptic loosening can be considered as a mechanical failure of the reconstruction although the prosthesis itself does occasionally fracture. The most likely site for mechanical failure is the bulk cement or its interfaces.

The cement mantle fulfils two functions; to provide stability and to act as a barrier to wear debris. The cement may lose its ability to provide these functions due to damage accumulation. Failure of the joint replacement may occur by one of a number of possible scenarios (Huiskes, 1993). Two failure scenarios are relevant to bone cement function; the first is the damage accumulation failure scenario whereby the cement mantle undergoes microcracking leading to loss of mechanical stability and resulting in prosthesis loosening. The second failure scenario is the particulate reaction scenario; as the cement degrades it may lose its ability to act as a barrier to wear particles, either PE particles formed at the articulating prosthesis head and polyethylene cup or PMMA particles formed by the relative movement of cement cracks or a mixture of PMMA and metallic particles formed by the relative movement of the femoral prostheses within the cement mantle. Wear particles at the cement-bone interface cause an inflammatory response causing osteolysis (Maloney, 1990).

Stresses within the cement in the *in vivo* loading situation have been predicted to be low, i.e. one third of the fatigue strength of bone cement (Prendergast *et al.*, 1989, Harrigan *et al.*, 1992). Nonetheless failure occurs. One possible explanation is a detrimental series of events which combine three different processes: creep, fatigue, and wear. The first destructive event is debonding of the stem from the cement mantle. Jasty *et al.* (1991) hypothesised that this event was the primary event in femoral prosthesis loosening. After debonding, stresses within the cement mantle increase (Verdonschot and Huiskes, 1996a); consequently the probability of fatigue cracks initiating also increases. Simultaneously, particles of UHMWPE produced at the head/cup articulating surfaces migrate along the debonded implant-cement interface. Defects in the cement mantle appear in the form of cracks. These cracks grow as time progresses and eventually form through-mantle cracks (Topoleski *et al.*, 1990) linking the stem-cement interface and bone-cement interface. Wear particles can then freely migrate to the bone-cement interface using fatigue cracks as their transportation network.

In a long-term follow-up study by Müller (1997) the amount of osteolytic sites was found to correlate with cement defects; similarly, Maloney *et al.* (1990) examined post mortem retrieved well-fixed femoral components and found that the area of osteolysis corresponded to either a defect in the cement mantle or an area of thin cement; at the osteolytic sites particulate PMMA was found and was assumed to be the stimulus for local osteolysis. At this juncture, the extent of creep/fatigue damage

may cause subsidence and loosening of the prosthesis (Gruen *et al.*, 1979, Topoleski *et al.*, 1990).

The interaction between the three failure modes of fatigue, creep, and wear, as described above, causes a complex and multifactorial failure mechanism; this interaction is illustrated schematically in Fig. 2.4.

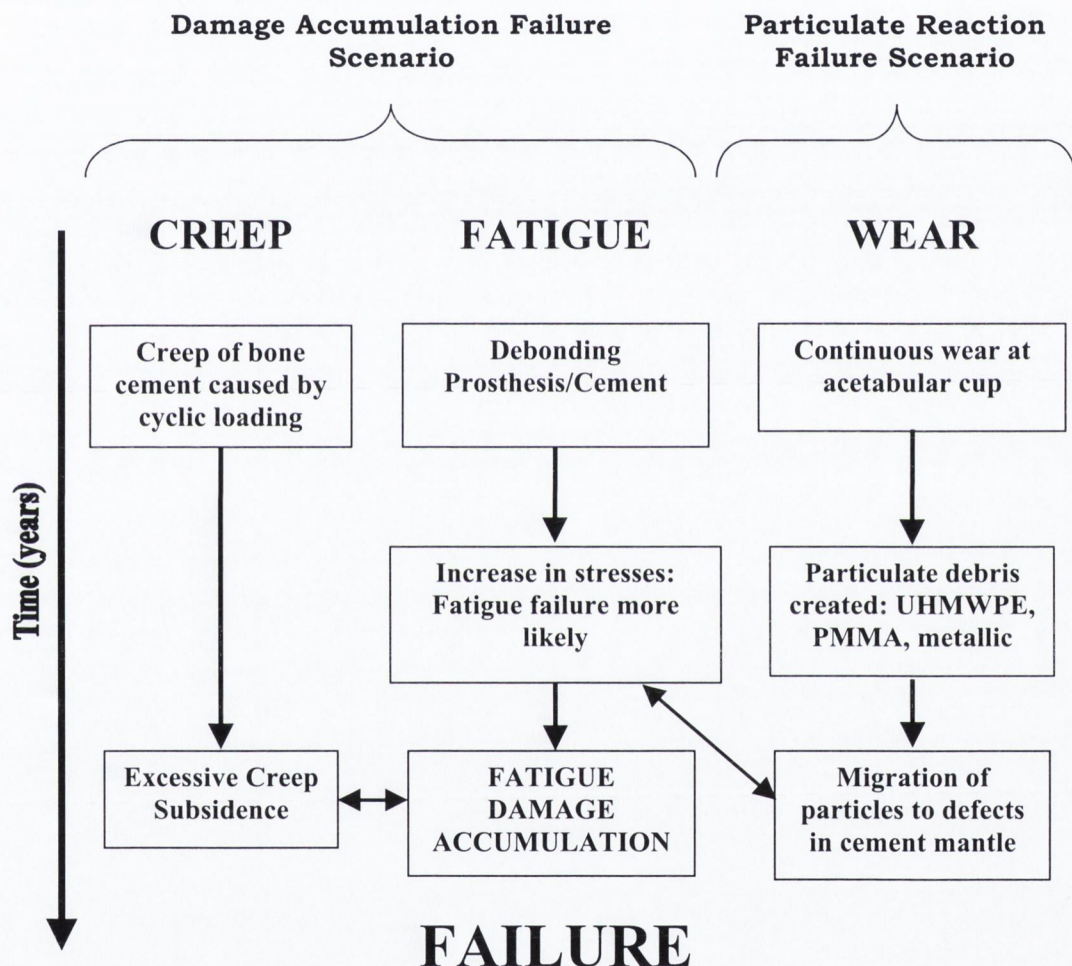


Figure 2.4 Schematic of the interaction between the damage accumulation failure scenario and the particulate reaction failure scenario.

2.3 Improved cementing techniques

One school of thought regarding advances to cemented joint arthroplasty is that improved cementing will prove more beneficial than any innovation in prosthesis design or fixation mode. The history of innovation in the technology of joint arthroplasty would seem to bear this out. Early cementing techniques resulted in high rates of femoral loosening of 20% at five years (Beckenbaugh and Ilstrup, 1978), and at ten years, it increased to 30% (Stauffer, 1982). These “first generation” cementing techniques involved hand-mixing, and finger-packing of the cement into the femoral canal. Second-generation cementing techniques improved the cementing process by use of a cement gun and retrograde filling of the canal and the addition of a distal plug. Now a “third generation” of cementing techniques are in use; these techniques involve pressurisation of the cement, vacuum or centrifugation mixing, and pulsative lavage of the femoral canal.

Clinical results using second-generation techniques have shown a clear improvement over early cementing techniques, while third-generation cementing techniques result in yet further improvement, although these results are only for seven years postoperatively (Malchau and Herberts, 1996).

2.3.1 Second generation cementing

The introduction of a cement gun and retrograde filling of the femoral canal was thought to reduce laminations (defects) in the cement mantle, while the use of a distal plug allowed the cement to be pressurised upon prosthesis insertion and thus providing a stronger bone/cement interface. Beim *et al.* (1989) showed that PMMA distal plugs could withstand 340 kPa for a period of 5 minutes providing enough pressure for cement bone interdigitation. A clear difference in survival rates is evident when early cementing is compared to second generation cementing:

- (i) Malchau and Herberts (1996) found early cementing techniques have a survival rate of 86.5% compared to 93.5% for second-generation techniques at 16 years post operation
- (ii) Smith *et al.* (1998) found the use of second-generation cementing techniques, at 18 years post operation, caused only 5% of femoral replacements to be revised for aseptic loosening.

The result of an improvement in femoral stem survival compared to acetabular component survival suggests that the mechanical integrity of the cement mantle has been improved, reducing the rate of damage accumulation; but the failure mechanism of the acetabular cup remains the particulate reaction scenario, as described by Schmalzried et al. (1992), and improvements to the mechanical integrity of the cement mantle do not have the same effect as they have for the femoral component.

2.3.2 Third generation cementing

Third generation techniques ensure a more consistent cement mantle by removing bone debris and blood and, by pressurisation of the cement mantle, a stronger bone cement interface is realized. Porosity reduction is achieved through vacuum-mixing or centrifugation of the bone cement (Wang *et al.*, 1996; Jasty *et al.*, 1990). A six to eight year follow-up study using third generation cementing techniques (pressurisation, pulsatile lavage, centrifugation of bone cement, in addition to second generation cementing techniques) shows a 1% failure rate in femoral component loosening can be achieved (Oishi *et al.*, 1994). Similarly third generation cementing techniques show excellent results in the Swedish Hip Register with a survival rate of 99% after seven years (Malchau and Herberts, 1996). However concern has now arisen over the use of vacuum-mixed cement (Malchau and Herberts, 1998), in comparison to earlier reports stating that vacuum-mixing gives a stronger cement (Malchau *et al.*, 1993). One of the conclusions reported by Malchau and Herberts (1998) in the 1998 Swedish Hip Register annual report was:

“No positive effect was associated to porosity reduction of bone cement in the short to mid-term follow-up perspective.”

Vacuum-mixed cement now has a greater risk associated with it for the first five years post-operation compared to hand-mixed cement, see Fig. 2.5 (Malchau *et al.*, 2000). This clinical evidence contradicts *in vitro* fatigue testing and static tests where vacuum-mixed cement outperforms hand-mixed cement, see Lewis (1997) for a review. One of the objectives of this thesis is to solve this seeming contradiction.

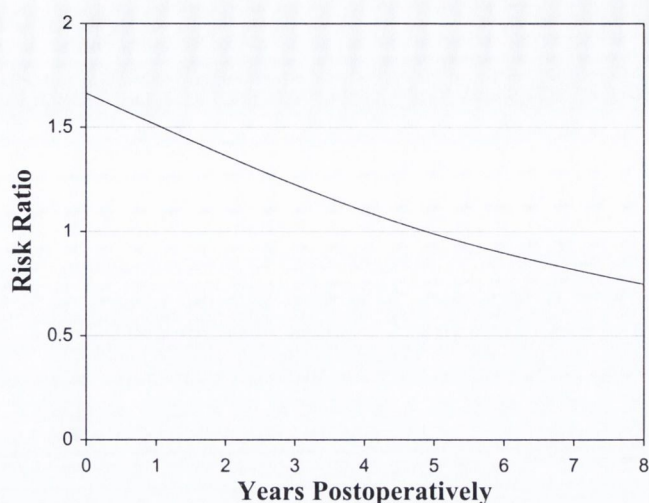


Figure 2.5 Risk ratio for Cement mixing technique, Vacuum vs. manual mixing. When the line is greater than one vacuum-mixing has an increased risk associated with it compared to hand-mixing (Malchau *et al.*, 2000).

2.4 Porosity reduction and sources

Pores have been observed to act as crack initiation sites in many retrieval studies (Jasty *et al.*, 1991; Culleton *et al.*, 1993; Topoleski *et al.*, 1990) and in *in vitro* studies (James *et al.*, 1992; Davies and Harris, 1990). However, some researchers have hypothesised that pores may also have a positive effect by acting to blunt crack growth (Rimnac *et al.*, 1986; Kadakia *et al.*, 2000). Porosity within the bulk cement can range between 5 and 16% (James *et al.*, 1993); the main sources of porosity are air entrapment during the mixing stage and evaporation of the liquid monomer during the curing stage. Most of the attention has focused on reducing the porosity by means of modifying the mixing technique; centrifugation was introduced as a method of preparing bone cement (Burke *et al.*, 1984); similarly, vacuum-mixing was introduced by Dearnast *et al.* (1983). Both techniques have the same aim—reducing porosity in the cement mantle.

Linden and Guillquist (1989) compared three mixing methods: hand-mixing and mechanical mixing with or without centrifugation or vacuum. The results showed that vacuum-mixing combined with mechanical mixing produced the most consistent material, while mechanical mixing combined with centrifugation reduced the percentage porosity by 50% in comparison to manual/centrifugation mixing, see Fig 2.6. However, it was noted that centrifugation concentrated pores in one part of the

cement resulting in a density gradient in the material. Huiskes (1993a) suggested a similar fate would occur to the heavier BaSO₄ particles under centrifugation resulting in an even greater density gradient within the material.

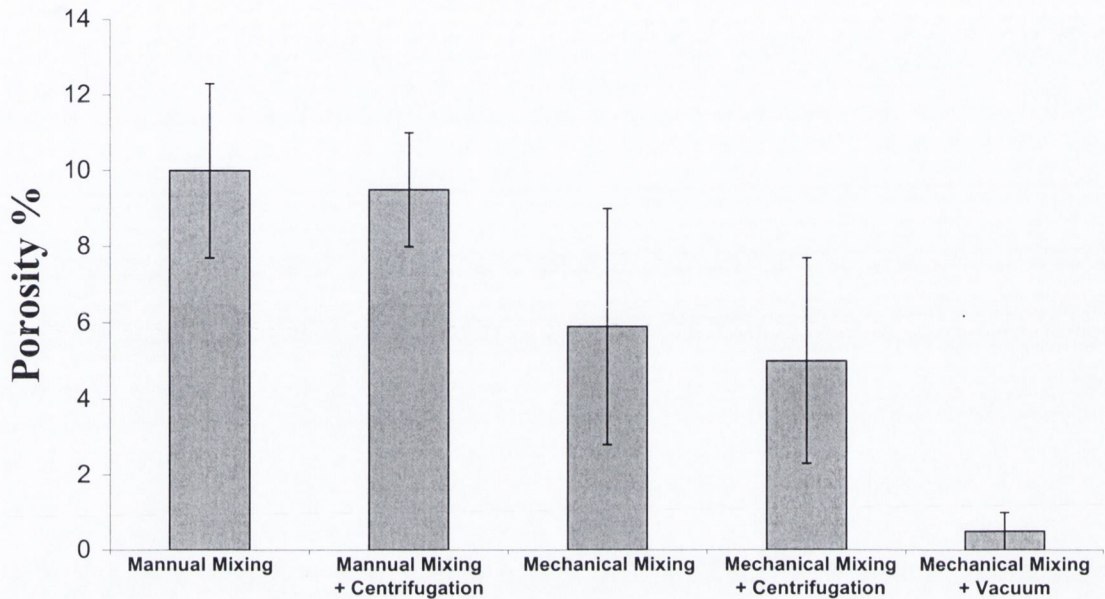


Figure 2.6 Porosity results from Linden and Guillquist (1989) showing that the combination of vacuum and mechanical mixing significantly reduced porosity in acrylic bone cement compared to other mixing methods.

Jasty *et al.* (1990) investigated the effect of centrifugation on percentage porosity of five commercial bone cement formulations. A control set was hand-mixed at 21°C and 50% humidity at a mixing rate of 2 Hz. Centrifuged specimens were mixed in the same manner but immediately after mixing they were spun at 4000 rpm for 30 s. Centrifugation reduced the percentage porosity and the mean pore size in all cement formulas, see Fig. 2.7. However, the number of voids/cm² increased for four of the five formulations. The experiments were repeated with the monomer chilled to 0°C this was shown to increase the amount of porosity for all cements. This study was repeated with a centrifugation time of 2 min; after centrifugation the cement was too viscous to be of any practical use.

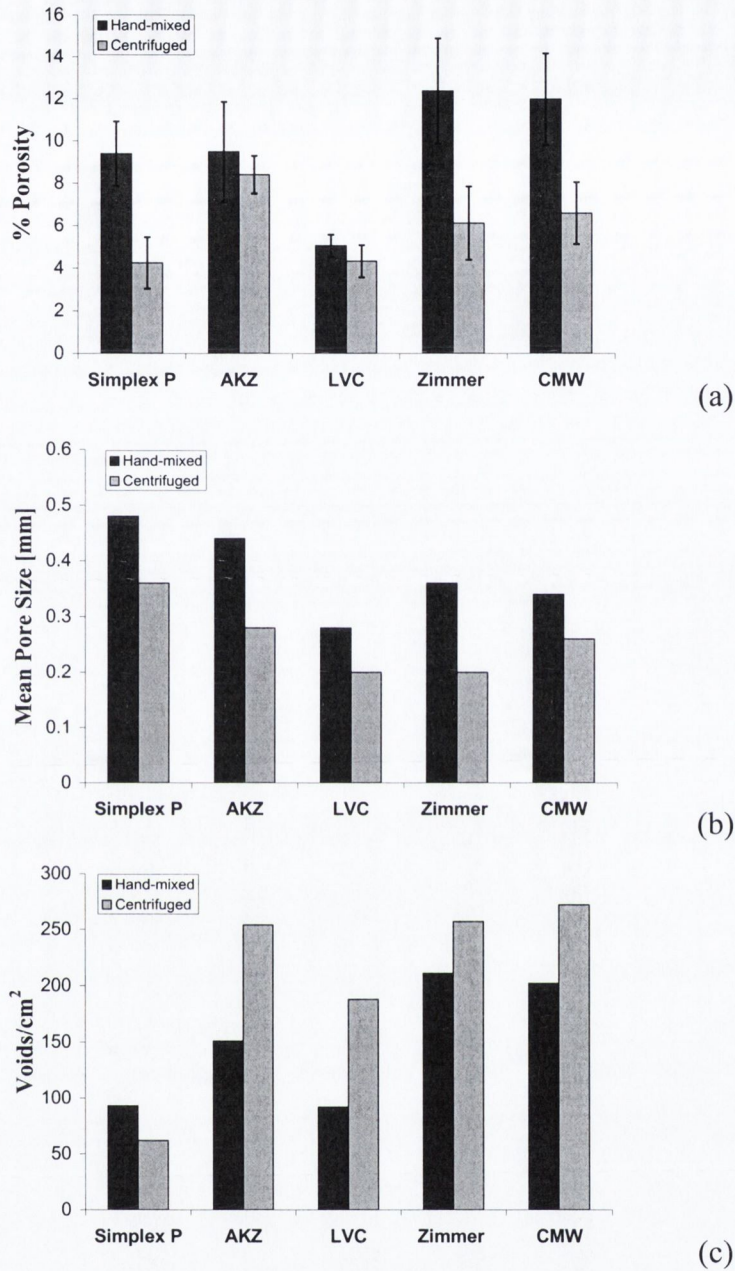


Figure 2.7 Centrifugation decreases percentage porosity (a) and the mean pore size (b). However the number of pores/cm² is increased after centrifugation (c).

Wang *et al.* (1996) investigated the difference between six commercial vacuum-mixing systems and their effectiveness in reducing porosity. All vacuum-mixing systems reduced porosity in high viscosity cement (Palacos R) and similarly in low viscosity cement (Simplex P) compared to hand-mixed cement, see Table 2.1. All the systems were successful in reducing micropores within the cement; however, macropores were not entirely eliminated from the cement resulting in a non-consistent material. This phenomenon of large pores in vacuum-mixed cement was also noted

by Davies and Harris (1990); vacuum-mixed cement specimens were generally pore free but some contained substantial voids; in contrast, centrifuged cement specimens appeared to be uniform and free of all large voids.

Table 2.1 (a) Porosity results for Palacos R[®] bone cement using different vacuum-mixing systems (Wang et al., 1996).

Mixing System	Macropores ^a	Micropores ^b	Density (g/cm ³)
Optivac [®]	0.1 ±0.1	0.1±0.1	1.282±0.002
Stryker [®]	0.4 ±0.2	0.7±0.6	1.282±0.004
Merck [®]	0.4±0.4	0.4±0.5	1.284±0.002
Osteobond [®]	0.6±0.3	1.7±1.3	1.279±0.005
Mitvac [®]	0.7±0.2	1.0±1.7	1.266±0.025
Cemvac [®]	1.0±0.5	6.0±2.9	1.263±0.013
Control	1.2±0.2	95±23	1.193±0.008

Table 2.1 (b) Porosity results for Simplex P bone cement

Mixing System	Macropores ^a	Micropores ^b	Density (g/cm ³)
Optivac [®]	0.1 ±0.1	0.7 ±0.6	1.240±0.003
Stryker [®]	0.1 ±0.1	0.8 ±0.5	1.241±0.001
Osteobond [®]	0.4 ±0.3	3.4 ±4.4	1.232±0.015
Control	1.8 ±0.2	90 ±48	1.176±0.020

^a Number of pores/cm³

^b Number of pores/78.5mm²

James *et al.* (1993) investigated autopsy-retrieved cement mantles and revealed that average cement porosity at the stem/cement interface was 17% compared to 8% in the bulk cement—a significant difference in porosity. *In vitro* experiments using centrifuged cement were conducted to try and reduce interface porosity; however, no reduction in interface porosity resulted—the results were similar to the autopsy-retrieved specimens. A further set of experiments was conducted to observe the source of interfacial porosity: glass test tubes were used to mimic prostheses; interface porosity could be observed during insertion and curing of the cement. The majority of the pores formed immediately upon contact of the glass tube with the cement, more pores appeared when the cement temperature began to rise. Interfacial porosity was found to be present in all specimens in the study ranging from 16-50%, while bulk cement porosity ranged from 5-16%. The conclusion that can be drawn from this study is that the use of third generation mixing techniques will not reduce interfacial porosity.

2.5 Fatigue behaviour

2.5.1 Fatigue testing conditions

Direct comparisons of fatigue lifetimes from different studies are difficult to make because of differences in specimen geometry, preparation methods, fatigue loading modes, testing environment, and loading frequency.

In the last few years, studies have emerged in which a large number of different bone cement formulations are tested under identical conditions. For example Harper and Bonfield (2000) tested ten different bone cement formulations under identical conditions. The only potential problem in this study was that testing was done in air at room temperature.

Frequency of cyclic loading: Fatigue crack propagation in polymers is frequency dependent (Hertzberg and Manson, 1980). As frequency increases fatigue crack propagation rate decreases due to crack blunting caused by local hysteretic heating and the inhibition of molecular motion due to a shortened deformation time. Cheng *et al.* (1990) measured the temperature near the crack tip in PMMA during a fatigue test. Using an infrared microscope at room temperature, they showed a negligible change in temperature at the crack tip for a cyclic frequency of 10 Hz. Humpreys *et al.* (1989) investigated the effects of frequency on temperature rise in acrylic bone cement. Their experiment involved testing a prosthesis cemented in a femur; temperature was measured using thermocouples embedded in the cement mantle. Two frequencies were investigated; 1 Hz and 6 Hz. Their results concluded that a maximum temperature rise of 3.8°C occurred at 6 Hz when a force of 4.5 kN was applied to the head of the prostheses.

Johnson *et al.* (1989) determined the effect of frequency on the fatigue life of acrylic bone cement and concluded that fatigue life increased as test frequency increased, and testing at high frequencies would therefore lead to an overestimate of the fatigue life. Analysis of the results was limited to a comparison of Weibull distributions. Notably absent from this study were figures for the mean failure life and standard deviation. The plotted Weibull distributions for the different frequencies crossover and converge at a survival probability of 80% for the 1, 2, 5 Hz frequencies. In the case of the 5 Hz frequency, one specimen that had a significantly increased

fatigue life in comparison to the other specimens in the group caused the distribution to crossover the 10 Hz distribution at a probability of failure of 50%, and the 20 Hz distribution at a probability of failure of 90%, see Fig. 2.8.

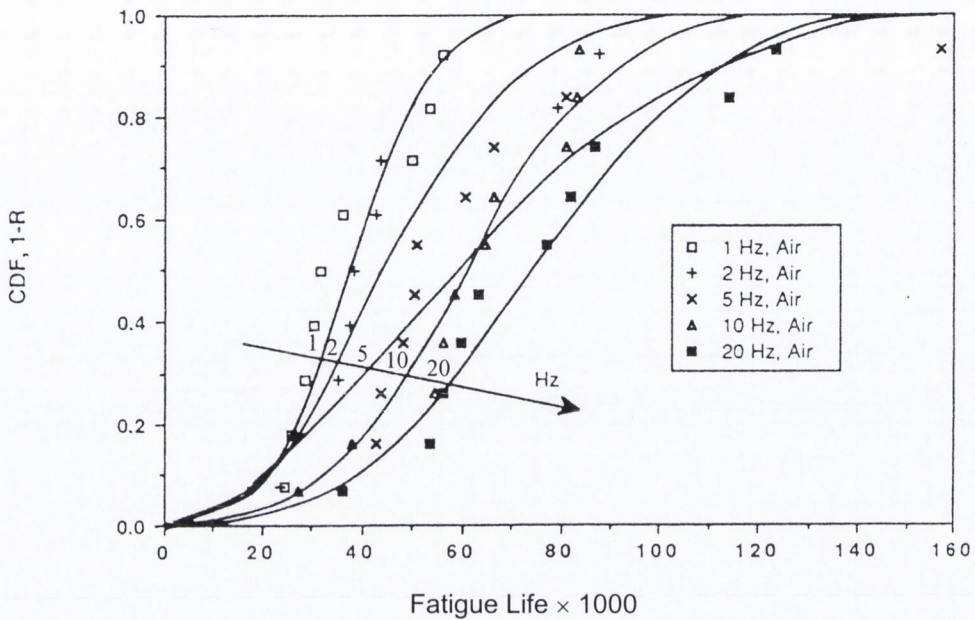


Figure 2.8 Weibull distributions from Johnson *et al.* (1989) showing that the 5 Hz distribution is wildly skewed because of one outlier.

A number of authors have compromised on accelerated testing and physiological conditions, by testing at 5 Hz (Molino and Topoleski, 1996, Rimnac *et al.*, 1986, Askew, *et al.*, 1994) and also at 10 Hz (Topoleski *et al.*, 1995, Krause *et al.*, 1988).

Environmental conditions: It is clearly desirable to evaluate the mechanical properties of acrylic bone cement in an environment as close to the *in vivo* condition as possible. Bone cement has been tested under different environmental conditions from air at room temperature, to saline solution, to water, to Ringer's solution all at 37°C. However, Johnson *et al.* (1989) proved that a considerable decrease in fatigue life (40%) exists when bone cement is tested in saline solution at 37°C compared to testing at room temperature in air. Most studies have adopted a fatigue test that is conducted at 37°C and in a water bath (James *et al.*, 1992, Davies *et al.*, 1987, Davies and Harris, 1992 and Carter *et al.*, 1982). Testing in saline solution is generally avoided because the NaCl causes corrosion of the testing grips, and moreover the corrosion products may influence the fatigue test.

Loading mode: The fatigue life of bone cement is highly dependent on the loading mode. Stress tests (load control) or strain tests (displacement control) can be implemented. Under strain control, the force on the specimen falls off due to creep and crack extension and thus the stress decreases as the test proceeds. In a stress controlled test the force on the specimen remains constant and does not fall off; therefore it is a more difficult test to pass. A compromise to testing in strain control is to load the specimen to an initial strain (maybe a physiological strain) and then run the test in load control (Davies *et al.*, 1987, and Burke *et al.*, 1984); this is simply an altered stress controlled fatigue test whereby the initial strain is known but the test is then run at the stress level which causes the initial strain. Even if bone cement can be considered as being under displacement control fatigue *in vivo*, testing under stress control will draw attention to weaker cements and is therefore to be preferred.

As bone cement is weakest in tension (Lewis, 1997), a fatigue test generally incorporates tension into its loading cycle.

2.5.2 Specimen preparation

Bone cement specimens are usually moulded in a polymer mould (Carter *et al.*, 1982, Krause *et al.*, 1988). Two distinct specimen geometries exist: flat “dog-bone” shaped specimens (Krause *et al.*, 1988, Fritsh, 1996) and cylindrical waisted specimens (Carter *et al.*, 1982, Davies and Harris 1990). Cylindrical specimens are machined after moulding to incorporate a reduced diameter within the gauge length and to aid gripping (Davies and Harris, 1990, Lewis, 1999). Machining of the gauge length may cause defects to appear on the surface of the sample (i.e. pore extremities) reducing the strength of the sample and thereby adding or perhaps increasing the variability of the measured fatigue strength. Dog-bone shaped specimens tend to be used in tensile loading tests, while cylindrical specimens are used in mechanical tests which involve a compressive load (Lewis, 1997).

Previous investigators have removed specimens containing large pores from their test group with the justification that these specimens were improperly made, although the conditions of specimen preparation used are comparable, or better, than those used in surgery. Some researchers have even gone as far as to propose a quantitative criteria for rejection of specimens with large pores (Cristofolini *et al.*, 2000) even though retrieval studies show they occur *in vivo*. This practice varies and

is not consistent between research groups or within individual groups (see Table 2.2). Therefore caution must be addressed in examining these results as this practice will lead to an overestimation of fatigue life. More importantly, the true variability of the fatigue results is will not be determined by such studies. The presence of large pores in cemented joint replacement is a natural consequence of the use of self polymerising PMMA and consequently should be accepted and evaluated in laboratory tests.

Table 2.2 *The removal of specimens with large pores is not consistent in the literature.*

Article	Pore Size
Johnson <i>et al.</i> , (1989)	> 500µm removed
Lewis and Mladsı (1998)	> 2 mm removed
Lewis and Austin (1994)	> 3 mm removed
Lewis (1999)	> 1 mm removed
Fritsh (1996)	No size stated but “large air inclusions” removed

Specimen storage: As bone cement absorbs water and its mechanical properties are affected by absorption of water, the pre-testing storage environment is important. Bone cement has been stored in Ringer’s solution (Soltész, 1994), saline solution (Verdonschot and Huiskes, 1994), and water (James *et al.*, 1992), all at 37°C. Davies *et al.* (1987) observed no deterioration in mechanical properties when stored in solution at 37°C for a time period of two weeks to two years. A general consensus for a recommended minimum storage time is between 1-7 days (Lewis, 1997), while ISO 5833 recommends a storage period of 48 hr. According to Kühn (2000) the glass transition temperature (T_g) reduces after storage in water at 37°C; therefore storage in water and testing in water at 37°C will accelerate the creep rate of bone cement and may have disastrous consequences if T_g reduces below body temperature.

2.5.3 Effect of additives and sterilisation method on fatigue properties

Fibres: The fatigue strength of PMMA bone cement is affected by additives. Pilliar *et al.* (1976) suggested the need for development of a tougher material (more fatigue resistant) and compared carbon fibre reinforced bone cement to normal bone cement. The Young’s modulus of the cement doubled from 2.76 GPa to 5.5 GPa and an increase in fatigue life also resulted. However, poor intrusion characteristics were

noted. Similarly, Topoleski *et al.* (1998) found a significant increase in fracture and fatigue resistance of a commercially available bone cement with the addition of short Ti fibres (200 μm). The use of fibres performed into a metal mesh and incorporated into a cement mantle improved the fatigue life of the cement mantle by a factor of 30 times (Taylor *et al.*, 1989). Even though clinical trials of this design did begin, no clinical results are available in the literature.

Radiopacifiers: The effect of the addition of a radiopaque filler was analysed by Molino and Topoleski (1996). Different fracture paths resulted for the radiopaque cement in comparison to radiolucent cement: in radiopaque cement cracks propagated through the interbead matrix, whereas in radiolucent cement cracks propagated through PMMA beads and the interbead matrix. Small pores (1 μm) were seen to form around BaSO_4 particles and it is likely that the interbead matrix was weakened by the radiopacifier. The crack propagation rate was lower for the radiopaque cement even though the interbead matrix was hypothesised to be weaker; this was probably due to the fact that the crack had a longer distance to travel as it propagated through the field of PMMA beads compared to the flat cracking in the translucent cement. James *et al.* (1992) and Bhambri *et al.* (1995) have shown that BaSO_4 particles can affect the crack initiation stage in bone cement. Both noted BaSO_4 particles acting as crack initiation sites—it is thought that they act in a similar way to voids/cracks in the cement mantle when associated in a “clump”.

Antibiotics: Antibiotic additives can decrease the fatigue strength of PMMA bone cement. Davies *et al.* (1989) showed a reduction in mean fatigue strength was associated with gentimacin in Palacos R bone cement. In the case of a low viscosity cement there was no statistically significant difference in fatigue life between Simplex P and its antibiotic impregnated counterpart. Klekamp *et al.* (1998) showed that fatigue life decreased with increasing amounts of Vancomycin P or Tobranycin.

Sterilisation: Lewis and Mladi (1998) showed that a statistically significant increase in fatigue strength was associated with ethylene oxide sterilised cement compared to cement sterilised by gamma irradiation. It is known that ethylene oxide sterilisation of the powder component produces a cement with higher molecular weight compared

to gamma irradiated cement (Kühn, 2000) and fatigue crack propagation in PMMA is directly proportional to molecular weight (Hertzberg and Manson, 1980).

2.5.4 Effect of mixing method on fatigue life

Mixing technique severely affects the fatigue strength of acrylic bone cement, as the majority of pores are attributable to the mixing process. Two prominent mixing techniques have emerged as third generation cementing techniques: vacuum-mixing and centrifugation post mixing.

Wixson *et al.* (1987) carried out fatigue tests on vacuum-mixed and hand-mixed specimens and found a 7.5 fold increase in fatigue strength for the vacuum-mixed specimens at 20 MPa, 25 MPa, and 30 MPa. The superior fatigue strength was attributed to the reduction in large and small pores caused by vacuum-mixing. Linden (1989) compared vacuum-mixed and hand-mixed cement in four-point bending and found that a combination of vacuum (custom system) and mechanical mixing significantly increased ($p < 0.01$) the fatigue life of CMW, Simplex P, and Zimmer LVC bone cement in comparison to hand-mixing.

Davies and Harris (1990) investigated three commercial vacuum-mixing systems and their effect on fatigue life. The three systems were the Mitab system, Mixevac II and the Enhancement Mixer; these systems were compared to centrifuged and hand-mixed cement. Fatigue tests were conducted on Simplex P bone cement at 2 Hz, at ± 15 MPa and in water at 37°C. The main results are:

- (i) The average fatigue strength increased 2-5 times the hand-mixed value for the three mixing techniques (see Fig. 2.9),
- (ii) No statistically significant increase in fatigue strength was noted for the three vacuum-mixing systems compared to hand-mixing.
- (iii) The vacuum-mixed test groups produced some specimens that were extremely strong and others that were extremely weak; this result correlated to x-rays taken of the specimens, some specimens had substantial pores, while others were pore-free.
- (iv) The fatigue results were improved when two packs of cement were used (see Fig. 2.9), this resulted in a further increase in mean fatigue strength and a statistically significant difference ($p < 0.05$) between the hand-mixed and the vacuum-mixed mixed cements. Vacuum-mixing

still produced some extremely weak specimens; in the most extreme case the range of the Enhancement Mixer was from 30 cycles to 139,200 cycles, resulting in an extremely non-consistent cement mix.

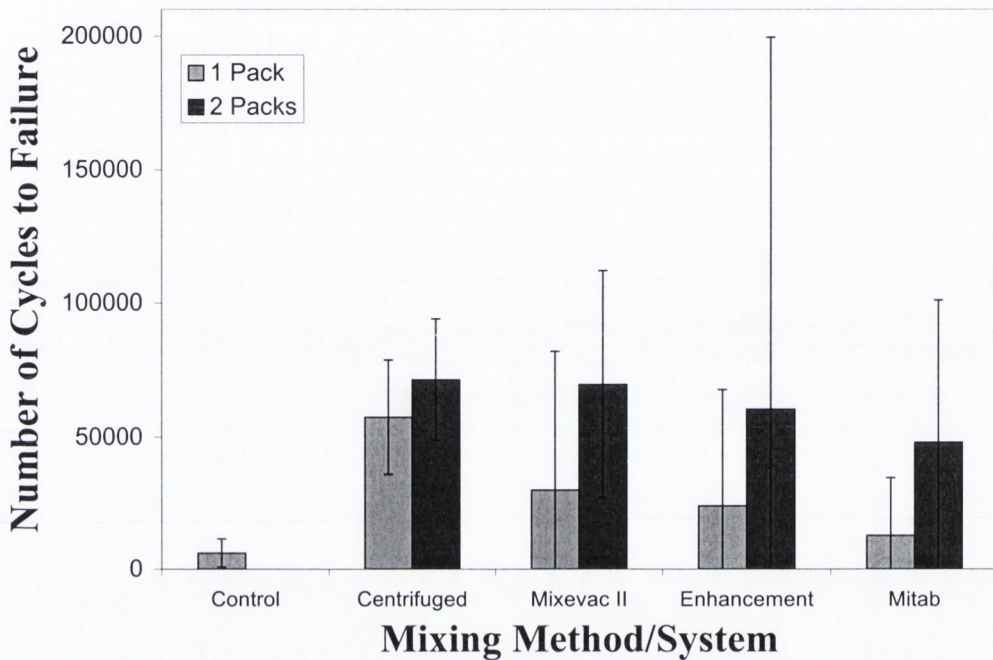


Figure 2.9 *Fatigue Results from Davies and Harris (1990) showing that vacuum-mixing and centrifugation increased the mean fatigue life; however, the large variation of fatigue strength for the vacuum-mixed specimens does not cause a significant increase in fatigue strength compared to hand-mixed cement (one cement pack).*

Fritsh *et al.* (1996a) investigated the fatigue properties of high viscosity bone cement mixed using a “custom-made” vacuum-mixing device for one test series and the Draenert system for the second vacuum-mixing series. Fatigue tests were conducted on Palacos R bone cement at 25 Hz and in 0.9% saline solution at room temperature. Surprisingly no significant increase in fatigue strength was observed compared to hand-mixed cement. Fatigue stability (i.e. the fatigue limit) quoted for the three mixing techniques is similar. However, in all three cases some experimental data falls below the quoted fatigue limit, which is rather strange. Moreover, the test must be questioned as specimens with large pores were removed from the test group.

The effect of vacuum-mixing of Palacos R bone cement was also investigated by Lewis (1999) using the Simplex Enhancement vacuum-mixing system. Fatigue tests were carried out at 15 MPa at a frequency of 2 Hz on hand-mixed cement with

components chilled to 4°C or 21°C and similarly for vacuum-mixed cement. No statement is made on the environmental test conditions. Specimens with pores greater than 1 mm in diameter were excluded. The results showed a significant ($p < 0.05$) increase in fatigue life of the vacuum-mixed cement, see Table 2.3. Furthermore vacuum-mixed cement showed a reduction in variation in fatigue results. The two studies use the same cement and mixing method; however they have contradictory results due to different testing methods and specimen preparation methods.

Table 2.3 *Fatigue results of Palacos R bone cement from Lewis (1999), vacuum-mixing increases mean fatigue life by over 50%.*

	Hand-mixed 21°C	Hand-mixed 4°C	Vacuum-mixed 21°C	Vacuum-mixed 4°C
Average	53219	54570	130749	132157
SD	17967	18968	36974	39275
SD as % of Av	34%	35%	28%	30%

In a further study by Lewis (1999a) the effect of vacuum-mixing Osteopal bone cement (a low viscosity cement) was measured using the same methods as Lewis (1999). A five-fold increase in fatigue strength was found, with a highly statistically significant increase ($p < 0.001$) in fatigue life of vacuum-mixed Osteopal compared to hand-mixed Osteopal, see Table 2.4. These results can be compared to the results of the previous study by Lewis (1999) where no statistical difference is noted between Osteopal hand-mixed versus Palacos R hand-mixed; however, a notable increase in strength is observed for vacuum-mixed Osteopal compared to any other formulation.

Table 2.4 *Fatigue results for Osteopal bone cement from Lewis (1999a); there is an increase of approximately ten times the hand-mixed value compared to only double the strength for the high viscosity Palacos R cement, see Table 2.3.*

	Hand-mixed 21°C	Vacuum-mixed 21°C
Average	172,429	1,028,836
SD	272,244	238,318
SD as % of Av.	158%	23%

Lewis and Austin (1994) investigated the fatigue strength of vacuum-mixed low viscosity cement (CMW 3). The cement was vacuum-mixed in the Enhancement Mixer and the specimens were stored in Ringer's solution for seven days. Fatigue tests were performed in fully reversed tension-compression loading at 6 stress levels (± 5 MPa, ± 10 MPa, ± 15 MPa, ± 20 MPa, ± 25 MPa, and ± 30 MPa) at a frequency of 2 Hz. Specimens with pores greater than 3 mm were removed from the study. Fatigue failure within two million cycles did not occur in any of the specimens tested at ± 5 MPa. The fatigue results were fitted to an Olgive curve and the estimated endurance limit was 8.1 MPa (see Fig. 2.10); however, the data trend would estimate that the fatigue life at ± 5 MPa would be in the range of 3-5 million cycles. A three-parameter Weibull distribution was fitted to the data and guaranteed fatigue lives are quoted for five stress levels. Plotting the guaranteed fatigue life against stress amplitude indicates that the fatigue limit is not 8.1 MPa as the Olgive curve fit would imply, see Fig. 2.11. The minimum predicted fatigue life at 5 MPa is approximately 200,000 cycles if the trend-line is extrapolated to lower stresses; this trend surely indicates that fatigue failure will occur below 8.1 MPa.

A conclusion can be drawn from the above studies that the effect of vacuum-mixing is greatest on low viscosity cements: CMW 3, Simplex P, and Osteopal, while in the case of high viscosity cements like, Palacos R, fatigue life does not increase substantially with vacuum-mixing.

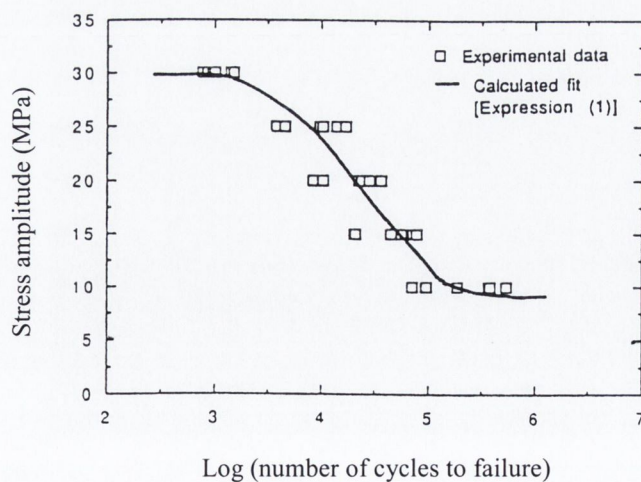


Figure 2.10 Uniaxial fully reversed tension-compression fatigue test results, fitted to an Olgive curve. (Lewis and Austin, 1994).

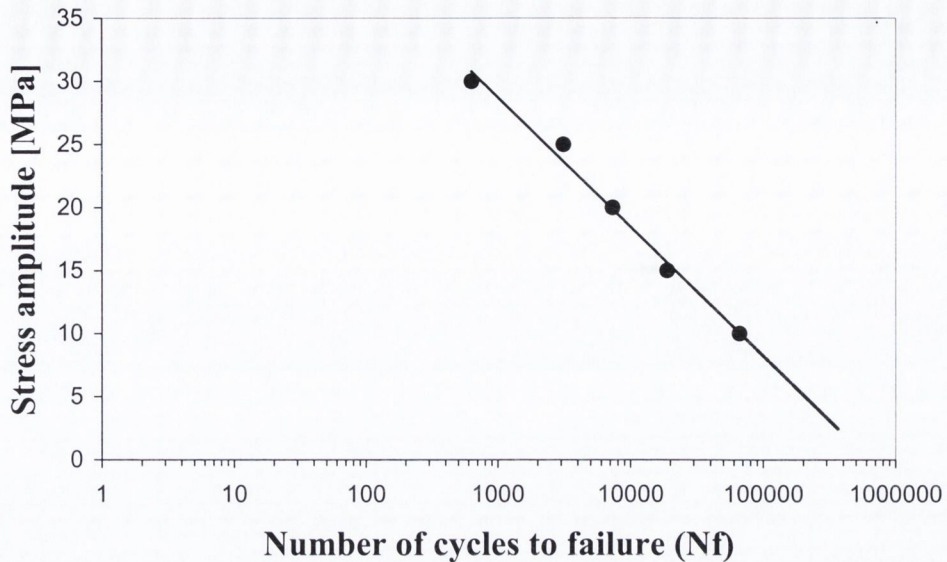


Figure 2.11 Guaranteed fatigue life (estimated from the three-parameter Weibull distribution) plotted against stress amplitude, from Lewis and Austin (1994).

2.6 Review of methods for analysis of results

S-N Curves: Reporting of fatigue results usually comes in the form of a typical stress/strain versus number of cycles to failure curve (S-N Curve). Regression lines are fitted to the complete data set so a trend within the data can be observed and correlation coefficients are normally quoted for the data (Davies *et al.*, 1987). The association of fatigue data is generally quite low, whereby low correlation coefficients are associated with bone cement fatigue results (Burke *et al.*, 1984). A particular curve fitted to S-N data is the Olgive type curve (Krause *et al.*, 1988a), which takes the form:

$$\sigma(N_f) = A + \frac{B - A}{1 + (\log(N_f) / C)^D}, \quad \text{Eqn. 2.1}$$

where A , B , C , and D are material constants whose values may be obtained using non-linear regression of the σ/N_f data. B is the upper asymptote of the curve and A is the lower asymptote of the curve, i.e. the fatigue limit of the material. This type of curve fitting could prove quite controversial as bone cement can be described as having an undefined fatigue limit due to the random distribution of pores within the material (Huiskes, 1993a). In a study by Lewis and Austin (1994) an Olgive curve predicted

the fatigue limit of CMW 3 bone cement as 8.1 MPa; however the trend of the data indicates that at 5 MPa failure would occur at approximately 3-5 million cycles, see Fig. 2.10.

Weibull Analysis: As the variability in fatigue results is high in bone cement, a statistical distribution is usually chosen to model the variability. The two-parameter Weibull distribution is a useful statistical tool for reporting the probability of survival/failure of the material at a certain number of cycles to failure. A full description is given in Chapter 3. The Weibull distribution is a positively skewed distribution ranging from zero to a positive value; unlike the normal distribution negative numbers are not allowed. Johnson *et al.*, (1989) found that, out of eight statistical distributions, the two-parameter Weibull distribution best fitted the fatigue results of acrylic bone cement. Many researchers perform this analysis on their data (Burke *et al.*, 1984, Gates *et al.*, 1983, Lewis, 1997).

The three-parameter Weibull distribution is also used to model the distribution of fatigue results and a “guaranteed fatigue life” can be quoted when this method is used (Lewis, 1997). The equation of the three-parameter distribution is given as:

$$P_s = \exp \left[- \left(\frac{(N_f - N_o)}{(N_a - N_o)} \right)^b \right], \quad \text{Eqn. 2.2}$$

where N_o is the guaranteed fatigue life, N_a is the characteristic fatigue life (or location parameter), b is the shape parameter, P_s is the probability of survival, and N_f is the number of cycles to failure. The parameters b and N_a are determined using a least squares regression analysis to the linearised form of the three-parameter Weibull distribution. The linearised form of Eqn. 2.2 is given as:

$$\ln(\ln(-P_s)) = b \ln(N_f - N_o) - b \ln(N_a - N_o), \quad \text{Eqn. 2.3}$$

where:

$$P_s = 1 - \left(\frac{Y - n}{M - n - m + 1} \right), \quad \text{Eqn. 2.4}$$

Y being the failure order number of the specimen in a set of M test specimens; $Y=1$ is the specimen with the shortest fatigue life and $Y=M$ is the specimen with the longest fatigue life, and n and $m = 0.3$.

The guaranteed fatigue life is estimated from a plot of $\ln(\ln(-P_s))$ versus $\ln(N_f)$ and is given as the y-asymptote of a curve fitted to the data, see Fig. 2.12. Lewis and Austin (1994) suggested the guaranteed fatigue life could be used as a design parameter, also it has been described as the minimal fatigue life at a certain stress level (Lewis, 1997); however, specimens with large pores are removed from their tests and thus the variation in fatigue strength is underestimated, and consequently specimens will have a lower fatigue life than the so-called “guaranteed fatigue life”. Therefore the use of the two-parameter Weibull distribution where N_o is set to zero is a better option for bone cement, as it does not assume a guaranteed fatigue life, which might be incorrect when large variation in fatigue strength is present.

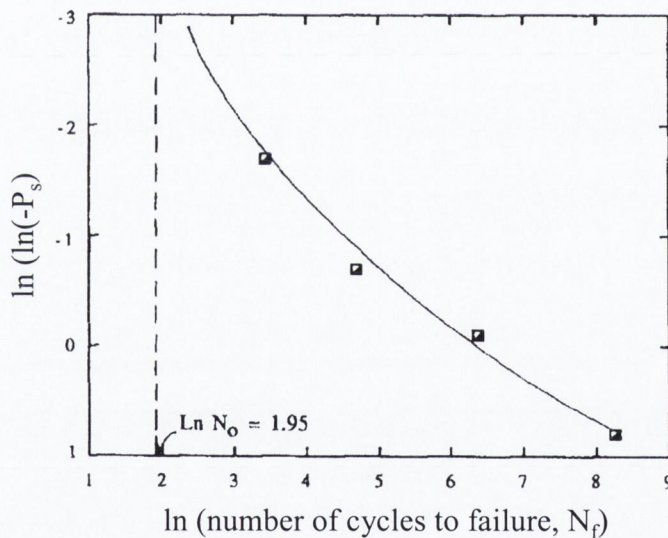


Figure 2.12 An estimation of the guaranteed fatigue life for acrylic bone cement, adapted from Lewis and Mladi (1998)

2.7 Fatigue damage accumulation in bone cement

2.7.1 Fatigue observations *in vivo*

A number of studies have shown that fatigue damage accumulation must occur in bone cement *in vivo*. In the study by Jasty *et al.* (1991) of cement mantles retrieved post-mortem (*i.e.* cement mantles that have performed successfully over their required life), microcracking was present in all specimens implanted for more than three years;

the presence of striations on the fracture surfaces confirmed that microcracking was due to fatigue. It was noted that specimens less than 10 years old had small incomplete fractures, while specimens greater than 10 years had complete through-mantle fractures. A similar fractographic study by Topoleski *et al.* (1990) considered failed cement mantles and found that fatigue cracking was present in all specimens, as were a number of through-mantle cracks. They also observed wear of crack surfaces including one specimen that was known to have had cement failure for at least three years prior to revision. Culleton *et al.* (1993) corroborated these findings, in an examination of a revision retrieved cement mantle; complete failure of the cement mantle at a large pore was noted. Furthermore fatigue was suspected as the main failure mechanism due to evidence of fatigue cracking in the form of striations on one of the fracture surfaces. In the studies by Topoleski *et al.* (1990) and Culleton *et al.* (1993) PMMA particulate debris must have been generated as the presence of wear patterns on cement crack surfaces was evident in both studies. Gelb *et al.* (1994) showed that an inflammatory response occurred when small (<20 μ m) irregularly shaped particles of PMMA bone cement were implanted into air pouches in rats; these particles are of the order of particle size associated with wear debris *in vivo*. In all three studies (Jasty *et al.*, 1991, Topoleski *et al.* 1990, Culleton *et al.* 1993), pores in the bulk cement mantle had a clear influence on damage accumulation by acting as crack initiation sites or by allowing microcracks to coalesce to form larger catastrophic cracks.

2.7.2 Damage accumulation – experimental

The phenomenon of damage can be described as the continuous accumulation of irreversible discontinuities (in the form of microcracks) within a structure. A material can be considered to be in an undamaged state ($D = 0$) at time zero. After a certain load history, damage within the structure evolves, eventually leading to failure ($D = 1$). Damage accumulation in acrylic bone cement has been shown to take the form of continuous growth of microcracks *and* increase in the number of microcracks over the lifetime of a hip replacement (McCormack and Prendergast, 1999); this process was aptly described as “a gathering storm of microcracks” by Dr. Brendan McCormack (1997) in his PhD thesis. Considerable clinical evidence of this phenomenon exists, and a number of research groups have simulated damage

accumulation (Verdonschot and Huiskes, 1997) and experimentally observed damage accumulation (McCormack and Prendergast, 1999). As yet, however, a precise relationship between stress level and damage accumulation rate has not been determined.

Topoleski *et al.* (1993) proposed that the fatigue crack damage zone in PMMA bone cement is expanded due to the presence of pores, see Fig. 2.13. McCormack and Prendergast (1999) confirmed that the entire cement mantle is the damage zone; microcracks were observed to propagate in every zone within the cement mantle; at the bone-cement interface, stem-cement interface and within the bulk cement mantle. In their study of the femoral reconstruction the majority of the cracks (approximately 90%) initiated from pores within the bulk cement mantle, rather than at the interfaces. Microcracks initiated continuously until the test was stopped at 5 million cycles; the rate at which new cracks initiated slowed down as the test approached 5 million cycles, presumably the number of crack initiation sites ran out. The dominant role of pores in the crack initiation stage was noted, and it was thought that factors such as pore size and pore location would influence the damage accumulation process.

In a separate study by McCormack *et al.* (1999a) torsional loads were applied to a bone cement mantle and rather than pores in the bulk cement mantle acting as the main crack initiation sites, instead pores on the stem-cement interface acted as the crack initiation sites for the majority of cracks and occasionally cracks grew from the sharp corners of the stem cross section. This was explained in terms of the stress concentration ahead of a bimaterial interface crack, see McCormack and Prendergast (1996).

2.7.3 Damage accumulation – computational

Verdonschot and Huiskes (1997) analysed the damage accumulation failure scenario with a combination of finite element analysis and continuum damage mechanics. The effect of prosthesis debonding on damage accumulation in the cement mantle was investigated. When an unbonded stem-cement interface was modelled, stresses within the cement mantle increased by a factor of 2-3, resulting in a damage rate that was approximately four times higher compared to the case with the bonded stem-cement interface. In these analyses, Miner's law (i.e. a linear damage accumulation rate, see Fig. 2.14) was used to describe the damage accumulation rate. Similarly, when

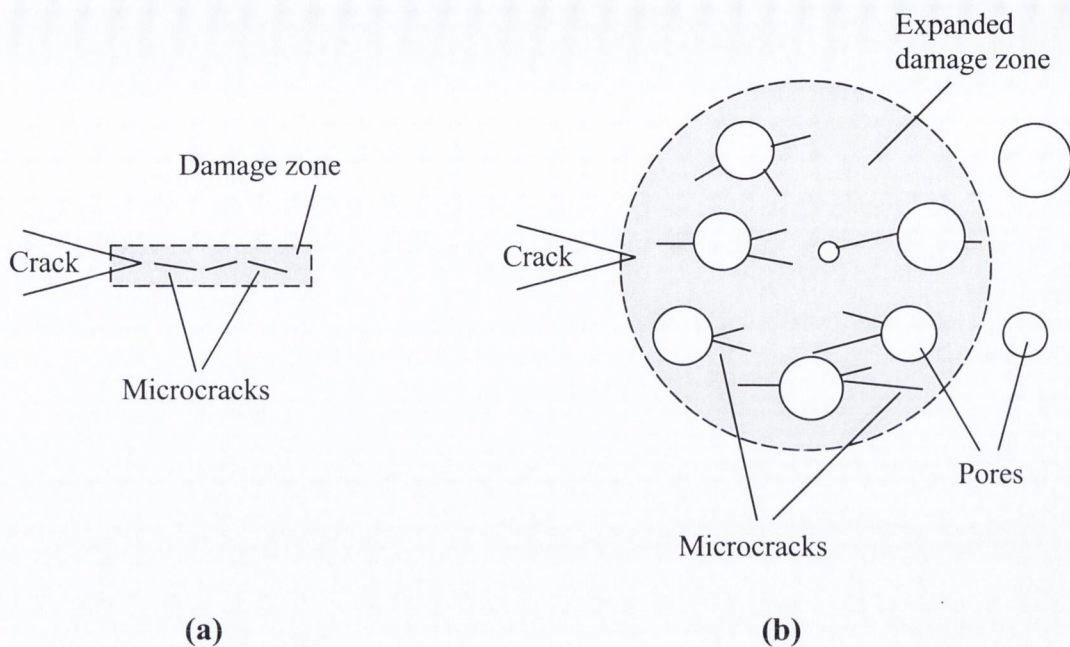


Figure 2.13 A schematic of the suggested model of expansion of the fatigue crack damage zone in the presence of the porosity phase in the vicinity of the crack tip. (a) The damage zone through areas of PMMA where there are no pores is relatively linear. (b) When pores are in the vicinity of the crack tip, they expand the damage zone by acting as nucleation sites for microcracks. (Topoleski *et al.* 1993). This model was confirmed by McCormack and Prendergast (1999).

degraded bone was modelled (a decrease in stiffness of the layer adjacent to the cement mantle) stresses increased in the cement mantle and the damage accumulation rate increased considerably; this was only predicted in the unbonded case whereas in the bonded case no difference was predicted. The results of this study were replicated for the Lubinus SP II femoral stem by Stolk *et al.* (2000) where debonded cement stems produced a higher damage accumulation rate compared to bonded stems; again a linear relationship between damage rate and time was used to characterise the rate of damage accumulation. The relationship used between stress and number of cycles to failure was taken from Davies *et al.*, (1987) and does not account for the size of the cement mantle.

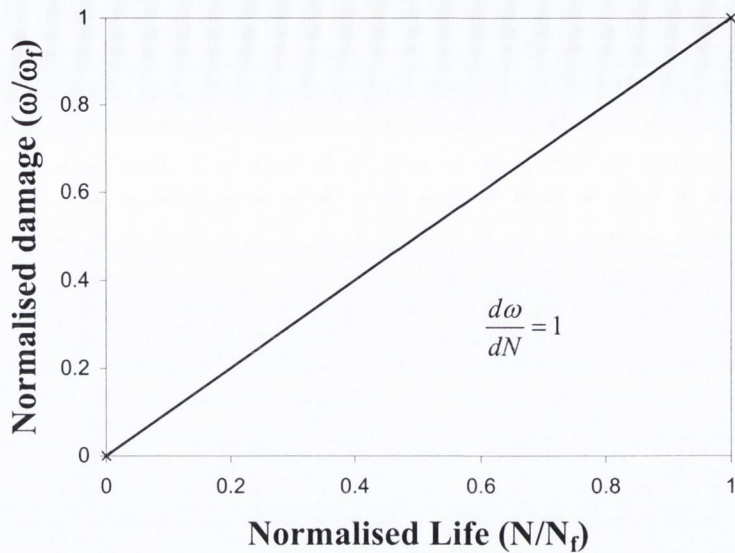


Figure 2.14 Miner's Law showing that damage accumulation is linear and the rate of damage accumulation is equal to one.

2.8 Multiaxial fatigue

Bone cement is subjected to multiaxial loading conditions *in vivo* (Prendergast *et al.*, 1989, Harrigan *et al.*, 1992). Failure due to multiaxial loading has been observed in the form of secondary cracks propagating in the plane perpendicular to the main crack (Topoleski *et al.*, 1990). However, there are no reports of investigations into the behaviour of bone cement under multiaxial fatigue conditions in the literature.

Leevers *et al.* (1979) investigated the effect of a biaxial stress state on fatigue crack growth in industrial PMMA. Centrally-notched plates of PMMA were subjected to biaxial stress states; the notch was perpendicular to one of the principal stresses. PMMA showed a reduction in crack growth rate with increasing stress biaxiality; it was suggested that the decrease in fatigue crack growth rate was due to crack closure caused by the tensile stress parallel to the fatigue crack.

One previous paper on the subject of multiaxial loading of PMMA bone cement involves static tests on cylindrical specimens subjected to an internal pressure and axial compression; specimens failed from the tensile hoop stress rather than the axial compressive force (Silvestre *et al.*, 1990). The experimental set-up was successful in applying a multiaxial stress state to acrylic bone cement; in this thesis a modified version of this set-up will be used to apply a multiaxial cyclic load to bone cement.

2.9 Creep properties

Creep can be defined as a time-dependent strain occurring under a stress which is less than the yield stress. Creep of polymers increases significantly when the working temperature is above one third of the glass transition temperature (T_g). The glass transition temperature of acrylic bone cement is approximately 90-110°C (Kühn, 2000) and it has been shown to decrease by about 20°C after absorption of water. Therefore, since the working temperature of bone cement is 37°C significant creep may be expected.

Perkins *et al.* (1989) showed that, under constant load, the creep rate is higher by a factor of 3 at 37°C compared to 20°C. While comparing Palacos R and Zimmer Regular bone cements, Norman *et al.* (1995) showed that vacuum-mixed cement had a lower creep rate than hand-mixed cement, see Fig. 2.15. Decreased creep in the vacuum-mixed specimens corresponded to decreased porosity. Creep tests in this study were conducted at 20°C if testing had been carried out at higher temperatures presumably the amount of creep would have increased approximately three-fold as Perkins *et al.* (1989) found.

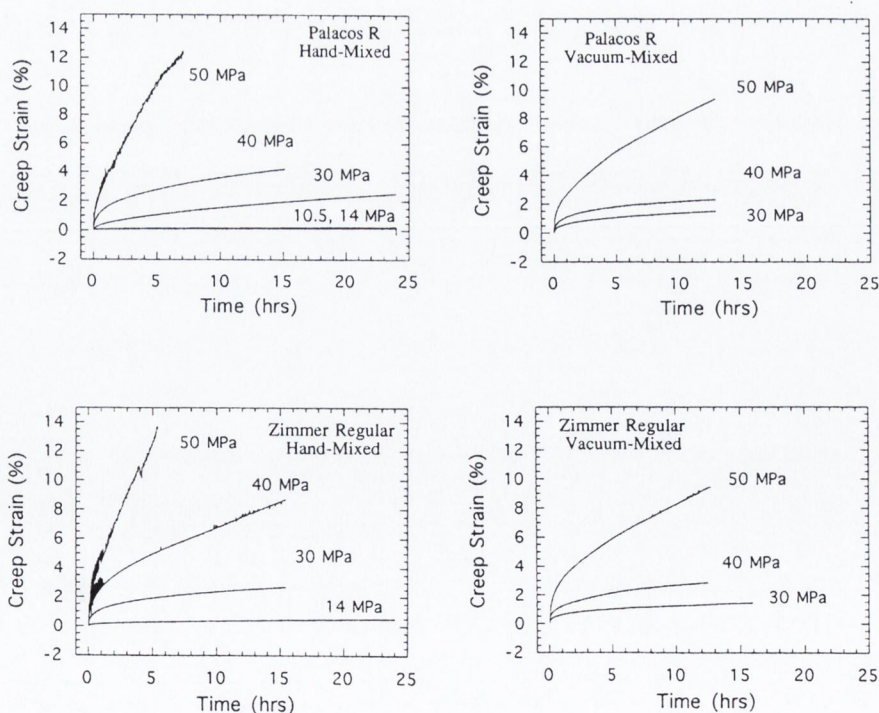


Figure 2.15 Typical creep strain curves for hand-mixed and vacuum-mixed Palacos R and Zimmer Regular bone cements at 20°C. The vacuum-mixed specimens showed reduced creep compared to hand-mixed specimens. (Norman *et al.*, 1995)

Chwirut (1984) investigated long-term compressive creep in acrylic bone cement and found that significant creep occurs in acrylic bone cement at 37°C in saline solution under stresses representing a worst case *in vivo* condition. Microcracks were found in tested specimens, with cracks originating at pores, and in the fractograph shown in the paper the propagation direction appeared to be random. Moreover, Chwirut (1984) found that carbon fibre reinforced cement exhibited the least amount of creep, which was a similar result to Pal and Saha (1982), who showed carbon fibre reinforcement reduced the creep strain by up to 45%.

Dynamic creep of acrylic bone cement (i.e. creep during cyclic loading) was measured under cyclic tension (Verdonschot and Huiskes, 1994) and under compression loads (Verdonschot and Huiskes, 1995). The creep curves were of a similar shape to the static creep curves of previous studies. A linear relationship was found between the logarithmic values of the number of loading cycles and the logarithmic values of creep strain; the creep rate was found to be 5-10 times greater under tension compared to compression for Simplex P bone cement. Verdonschot and Huiskes (2000) tested Cemex Rx bone cement under cyclic compression and found that the creep rate was 30% higher for Cemex Rx compared to Simplex P.

2.10 Summary

The literature points clearly to fatigue damage accumulation as the central mechanism of failure in cemented joint replacements. Porosity has been shown to have a significant role in promoting damage accumulation and accelerating failure. The use of second and third-generation cementing techniques reduces cement porosity and thereby improves the probability-of-survival for joint replacements. The literature suggests some form of early *in vivo* failure associated with vacuum-mixing, however this has not been explained in any experimental study to date.

The experimental studies and clinical retrievals have identified porosity as a key determinate of the damage accumulation failure scenario. One question in the literature remains unanswered: What is the interaction between stress level and porosity on the damage accumulation rate? Is reducing the stress only of minor importance compared to a reduction of porosity? Secondly the use of a linear damage

accumulation rate (Miner's Law) has never been validated for computer simulation of cement damage accumulation. Finally, no study has ever shown the effect of a multiaxial stress state on acrylic bone cement.

Further experimental investigations are therefore needed to more rigorously establish the fatigue behaviour of orthopaedic bone cement. The data that these experiments produce can be implemented in computer simulations to improve the prediction of failure in cemented joint replacements.

This literature survey has highlighted several factors that should be adhered to when fatigue testing bone cement; foremost acrylic bone cement should be tested at 37°C, firstly, to ensure the *in vivo* fatigue strength is not underestimated, and secondly if a cement is prone to creep damage it would be missed if testing was conducted at room temperature. The practice of removing specimens with large pores is not a good one as they are inevitable in surgical practice and should be accepted and evaluated in laboratory tests. The variation in fatigue life is significant and the need for correct methods to analyse it are evident. The assumption of a fatigue limit should not be used for bone cement because of the material's inconsistent nature.

Chapter 3

Materials and Methods

3.1 Introduction	43
3.2 Cement type	43
3.3 Cement mixing methods	44
3.3.1 Hand-mixing	44
3.3.2 Vacuum-mixing	45
3.4 Specimen/mould design	46
3.4.1 Macroscopic fatigue study: specimen and mould design	46
3.4.2 Mould design for the fatigue damage accumulation specimens	48
3.4.3 Mould design for multiaxial specimens	48
3.5 Design of testing rigs	52
3.5.1 Uniaxial fatigue test rig	53
3.5.2 Multiaxial fatigue test rig	53
3.6 Experimental protocols	57
3.6.1 Moulding procedure	57
3.6.2 Pre-test procedure	58
3.6.3 Fatigue test conditions	59
3.6.4 Data logging	59
3.6.5 Crack analysis	61
3.7 Statistical analysis	61

3.1 Introduction

In this Chapter the design of three experimental tests is presented. The objective is that the experimental results will unearth answers to the questions posed in Chapter one. The three experimental test series were as follows; the first and second test series consisted of uniaxial tensile fatigue tests carried out on “dog-bone” shaped specimens and the third test series involved testing tubular specimens of bone cement under a multiaxial stress state. In the first study, vacuum-mixing was compared to *baseline* hand-mixing using small dog-bone shaped specimens, while the damage accumulation study used larger dog-bone specimens, although the same grips and moulding methods were used in both studies. The final experimental test series was designed to observe the effect of multiaxial stresses on the fatigue strength of acrylic bone cement, whereby tubular specimens were pressurised and simultaneously tested in tension. This Chapter begins by describing the cement and mixing methods used in this study, and then proceeds to describe the design of the specimens, moulds, and testing rigs, and then concludes by describing the experimental protocols.

3.2 Cement type

Two cement types were used in this study; (i), a radiopaque Cemex Rx (Tecres, Verona, Italy) bone cement and (ii) a translucent Cemex cement. The only difference between the compositions of these two cements was the absence of a radiopaque filler within the powder component of the translucent cement. The absence of a radiopaque filler resulted in an increase in pre-polymerised PMMA and benzoyl peroxide; this ensured the same liquid to powder ratio remained, see Table 3.1. Cemex bone cement has a powder-to-liquid ratio of 3:1 and the maximum polymerisation temperature is quoted as 55°C (www.tecres.it). The liquid is sterilized by means of filtration and the powder by means of ethylene oxide treatment.

Table 3.1 Composition of the powder and liquid components of the bone cement used in this study. The monomer component is the same in both cements

40g of sterile powder	Radiopaque Cement	Translucent Cement	13.3g of sterile liquid Monomer	
Polymethylmethacrylate	88.27%	97%	Methylmethacrylate	99.10%
Barium Sulphate	9.00%	—	N-N dimethyl-p-toluidine	0.90%
Benzoyl Peroxide	2.73%	3.00%	Hydroquinone	75 ppm

3.3 Cement mixing methods

The handling and mixing properties are affected by ambient temperature, as temperature increases time-to-setting decreases; all cement was mixed at approximately 22°C which resulted in a setting time of approximately nine minutes, see Fig. 3.1.

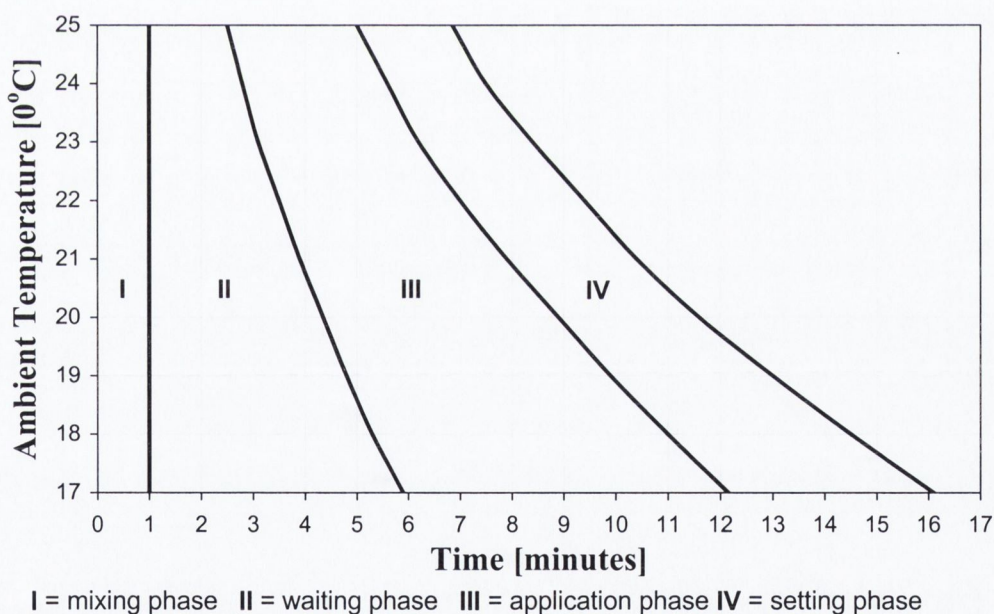


Figure 3.1 Working curves for Cemex bone cement for different ambient temperatures (adapted from Kühn, 2000)

3.3.1 Hand-mixing

Hand-mixing was carried out in a mixing bowl at atmospheric pressure. The liquid monomer was added to the mixing bowl followed by the powder. The liquid monomer and powder were mixed with a sterile spatula for approximately 60 seconds at one

beat per second. Once a doughy state was reached, the cement was transferred into a cement syringe and allowed to rest for 30-60 seconds. The cement was then injected into the appropriate mould. Figure 3.2 illustrates a schematic of the mixing process.

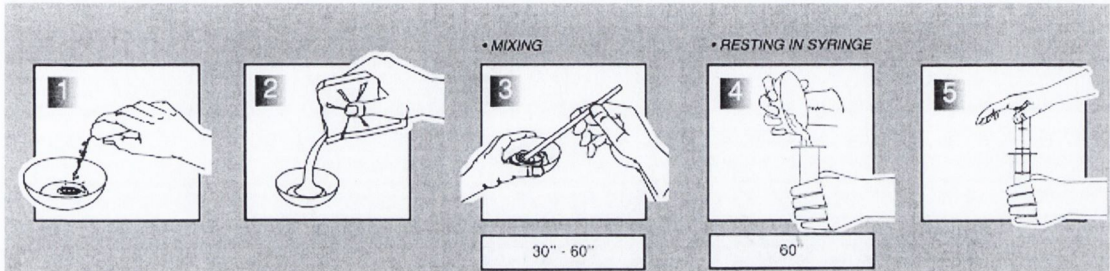


Figure 3.2 *Hand-mixing schematic*

3.3.2 Vacuum-mixing

Vacuum-mixed specimens were prepared using the Optivac[®] system (Scandimed A.B., Sjöbo, Sweden). The following procedure was followed: the cement constituents (PMMA powder and the liquid monomer) were added to the Optivac cartridge (see Fig. 3.3). Next the cartridge was sealed and the vacuum applied to the chamber for 10 seconds—to allow complete air evacuation. The cement was then mixed for one minute at a consistent rate and collected at the top of the chamber before the vacuum was released. After a 30-60 second resting period the cement was injected into the mould— injection was carried out only after the cement formed a meniscus in the syringe (personal communication, F. Robbotti, Tecres, Verona, Italy).

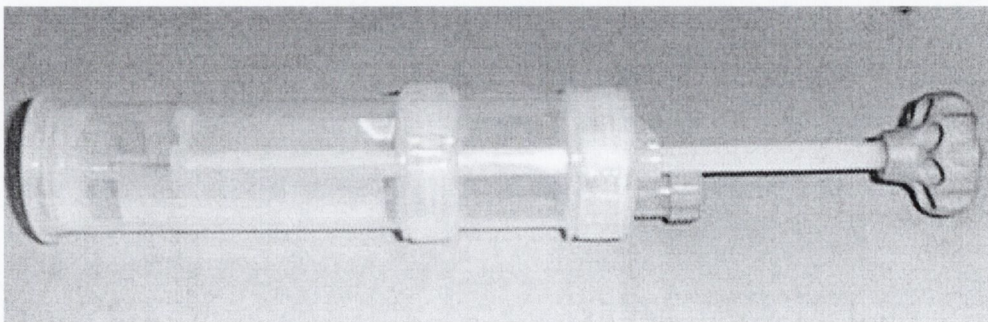


Figure 3.3 *Optivac Vacuum-mixing cartridge*

3.4 Specimen/mould design

A number of factors influenced the methods of specimen design for this project:

- (i) All specimens had to be produced from moulds where no machining of the cured specimen would take place. This constraint was placed on specimen design as previous studies have reported specimen breakages due to machining (Carter *et al.*, 1982).
- (ii) All fatigue testing was carried out in zero-to-tension because bone cement is weakest in tension (Krause and Mathis, 1988) – a tensile load would provide the worst-case loading situation.

In this thesis, three designs of PMMA specimens were used; a smaller one to determine S/N behaviour and a larger one for a study of damage accumulation, and a tubular specimen to determine the effect of off-axis stress on the fatigue life of acrylic bone cement.

3.4.1 Macroscopic fatigue study: specimen and mould design

The specimen used in this test series was rectangular in cross section and dog-bone shaped. The dimensions of the specimen are given in Fig. 3.4. A thickness of 3.5 mm was chosen as it represents the approximate thickness of a cement mantle *in vivo* (Petty, 1991). Large tab ends are present on the specimen to aid gripping; alignment holes were drilled into the tab ends of the specimen so that the specimen could be aligned with the uniaxial load in the materials testing machine.

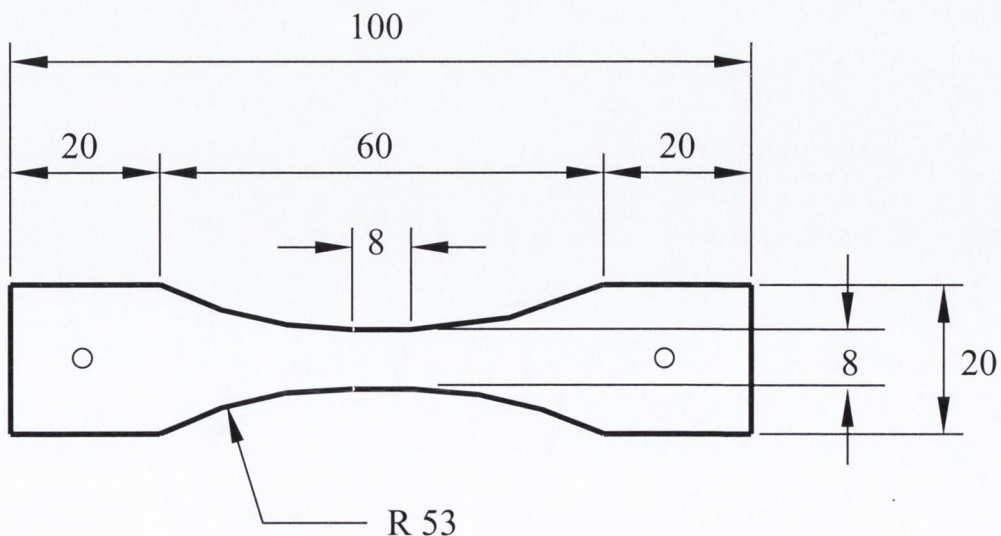


Figure 3.4 Dimensioned drawing of moulded specimen. All dimensions are in millimetres.

The first design of the mould was a three-part aluminium mould, consisting of two external plates, and one internal plate that had the specimen profile machined from it. However, the specimens produced from this mould had rough edges and were troublesome to remove from the mould. Preliminary fatigue tests showed that these specimens tended to fail from stress concentrations caused by moulding defects. In order to remove the defects caused by moulding the mould material and machining method was changed to a mould consisting of two aluminium external plates, two polyethylene internal plates, and one polyethylene central plate: the central plate had the profile of three specimens machined from it, see Fig. 3.5 for an exploded view of the mould (excluding the aluminium plates). Three specimens were produced from one package of Tecres cement. The specimen profiles were machined into the central polyethylene plate using a slow feed CNC program to achieve a smooth finish on the polyethylene surface. The mould was sealed using eight bolts while pressure relief holes allowed the excess cement to escape. The three polyethylene plates made up the main part of the mould while the two aluminium plates were used for rigidity.

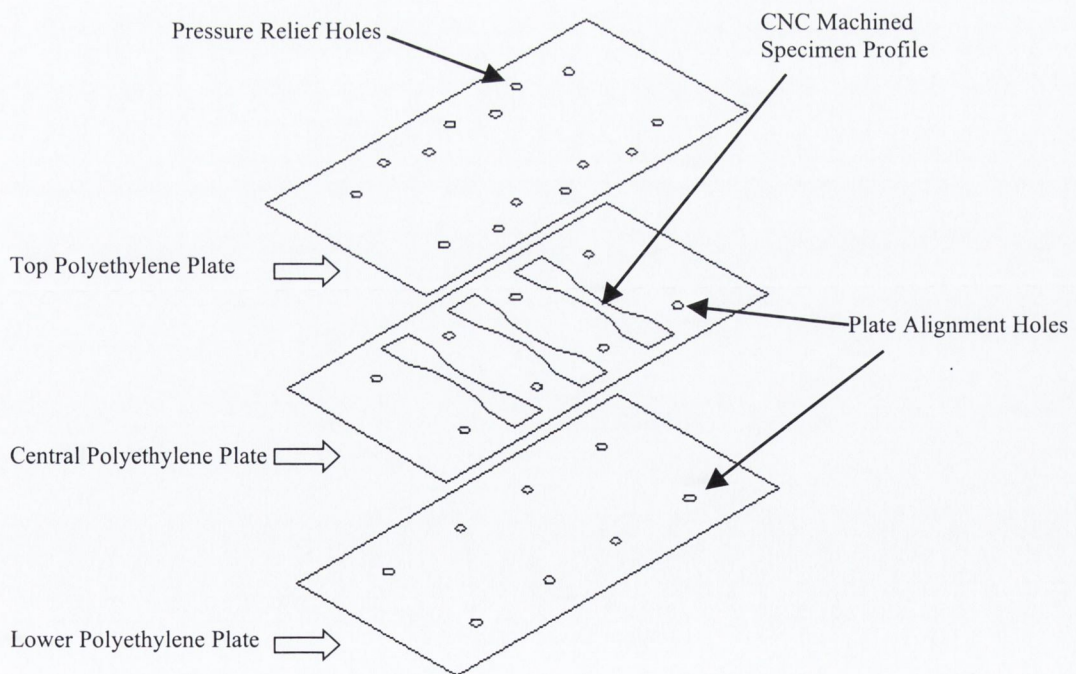


Figure 3.5 Exploded view of the mould, two aluminium plates 8 mm thickness were added for rigidity (complete engineering drawings of specimens, moulds, and test rigs can be found in Appendix I).

3.4.2 Mould design for the fatigue damage accumulation specimens

Similar to the previous specimen, this specimen was flat and dog-bone shaped; however, it was increased in size by a factor of two, see Fig. 3.6. The larger specimen allowed the use of a submersible extensometer (RDP Howden, Warwickshire, U.K.) to be placed over the gauge section of the specimen to monitor compliance during the fatigue test. The larger specimen was required so that there would be a sufficiently large area to monitor damage accumulation.

The mould consisted of the same aluminium and polyethylene plates as the previous specimen; however the central polyethylene plate was replaced with a plate that had one large specimen machined from it; larger pressure relief holes were added to the top polyethylene and aluminium plates. The central plate thickness was 3.5 mm producing a specimen with similar thickness.

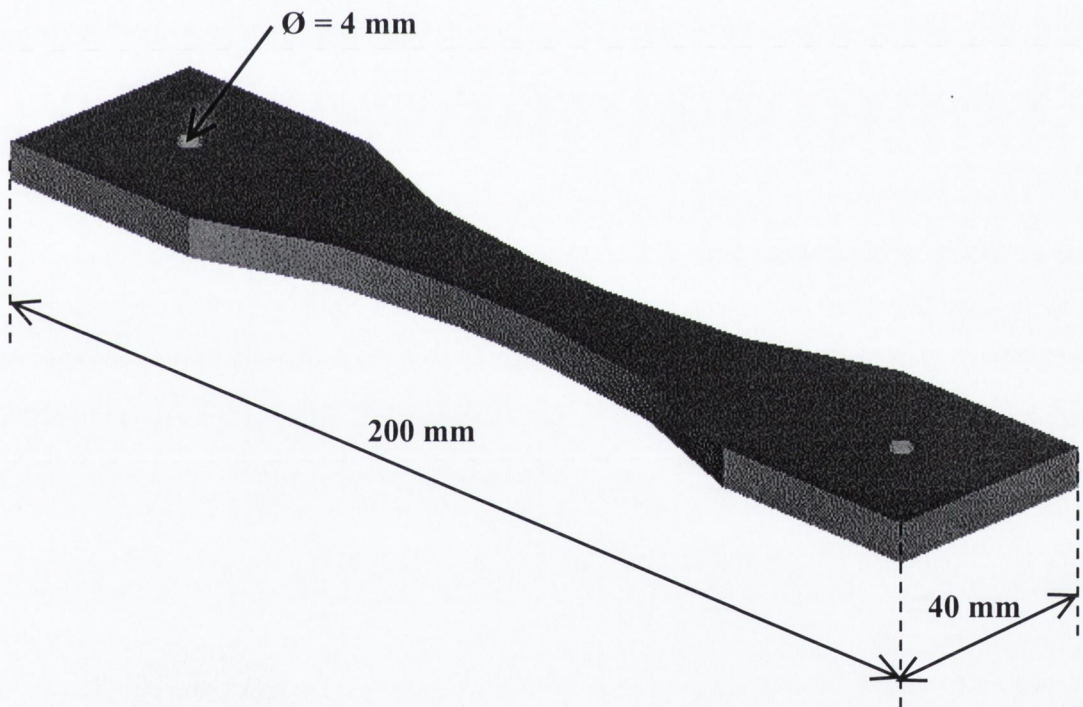


Figure 3.6 Schematic of a moulded damage accumulation specimen, with a 16 mm \times 16 mm gauge section and a thickness of 3.5 mm.

3.4.3 Mould design for multiaxial specimens

This specimen was designed to observe the effect of a multiaxial stress state on the fatigue and dynamic creep properties of acrylic bone cement. A hollow cylindrical specimen was chosen to create the multiaxial stress state. Applying a constant

internal pressure (P) to the cylinder radial and hoop stresses are generated. The cylinder acted as a thick walled cylinder as the ratio of wall thickness to radius was less than 10:1, therefore the stresses were not constant over the wall thickness (see Fig. 3.7) these stresses were calculated using equations given in Fig. 3.7. Applying a cyclic axial load (F) via a materials testing machine an axial stress is generated; with the two loading conditions applied to the cylinder a multiaxial stress state is created: with tensile hoop and axial stresses being the two principal stresses. There is also a compressive radial stress as a consequence of pressurisation.

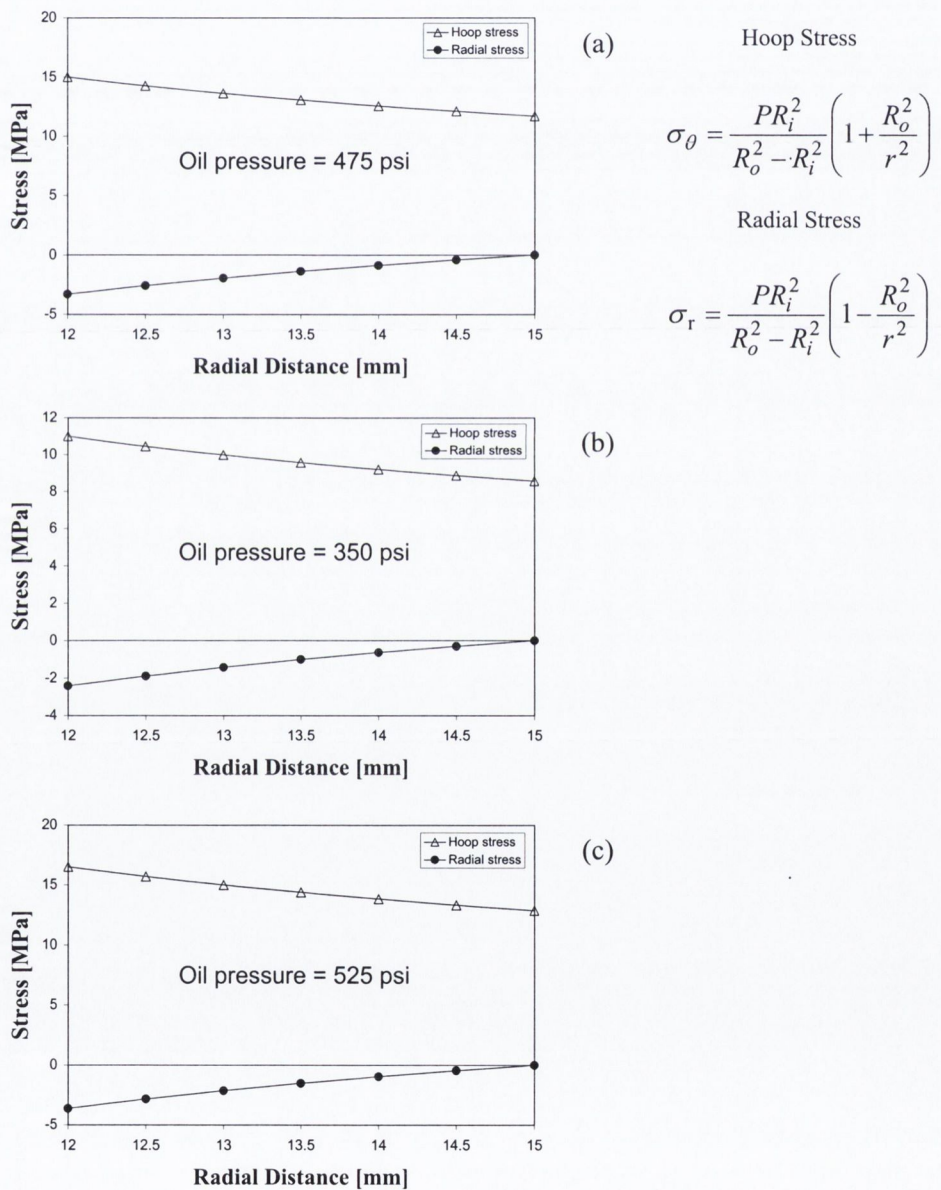


Figure 3.7 The application of an internal pressure to the tubular specimen resulting in the following testing conditions; (a) 1:1 ratio axial v's hoop at 15 MPa axial; (b) 1:1 ratio at 11 MPa axial and (c) 1:1.5 ratio at axial 11 MPa and hoop 16.5 MPa.

As the end conditions of the cylinder are not ideal, an additional static axial force is produced by pressurisation. This force was measured by setting up the experiment in position control (i.e. the specimen is not allowed to move when clamped); thus the tensile axial force that would act on the specimen due solely to internal pressurisation is read as the compressive force on the load cell. The axial force was measured for a number of different internal pressures and a relationship between load cell reading and internal pressure was determined, see Fig. 3.8.

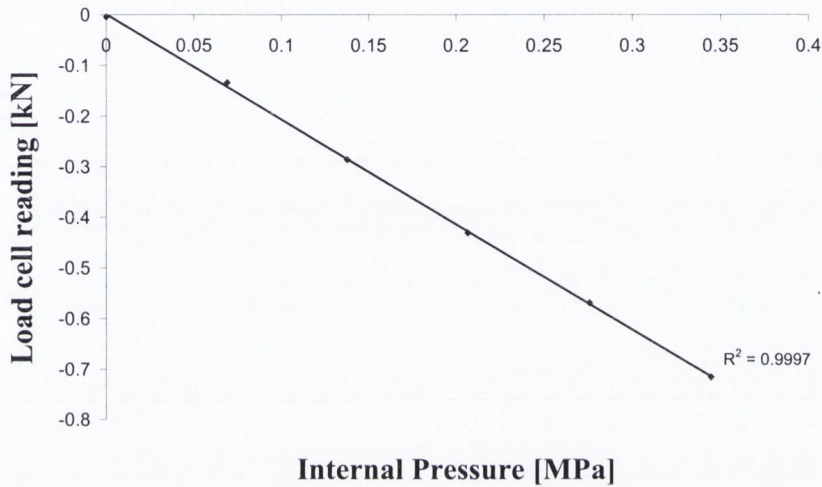


Figure 3.8 Plot of internal pressure and load cell reading while in position control.

The relationship between tensile axial force [kN] in the specimen and internal pressure [MPa] is given as:

$$F = 0.2074P - 9 \times 10^{-4} \quad \text{Eqn. 3.1}$$

Using Equation 3.1 the additional static stress was calculated to be: 2.88 MPa at 3.62 MPa (525 psi), 2.61 MPa at 3.28 MPa (475 psi), and 1.92 MPa at 2.41 MPa (350 psi); this was calculated to be the stress at zero load. This pressure reduces at the peak stress of the fatigue loading cycle due to enlarged pressurised cavity; the minimum and maximum cyclic stresses are given in table 3.2 along with the corresponding change in axial stress ($\Delta\sigma$) for each loading configuration.

Table 3.2 *Multiaxial loading conditions*

	Hoop stress 16.5 MPa	Hoop stress 15 MPa	Hoop stress 11 MPa
Minimum axial Stress [MPa]	2.88	2.61	1.92
Maximum axial stress [MPa]	13.61	17.27	12.81
$\Delta\sigma$ axial stress [MPa]	10.48	14.66	10.89

The change in axial stress is approximately the same as the $\Delta\sigma$ of the control specimens, and therefore the pressurised set will be compared directly against the control specimens. Furthermore, this data was confirmed with strain gauge measurements of the specimen while the materials testing machine was in load control (see Appendix II), which is the machine mode the tests are carried out in.

The specimen was designed as a hollow cylinder with two tapers; one internal, and one external, see Fig 3.8. Gripping of the specimen was achieved on the external taper at one end and on the internal taper at the other: Through this arrangement an axial tensile fatigue load could be applied to the bone cement, and an internal pressure was applied via the end with the external taper creating the hoop and radial stresses.

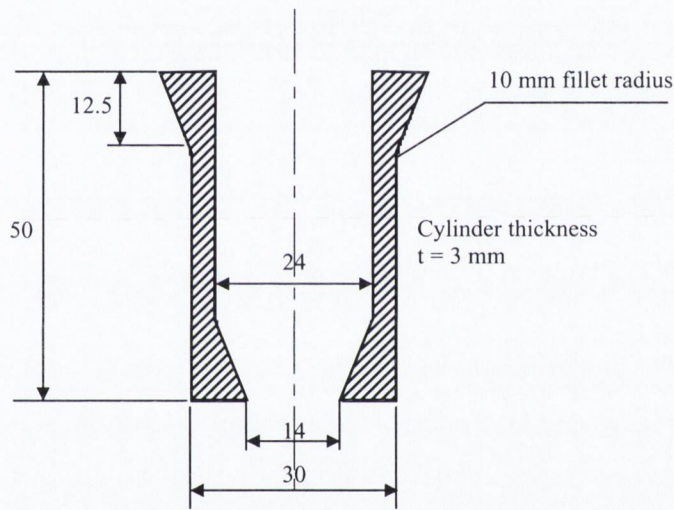
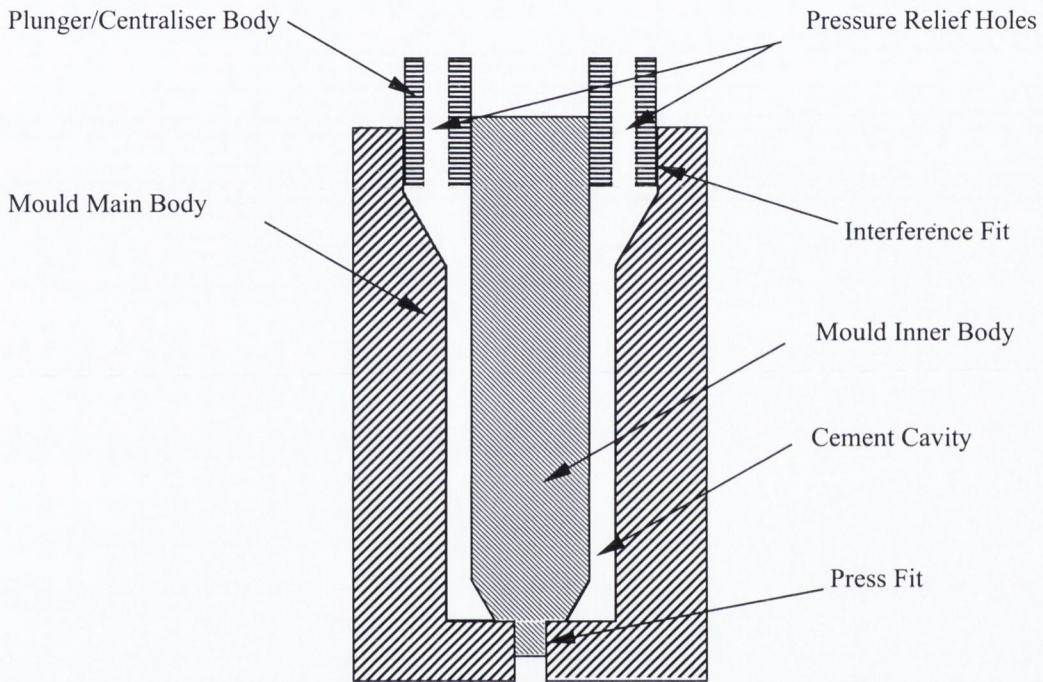


Figure 3.9 Dimensioned cross section of a moulded multi-axial bone cement specimen. All dimensions are in millimetres.

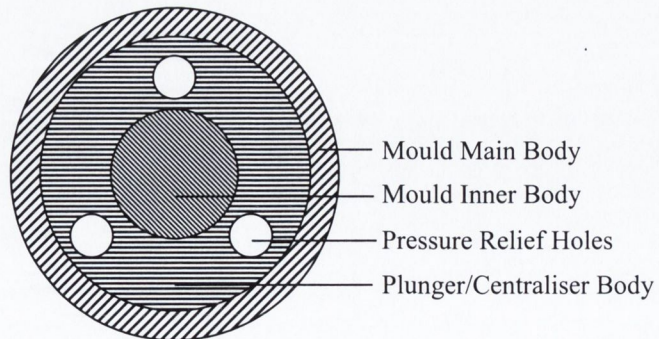
The specimen mould consisted of a three-part polyethylene design: a main body, an inner body, and a plunger/centraliser, see Fig 3.9. The inner body was slotted into a circular press fit hole in the main body, while the plunger/centraliser fitted over the inner body and between the main body. Both fits were zero-tolerance fits; this ensured centralisation of the inner piece. The plunger allowed excess cement to escape via pressure release holes. The inner and main body of the mould were CNC machined using a stainless steel tool piece with a slow feed rate; this ensured a smooth surface finish to minimise cement mechanical interlock with the mould.

3.5 Design of testing rigs

Two different experimental rigs were used in this project; one for the uniaxial fatigue tests and a second for the multiaxial fatigue tests. The experimental rigs were designed to test acrylic bone cement in a physiological environment under controlled cyclic loading conditions.



(a) CROSS SECTION



(b) PLAN VIEW

Figure 3.10 (a) Cross section and (b) plan view of the assembled mould for the multiaxial specimens. The clear section represents the area filled with cement.

3.5.1 Uniaxial fatigue test rig

This testing rig consisted of four main parts (see Fig. 3.10): an aluminium base, a Perspex container, a set of stainless-steel grips and a polyethylene tap. The Perspex container was sealed around the base by means of double o-rings. The stainless steel grips were precision machined by CNC machining. Alignment of the specimen was achieved through alignment holes drilled in the upper and lower grips. Similar holes were drilled in the specimens; steel pins were placed through the holes in the rig and through the alignment holes of the specimen (see Fig. 3.4 and Fig. 3.6) and a slight tension was applied after which the specimen was clamped in position thereby preventing bending and ensuring pure tension and consistent alignment for all specimens. The Perspex container was filled with water and heated up by means of a heating coil (Industrial Electrical Elements, Stafford, UK) the temperature was kept at 37°C ($\pm 1.5^\circ\text{C}$) during fatigue testing, a temperature probe providing a feedback loop to the heater ensured a constant temperature was maintained. The aluminium base was painted to avoid corrosion. An extensometer was clamped on the central region of the damage accumulation specimens to monitor compliance during a fatigue test.

3.4.2 Multiaxial fatigue test rig

The function of this rig was to apply the required pressure and force to the multiaxial specimen (Fig. 3.8) during a fatigue test in a physiological environment. This test rig was similar to the previous rig in so far as the same Perspex chamber was used to contain water at 37°C (see Fig. 3.11). The main differences were: different specimen grips, an improved temperature control system, and a pressurisation system passing through the upper specimen grip into the specimen.

Gripping of the multiaxial bone cement specimen was achieved with two stainless steel grips with a self-aligning gripping system; the gripping design ensured every specimen was gripped in the same manner, as the specimen was cylindrical, the centre line of the specimen always lined up with the centre line of the testing grips which were connected to the pre-aligned materials testing machine. The gripping arrangement consisted of an internal specimen grip which bolts into the lower grip and an external grip which slides over the specimen and bolts into the upper grip; both grips clamp against the tapers on the specimen, see Fig. 3.12. Temperature control within the test rig was achieved by passing a continuous flow of water through the testing tank; a water bath (Grant Instruments Ltd, Cambridge, England), with a pump

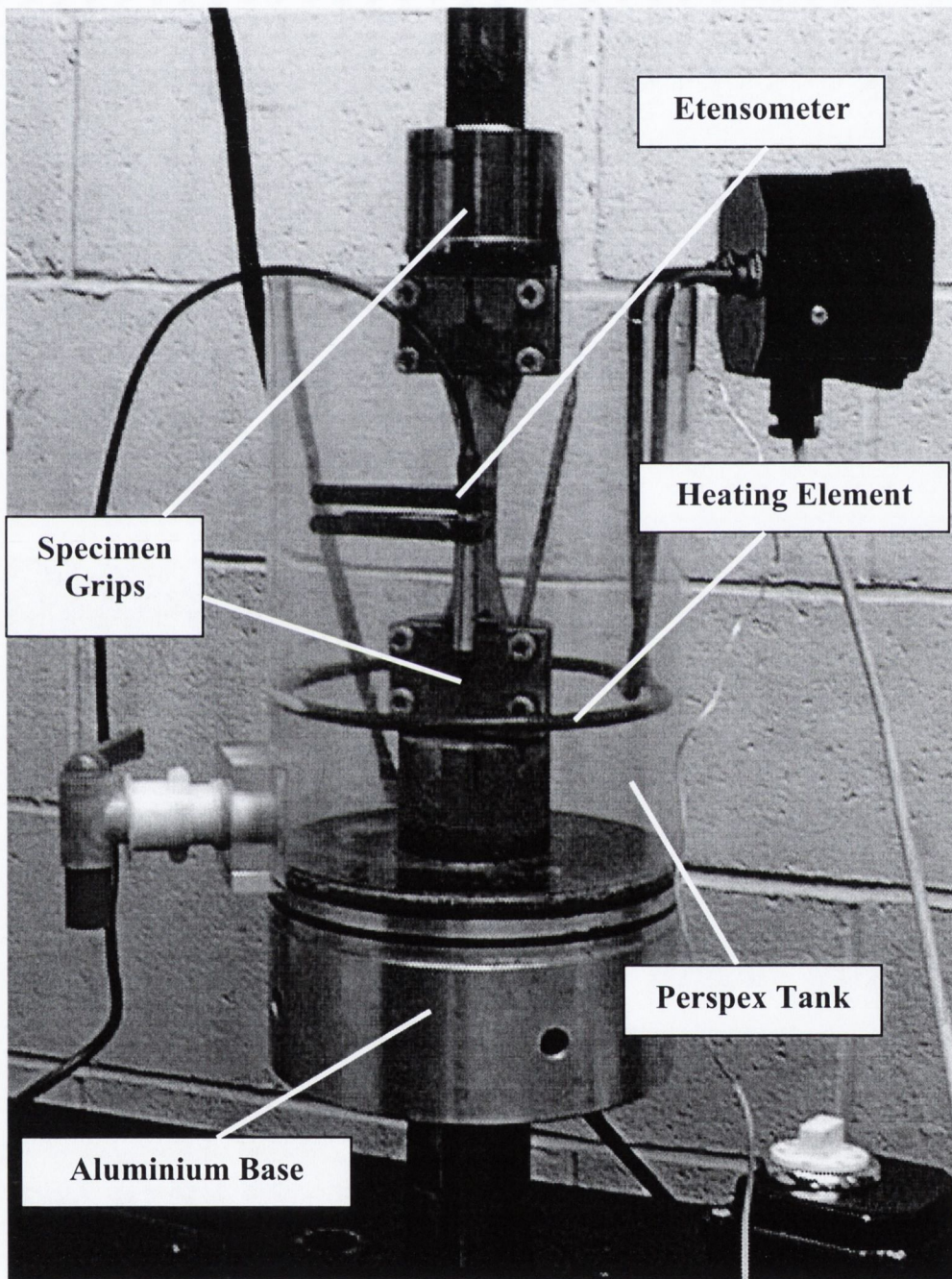


Figure 3.11 *Uniaxial experimental test rig*

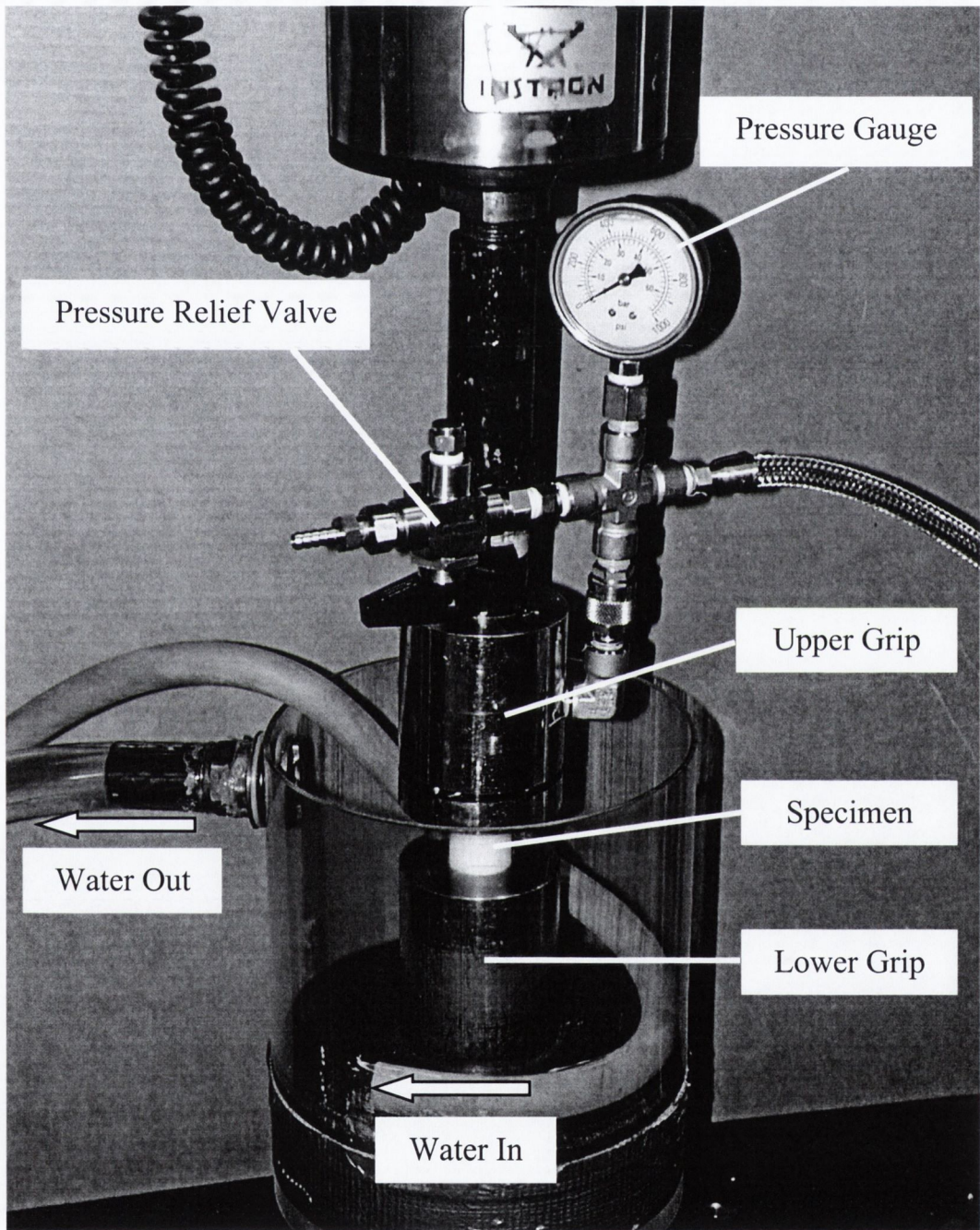


Figure 3.12 *Multi-axial experimental test rig*

attached, was used to heat and pump the water to the test rig; the resulting temperature control was $\pm 0.1^\circ\text{C}$.

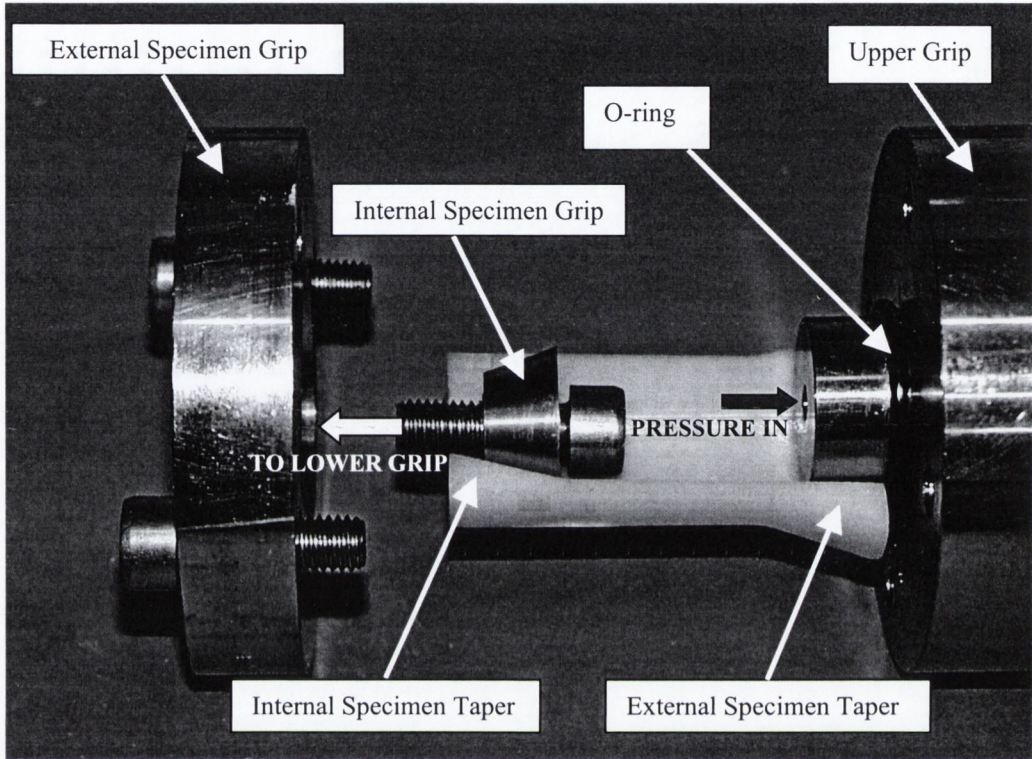


Figure 3.13 *Detail of multi-axial specimen gripping arrangement*

The specimen was pressurised by an air activated hydraulic foot pump (Power Team, SPX Corporation, MN, USA). Pressure was maintained in the set-up from a non-return valve to the specimen, see Fig. 3.13. The pressure could be read directly from a pressure gauge and released by a pressure relief valve. Pressure within the specimen was contained by o-rings on both ends of the specimen; one of the o-rings is visible in Fig. 3.12 between the upper grip and the specimen. To separate the oil from the specimen and to ensure *burst out* of the oil did not occur, a balloon was fitted over the section of the upper grip that fitted into the specimen; if a near through-thickness pore was present in the specimen burst out of the oil and loss of pressure would not occur due to the presence of the balloon.

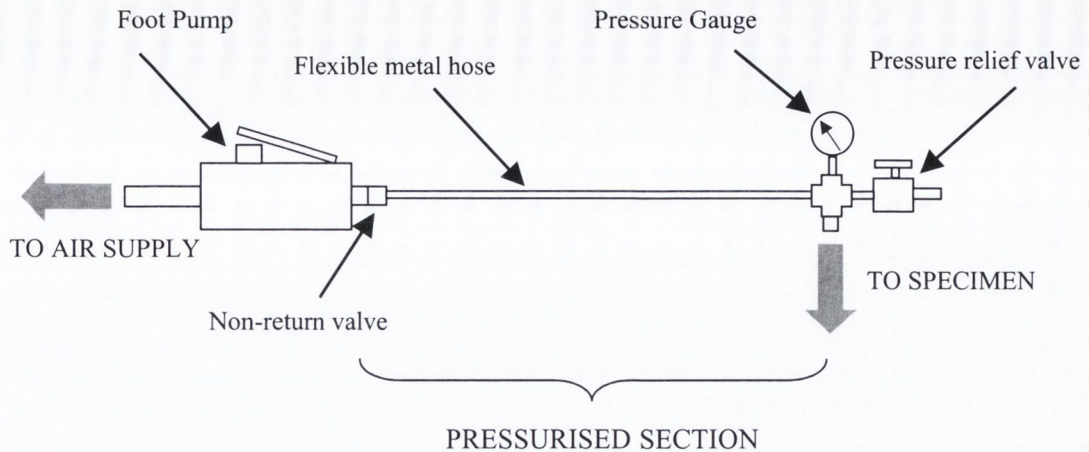


Figure 3.14 *Schematic of the pressure set-up.*

3.6 Experimental protocols

This section details the main points of the experimental procedure from specimen moulding through to the analysis of failed specimens. Step-by-step experimental protocols are included in Appendix II for comprehensive details of the testing procedure.

3.6.1 Moulding procedure

Uniaxial specimens: Prior to assembly of the mould all the polyethylene plates were cleaned with alcohol and allowed to dry. The following procedure was then followed for moulding of uniaxial bone cement specimens:

- The lower section of the mould was assembled with bolts passing through the eight alignment holes; depending on the type of specimen to be moulded the central plate was chosen.
- The cement was then mixed in the appropriate manner.
- The bone cement was placed in the specimen cavity with a cement gun filling one end of the cavity and progressing to the other.
- The two top plates were placed in position and nuts were tightened onto the bolts and the mould was sealed.

- The cement was allowed to set in the mould for 24 hrs at room temperature. After this time period the mould was disassembled and the specimen was easily removed from the central plate.

Multiaxial specimens

Moulding and removal of multiaxial specimens from the mould was slightly more complicated than the uniaxial case. However, the moulding method was similar to insertion of a femoral prosthesis. The main points involved in moulding and removing a multiaxial specimen are:

- The cement was vacuum-mixed and placed in the main body of the mould with a cement gun in a retrograde fashion.
- The inner body of the mould was inserted into the main body and pressed into the hole in the main body of the mould.
- The plunger was then placed over the inner body and into the main body of the mould. The plunger was pushed down into the main body to a certain level, which was indicated by a line on the side of the plunger.
- The bone cement specimen was allowed set in the mould for 24 hrs at room temperature.
- Removal of the specimen required the use of a lathe. The outer body was separated from the plunger, inner body and specimen in the first step. The second step involved removing the inner body from the plunger and the cement specimen; finally, the specimen was separated from the plunger (see Appendix II for full details of this procedure).

3.6.2 Pre-test procedure

Before the specimens could be tested a number of specimen preparation steps were required. Immediately after removal from the mould alignment holes were drilled in the uniaxial specimens, rough specimen edges were removed using 320 grit silicon carbide grinding paper. The specimens were then numbered with a permanent marker, and (in the case of the damage accumulation specimens, see Fig. 3.6) the region where damage accumulation was to be monitored was marked with a permanent marker. On the multiaxial specimens the region where the cement had extruded out via the pressure relief holes was grinded flat with 320 SiC grinding paper to ensure a flat region on the end of the specimen; this was necessary to ensure an effective pressure

seal. The specimens were then numbered with a permanent marker. All specimens were soaked for 14 days prior to testing to allow polymerisation and water absorption to take place. They were soaked in a Grant JB1 (Grant Instruments Ltd., Cambridge, England) water bath.

3.6.3 Fatigue test conditions

The following fatigue test conditions were maintained:

- Water at 37°C maintained for the duration of the test
- Uniaxial tests in pure tension cycling from zero to a tensile stress (i.e. an R-ratio equal to zero)
 - S-N tests conducted at four stress levels: 13, 17, 21, and 25 MPa.
 - Damage accumulation monitored at three stress levels: 9.76, 12.11, and 15 MPa.
- Control set of tubular specimens were tested in uniaxial tension at three stress levels: 11, 15, 19 MPa.
- Multiaxial fatigue tests were conducted at the following stress levels:
 - 1:1 ratio of axial stress: hoop stress on the inside wall, at 15MPa.
 - 1:1 ratio of axial stress: hoop stress on the inside wall, at 11MPa.
 - 1:1.5 ratio of axial stress: hoop stress on the inside wall, at 11MPa axial stress and 16.5 MPa hoop stress on the inside wall.
- All fatigue tests performed in load control
- Loading cycle was sinusoidal
- Test frequency
 - S-N specimens 10 Hz
 - Damage accumulation specimens 5 Hz
 - Multiaxial specimens 5 Hz

3.6.4 Data logging

During the damage accumulation and multiaxial fatigue tests the compliance (E) and the dynamic creep were monitored throughout a fatigue test. For the damage accumulation specimens the data was collected from the extensometer, while the multiaxial data was collected directly from the materials testing machine by monitoring the position of the actuator. Data was collected for two seconds at specified intervals; in the first 10,000 cycles data was collected every 500 loading

cycles. After this, 2 seconds of data was collected every 5,000 or 10,000 cycles depending on the length of the fatigue test. The two seconds of data consisted of 500 data points using a scan rate of 250 Hz this amounted to 50 data points per loading cycle when a fatigue testing frequency of 5 Hz was used. To determine the dynamic creep of the specimen the following procedure was used:

- The data was imported into Microsoft Excel. The first 500 data points were collected when the specimen had zero load applied, i.e. its original position, the average value was determined of these 500 data points
- The next set of 500 data points was the first data set taken during a fatigue test. The average minimum value of the ten sine waves was taken i.e. the position corresponding to the moment when no load was applied to the specimen.
- The specimen extension could be monitored from the subsequent data and compared to the original length of the specimen, see Fig. 3.14.

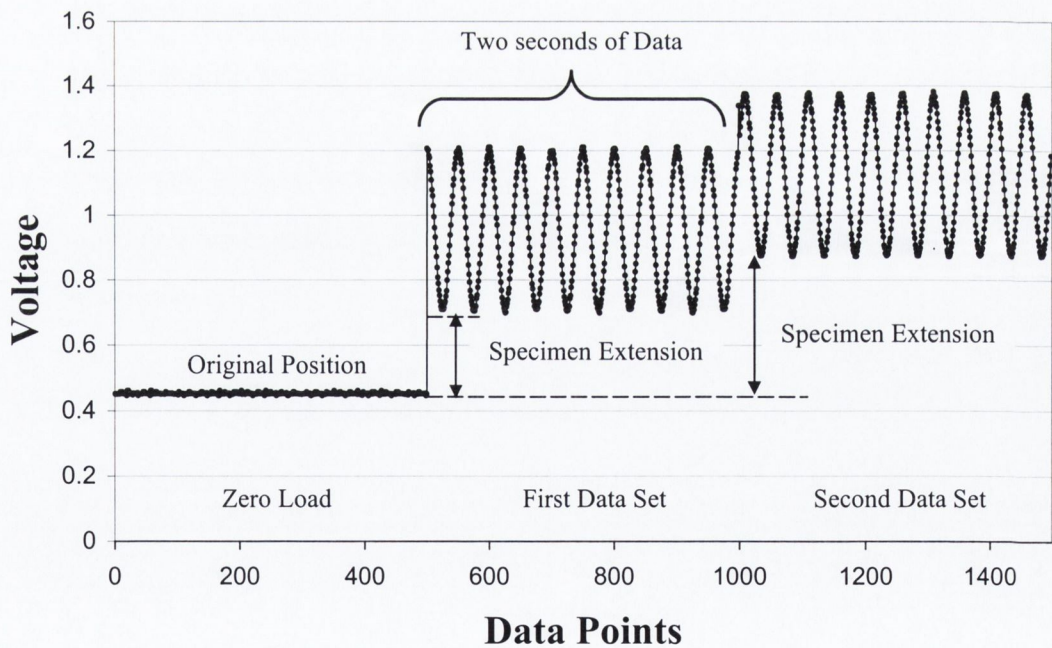


Figure 3.15 *Schematic of the data logging scheme.*

3.6.5 Crack analysis

S-N Specimens: The fracture surface of the uniaxial S-N specimens was examined by coating the specimens in gold and observing the fracture surface features with a scanning electron microscope (Hitachi Ltd., Model S-3500N, Japan).

Damage Specimens: Microcracking was observed over the course of a fatigue test following the procedure developed by Dr Brendan McCormack (1997).

- Specimens removed after certain number of cycles, n cycles.
- A red dye penetrant (J.A.P., Johnson and Allen, U.K) was applied to the specimen.
- The red dye penetrant was removed from the surface of the specimen by washing with water.
- Individual cracks were highlighted by the red dye and their crack tip and origin co-ordinates are recorded using a Mitutoyo Optical Comparator (Model PJ300) with a $\times 20$ lens.

This procedure was followed for five specimens were no loading was applied to the specimen (i.e. five control specimens).

3.7 Statistical analysis

A Weibull distribution (Weibull, 1951) was used to analyse the probability-of-survival for both mixing techniques (hand-mixing and vacuum-mixing) at each of the four stress levels. The Weibull distribution (Eqn. 3.2) may be used to describe the probability-of-survival to a given number of cycles under a known stress.

$$P_s = \exp \left[- \left(\frac{N_f}{\beta} \right)^\alpha \right], \quad \text{Eqn. 3.2}$$

where N_f is the number fatigue cycles to failure, P_s is the probability-of-survival and α and β are empirical constants. The constant α is referred to as the shape parameter of the curve, and β is the location parameter. Higher values of α indicate a narrower

distribution of data and therefore less variability. Higher values of β indicate a higher mean strength. The linearised form of the Eqn. 3.2 is:

$$\ln(-\ln P_s) = \alpha \ln(N_f) - \alpha \ln(\beta). \quad \text{Eqn. 3.3}$$

The probability-of-survival of each specimen was determined by the equation

$$P_s = 1 - \left(\frac{Y - n}{M - n - m + 1} \right), \quad \text{Eqn. 3.4}$$

Y being the failure order number of the specimen in a set of M test specimens; $Y=1$ is the specimen with the shortest fatigue life and $Y=M$ is the specimen with the longest fatigue life. Following Lewis (1997) and Carter *et al.* (1982), the parameters n and m were taken equal to 0.3, as this has been shown to give unbiased estimates of the parameters α and β (see Weibull [1961]). The probability-of-survival (P_s) is calculated for each specimen (from Eqn. 3.4) and is plotted in the form $\ln(-\ln(P_s))$ against $\ln(N_f)$ for each group of specimens (i.e., each stress level and mixing technique); the constants α and β can then be calculated from a least squares fit of Eqn. 3.3 to the data.

Chapter 4

Results

4.1 Introduction	64
4.2 Uniaxial fatigue results: vacuum-mixing versus hand-mixing	64
4.2.1 SEM analysis	67
4.3 Damage accumulation in acrylic bone cement	73
4.4.2 The determination of damage evolution curves	81
4.4 Multiaxial fatigue results	87
4.4.1 Effect of off-axis stress on fatigue life	87
4.4.2 Creep induced by cyclic loading	90
4.5 Calculation of the Monkman-Grant constant	97

4.1 Introduction

In this chapter the results are divided into three distinct sections; each section deals with a different aspect of the fatigue strength of acrylic bone cement.

- The first section deals with the fatigue strength of vacuum-mixed cement, comparing it to the *baseline* mixing technique, hand mixing.
- The second section presents the results of the damage accumulation study.
- Finally, the last section presents the results of the effect of multiaxial stresses on the fatigue strength of acrylic bone cement. Furthermore, this section presents the results of creep induced by cyclic loading under uniaxial tension and multiaxial loading conditions.

4.2 Uniaxial fatigue results: vacuum mixing versus hand mixing

Results confirm that vacuum mixing produces a cement with a higher fatigue strength; the increase in the average fatigue life is approximately one order of magnitude at each of the four stress levels tested. This data is shown in Table 4.1. The students t-test shows that a statistically significant increase in fatigue strength is found for three stress levels, although the Mann – Whitney significance shows that a significant increase in fatigue life is present at two stress levels. Table 4.2 shows this statistical data.

Table 4.1 *Stress to number of cycles to failure data for vacuum-mixed and hand-mixed cement*

Stress Level	Average N_f (SD ^a)		Average N_f (SD)		Factor increase in average strength
	Vacuum-mixed		Hand-mixed		
25 MPa	20,631	(±21,052)	1,581	(±868)	13.05
21 MPa	23,942	(±24,281)	8,985	(±12,802)	2.66
17 MPa	333,132	(±285,597)	43,683	(±26,058)	7.63
13 MPa	2,628,680	(±1,928,225)	462,054	(±398,793)	5.68

^a SD = Standard Deviation

Table 4.2 The results of statistical significance tests comparing the two mixing techniques.

Stress Level	p (Students T-test)	Mann – Whitney test ^b
25 MPa	0.02	S
21 MPa	0.07	NS
17 MPa	0.01	S
13 MPa	0.01	NS

^b Mann – Whitney test, Significance level = 0.05 (NS = no significant difference, S = significant difference)

The increase in fatigue strength is not as clear when the data is plotted as an S-N curve. At three of the four stress levels, several vacuum-mixed specimens have a lower fatigue life than the hand-mixed specimens causing overlap of the data sets, see Fig. 4.1.

Low correlation coefficients are associated with each data set, 0.89 for the hand-mixed and 0.76 for the vacuum-mixed cement; the lower correlation coefficient in the vacuum-mixed case shows that, even if the mean fatigue strength is higher, vacuum-mixed cement has a greater *variation* in fatigue strength. The regression lines plotted in Fig. 4.1 are calculated using a least squares fit to the entire data set; in both cases the trend in the data appears to be missed. Plotting lines through the *averages* of the data at each stress level allows the trend within the data to be more clearly established, see Fig. 4.2.

The equations of the S-N curves are as follows:

(i) Regression lines through all the data points:

$$\text{Hand-mixed} \quad \sigma = -3.76\text{Log}_{10}(N_f) + 34.95 \quad \text{Eqn. 4.1}$$

$$\text{Vacuum-mixed} \quad \sigma = -2.86\text{Log}_{10}(N_f) + 33.06 \quad \text{Eqn. 4.2}$$

(ii) Regression lines through the average values:

$$\text{Hand-mixed} \quad \sigma = -4.77\text{Log}_{10}(N_f) + 39.91 \quad \text{Eqn. 4.3}$$

$$\text{Vacuum-mixed} \quad \sigma = -4.82\text{Log}_{10}(N_f) + 43.99 \quad \text{Eqn. 4.4}$$

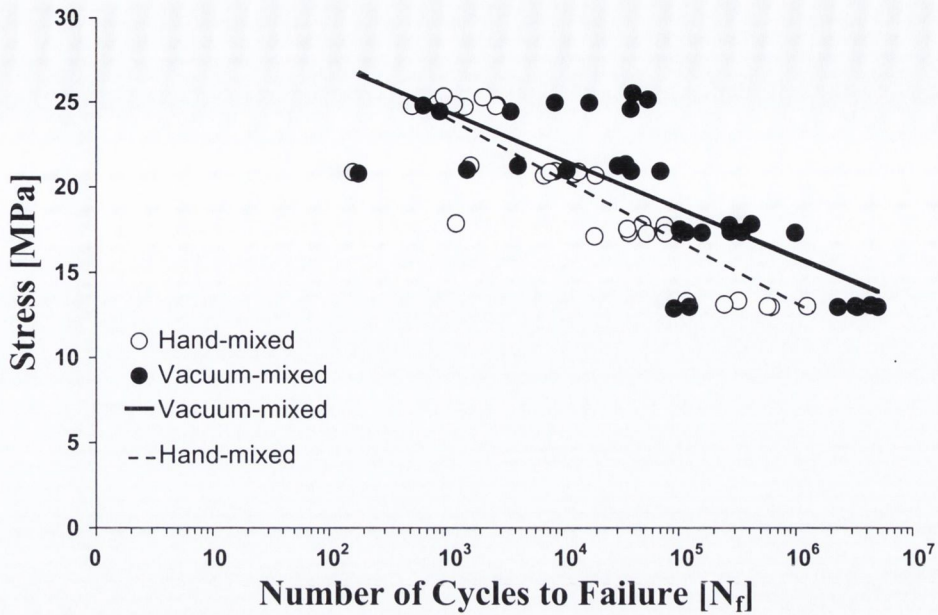


Figure 4.1 Stress versus number of cycles to failure curves for vacuum-mixed and hand-mixed Cemex Rx bone cement. The trend-lines were determined by a least squares fit through all the data points.

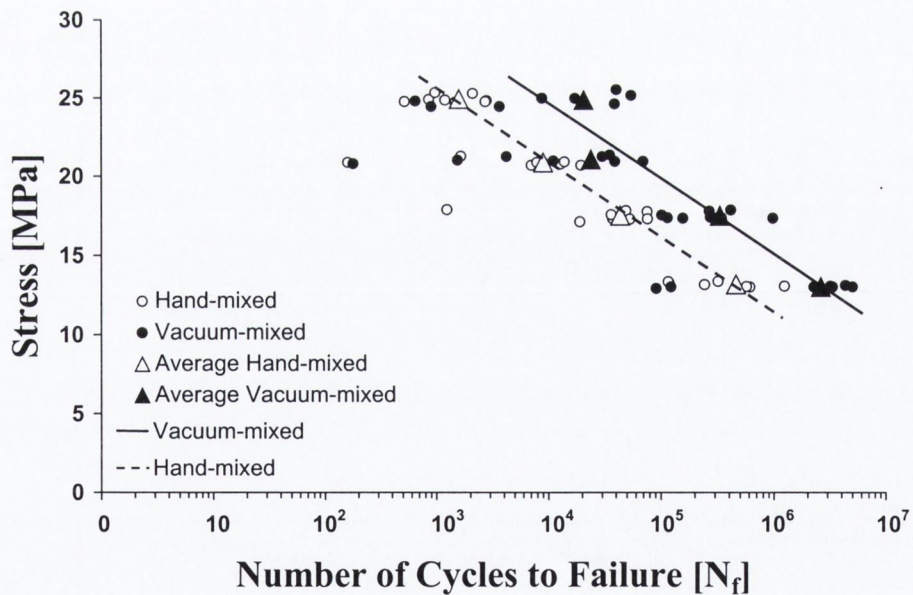


Figure 4.2 Stress versus number of cycles to failure curves for vacuum-mixed and hand-mixed Cemex Rx bone cement. The S-N curves for both mixing techniques have been fitted through the average $\log_{10}(N_f)$ values for the four stress levels.

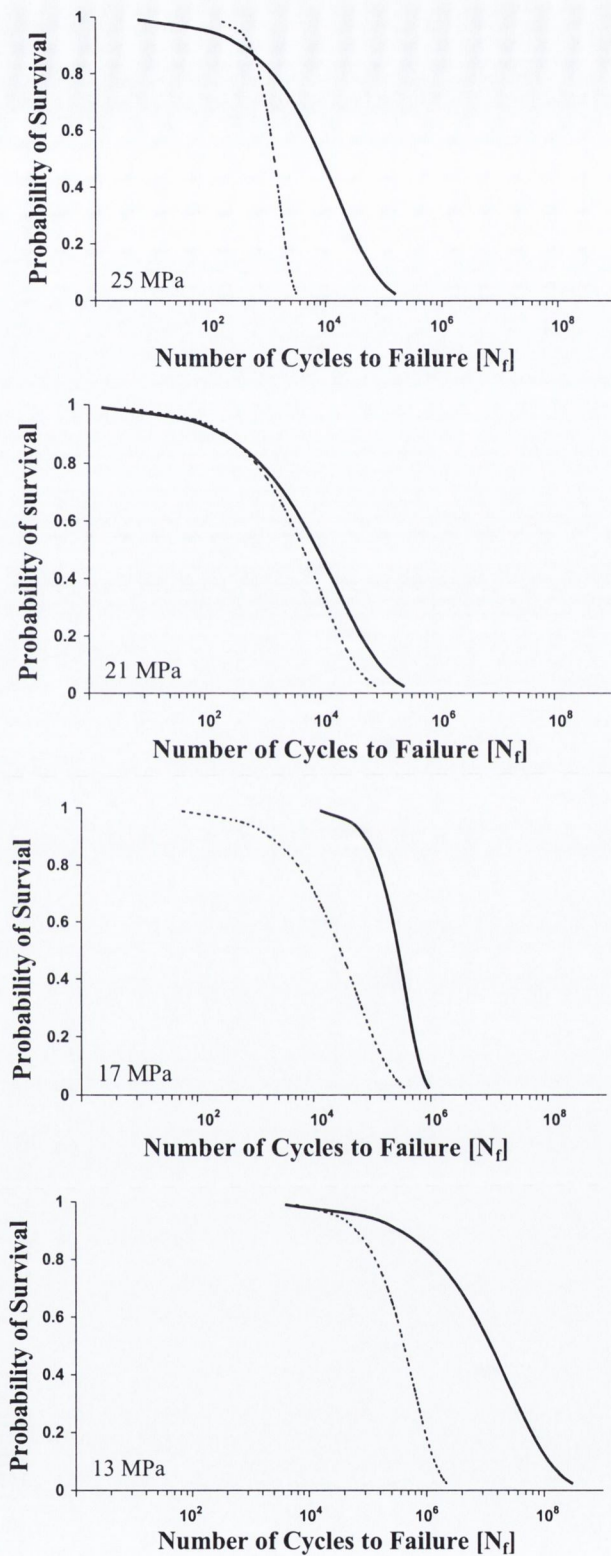
Using the Weibull theory described in Chapter 3 section 3.7, the probability-of-survival to a given number of cycles can be determined for each mixing technique and stress level. The Weibull distribution constants follow a trend where the α parameter is generally larger for hand-mixed cement indicating lower variability and the β values are lower for the hand-mixed indicating lower strength. Since the parameter α is generally lower for vacuum-mixed cement compared to hand-mixed cement, this further confirms the higher variability in the fatigue strength of the vacuum-mixed cement, see Table 4.3 for data.

Table 4.3 *Determined shape parameters (α) and location parameters (β) for the two-parameter Weibull distribution. Fig. 4.3 shows the cumulative distributions for each mixing technique and stress level.*

Stress Level	Hand-mixed		Vacuum-mixed	
	α	β	α	β
25 MPa	1	593,366	0.53	2,842,535
21 MPa	0.67	49,998	1.39	361,968
17 MPa	0.6	9,412	0.5	18,519
13 MPa	1.92	1,564	0.58	16,008

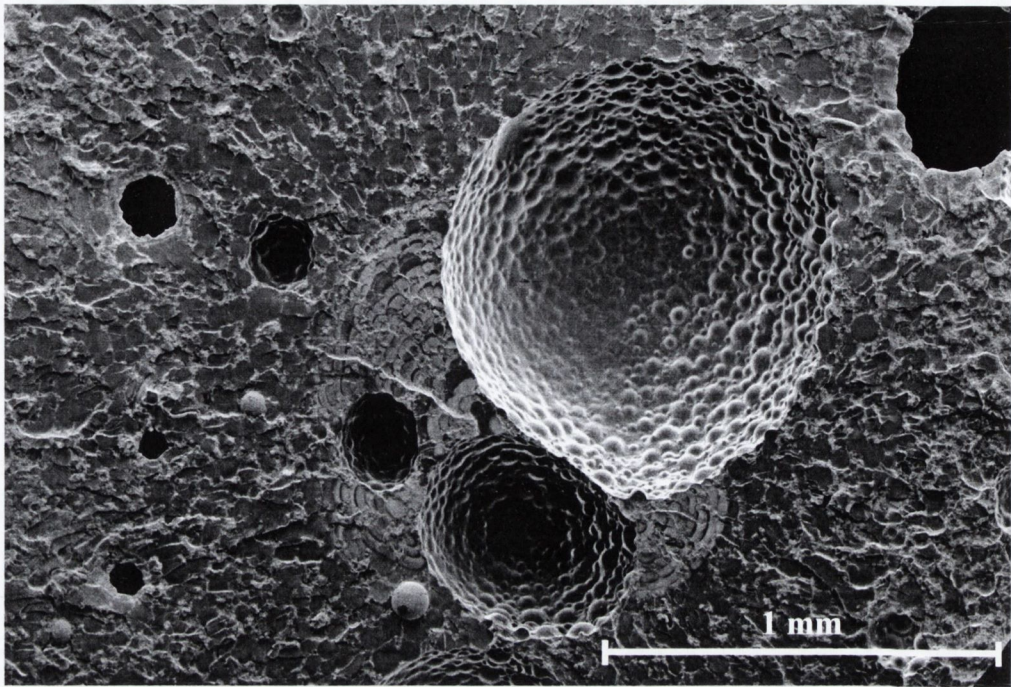
4.2.1 SEM analysis

Hand-mixed cement: The fracture surface features produced by the two mixing techniques are quite different under SEM analysis. Hand-mixed fracture surfaces are typified by a distribution of small pores with some relatively larger pores. On inspection of the hand-mixed specimens, it was found that pores interact to form crack initiation sites, see Fig. 4.4 (a); in this specimen the stress concentration between the large pore and the two smaller pores was large enough to form a crack initiation site. Crack fronts, or “discontinuous crack growth patterns” as Hertzberg and Manson (1980) call them, can be seen advancing out from the area between the three pores. A similar situation is present in Fig. 4.4 (b) where a small pore in close proximity to a large pore acted as the fatigue crack initiation site.

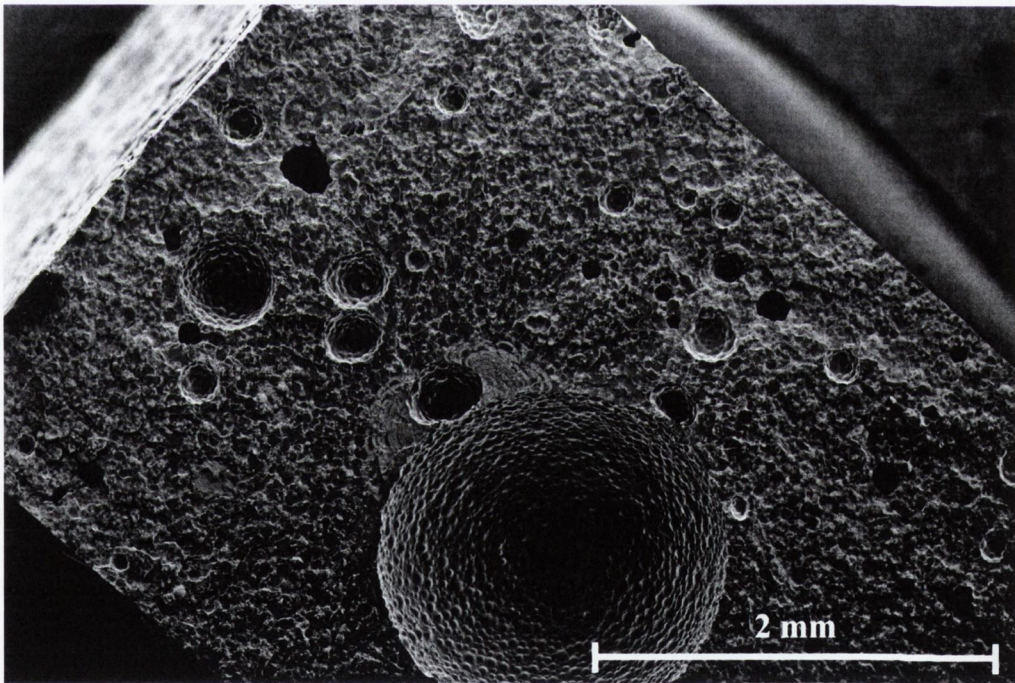


Legend: Hand-mixed ————— Vacuum-mixed

Figure 4.3 Probability-of-survival diagrams for the vacuum-mixed and hand-mixed fatigue tests. The vertical axis indicates the probability-of-survival and the horizontal axis indicates the number of cycles to failure. The graphs are based on the two-parameter Weibull distribution using the constants in Table 4.3.



(a)



(b)

Figure 4.4 (a) Three pores interact to form a stress concentration large enough to act as a crack initiation site. The pattern on the fracture surface is consistent with discontinuous crack growth bands. (b) The crack initiation site is located between the large pore and the smaller pore located in the light grey area.

The interaction of pores acted as the dominant fatigue crack initiation site in the hand-mixed cement; including small pores less than 100 μm interacting with larger pores as shown in Fig. 4.5. Moreover, acute closeness of pores formed large stress concentrations and acted as crack initiation sites, see Fig 4.6.

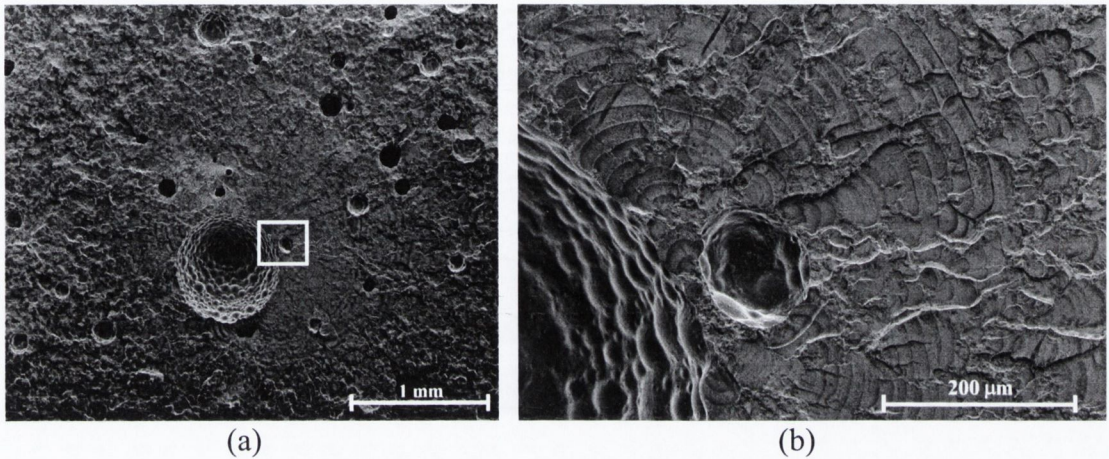


Figure 4.5 (a) The fracture surface of a hand-mixed bone cement specimen; the area around the large pore was suspected of acting as the crack initiation site and on closer inspection (the white box) (b) a pore of $< 100\mu\text{m}$ interacted with the large pore forming the crack initiation site; the crack propagated from this nucleus in the form of discontinuous crack growth bands. On close inspection both the pores are intersected by the same pre-polymerised PMMA bead.

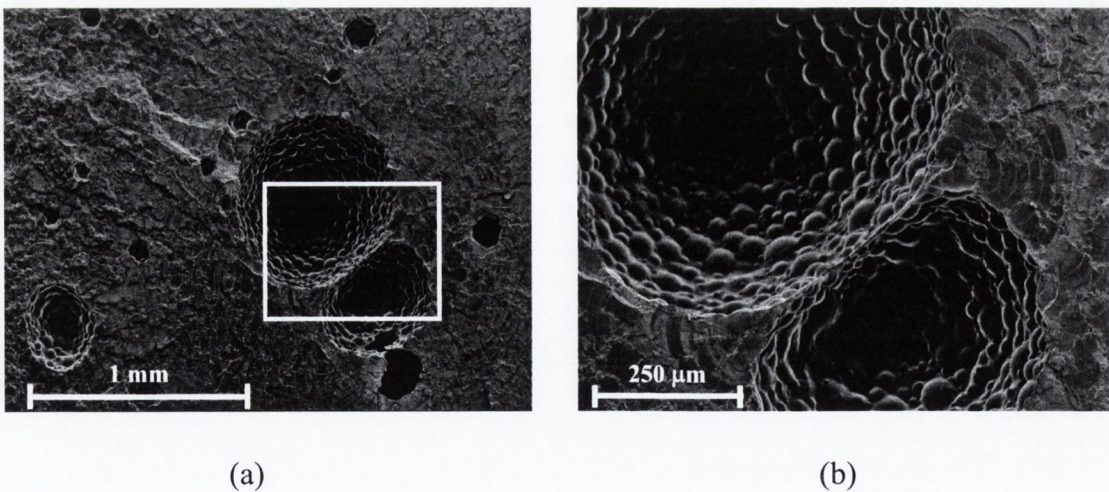


Figure 4.6 (a) The crack initiation site in this case was formed by two large pores. A close-up view (b) shows that only a narrow ridge separated the two pores. The fatigue crack can be seen to grow from both ends of this ridge.

Vacuum-Mixed Cement: The crack initiation sites within the vacuum-mixed specimens typically consisted of a single pore. Fatigue crack initiation sites were identifiable by the presence of *river lines* radiating out from the crack source. River lines are marked in Fig. 4.7 and can be observed in all the vacuum-mixed fractographs. Notably absent on the vacuum-mixed fracture surfaces was a distribution of pores, see Fig. 4.8 (a). Specimens with a high fatigue life were nearly devoid of pores on the fracture surface. Fig. 4.8 shows a good example of a vacuum-mixed specimen that is virtually free of pores on the fracture surface. On some occasions the lack of pores promoted clumps of barium sulphate to act as fatigue crack initiation sites (Fig. 4.9) — this occurred on two occasions. A number of specimens failed from single large pores; these specimens had a significantly reduced fatigue life compared to the average failure life of the vacuum-mixed specimens (see Fig. 4.10 (a) and (b)).

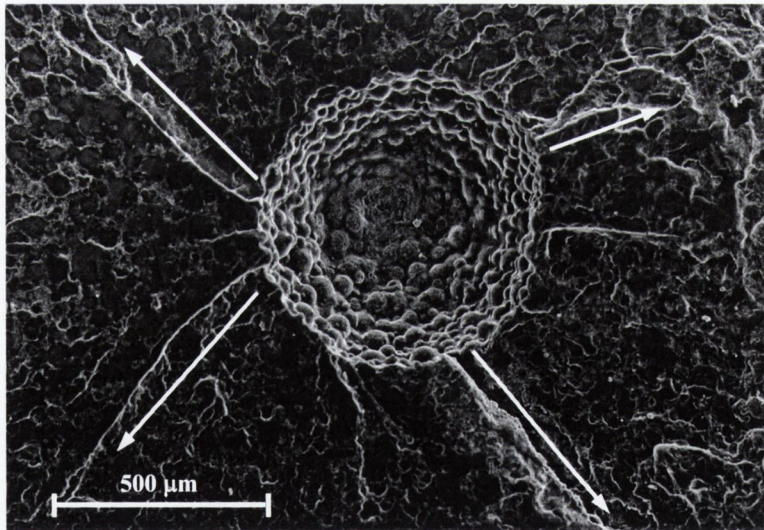


Figure 4.7 Failure site of a vacuum-mixed specimen, river lines are marked by the arrows radiating out from the pore; the direction of the arrow points in the direction crack growth.

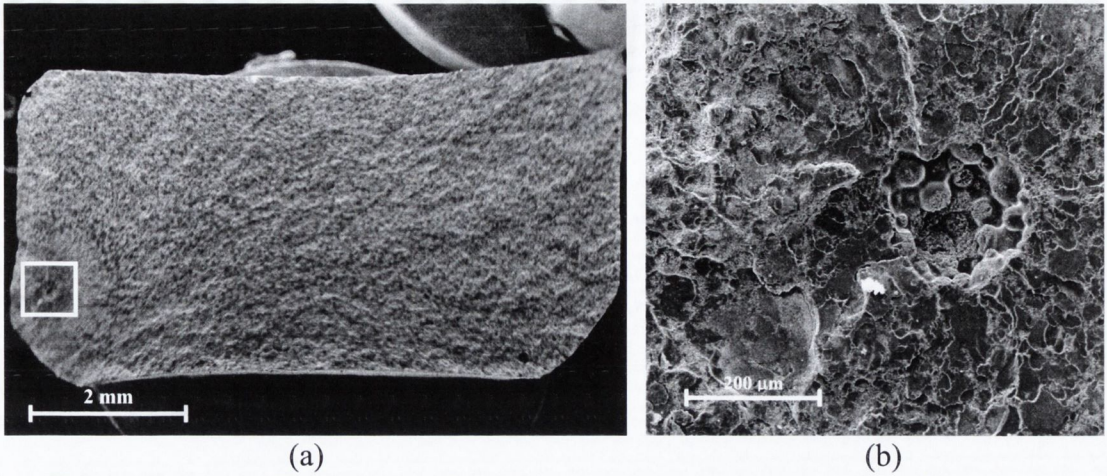


Figure 4.8 (a) Fracture surface of a vacuum-mixed specimen devoid of a porosity distribution. The close-up (b) is highlighted by the white box; an irregular pore of approximately 200 μm acted as the crack initiation site—river lines are present radiating out from the pore combined with a smoother fracture surface surrounding the pore.

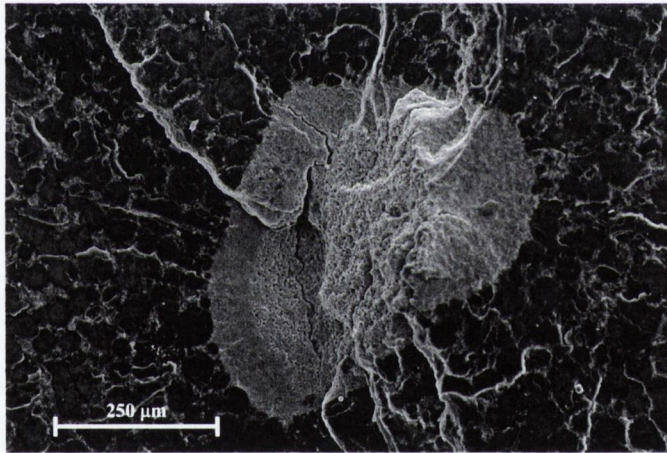


Figure 4.9 BaSO_4 clump acting as the crack initiation site, river lines are present propagating out from the BaSO_4 clump. Note the secondary crack passing through the BaSO_4 clump.

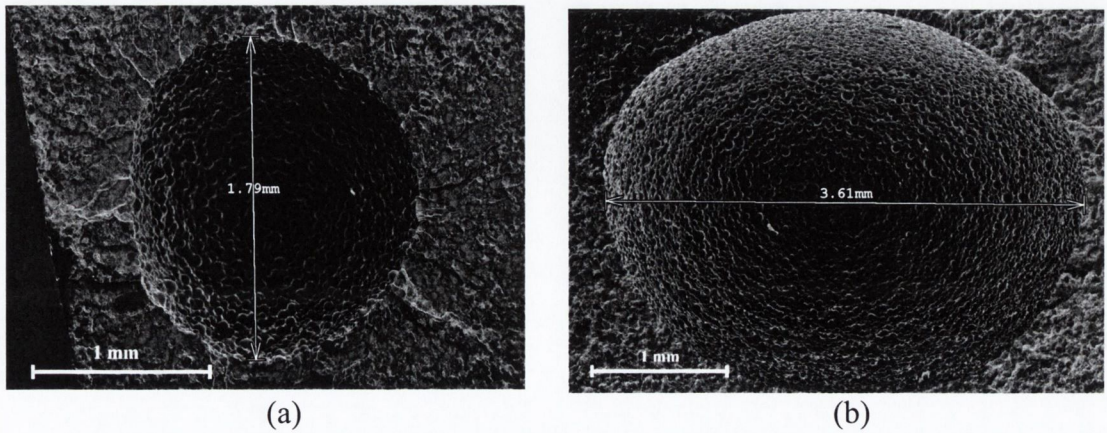


Figure 4.10 (a) A large pore on a vacuum-mixed fracture surface and (b) a considerably large pore acting as the fatigue crack initiation site.

4.3 Damage accumulation in acrylic bone cement

A total of 801 microcracks were observed in the 15 tested specimens; no cracks were observed in the control specimens. The length of the observed cracks varied between 30 μm and 2.4 mm. Cracks initiated between the pre-polymerised PMMA beads on the interior surface of the pores as shown in Fig. 4.11. The initial direction of crack growth seemed to be controlled by the stress concentrations on the inside of the pore, which comprised of a relatively sharp notch between two PMMA beads. Because of the irregular interior pore surface a distribution of crack growth direction was formed, and not all cracks propagated perpendicular to the applied load as would be expected if the apparent applied stress completely determined crack growth direction. The crack growth directions at the lower stress levels were found to be distributed normally about the direction perpendicular to the applied load; however, at the higher stress level the crack growth direction tended to be more broadly distributed, see Fig. 4.12.

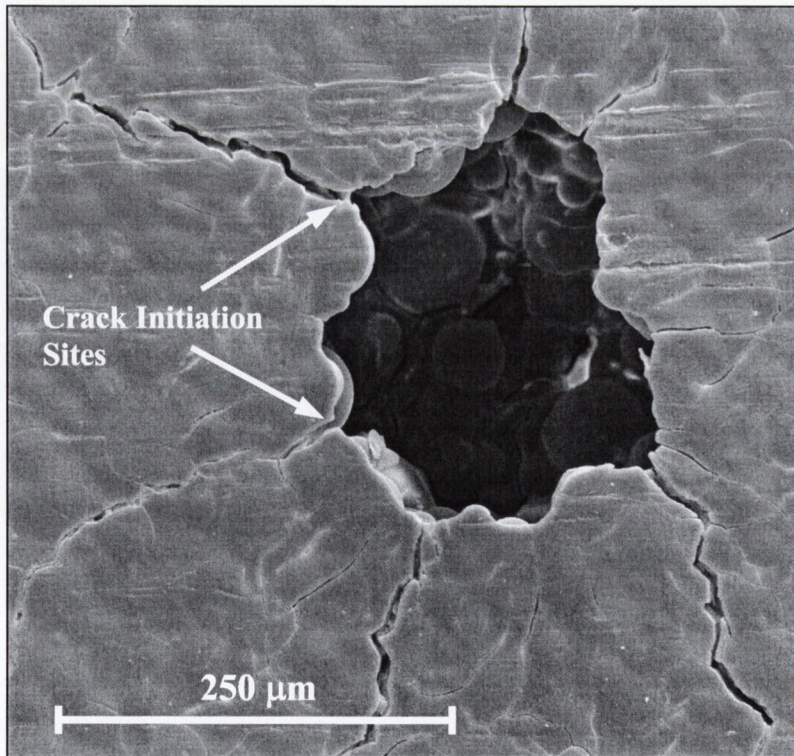


Figure 4.11 *Microcracks propagating from a pore. The direction of loading is in the horizontal direction.*

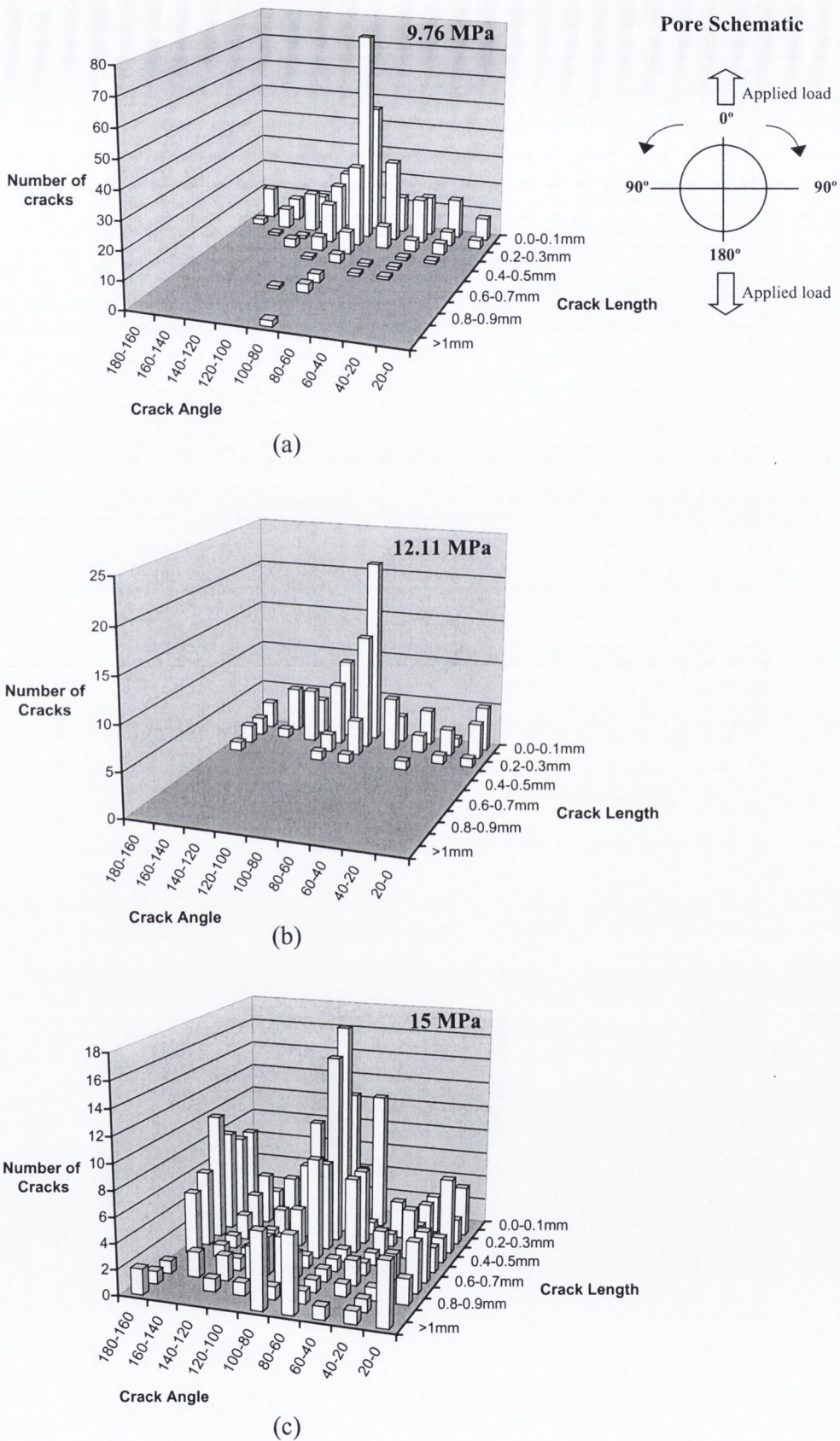


Figure 4.12 Crack angle and crack length distributions for all cracks at failure. (a) the crack angle versus crack number distribution for the 9.76 MPa stress (b) the crack distribution for the 12.11 MPa stress and (c) the crack distribution for the 15MPa stress.

The number of cracks initiating per pore varies for the three stress levels; at the lower stresses approximately three cracks initiate for every two pores whereas at the higher stress level over three cracks initiate per pore, see Table 4.4. The data in Table 4.4 is taken at failure for each specimen and has been summed for the five specimens tested at each stress level. It can be noted that the average crack length would seem to increase with increasing stress, although at the intermediate stress a decrease in the average crack length is observed, see Table 4.4. The measure of fatigue damage decided on was the sum of the crack lengths.

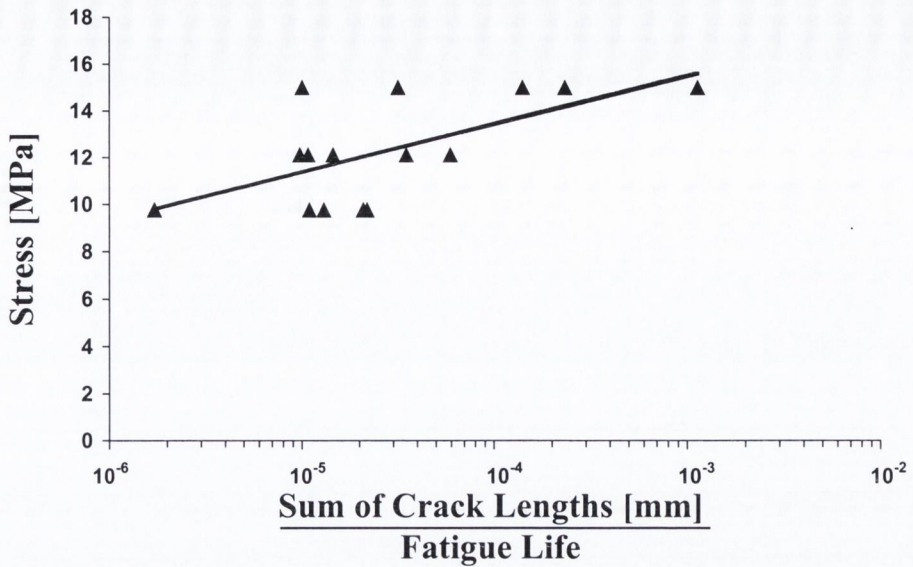
Table 4.4 Summary of crack results at failure*

Stress [MPa]	9.76	12.11	15
n_c	409	112	280
n_p	237	77	84
$\sum_{i=1}^{n_c} a_i$ [mm]	67.47	13.5	134.35
$\sum_{i=1}^{n_c} \frac{a_i}{n_c}$ [mm] (\pm)	0.165 (0.14)	0.121 (0.07)	0.479 (0.35)
$\sum_{i=1}^{n_c} \frac{a_i}{n_p}$ [mm/pore]	0.285	0.175	1.59

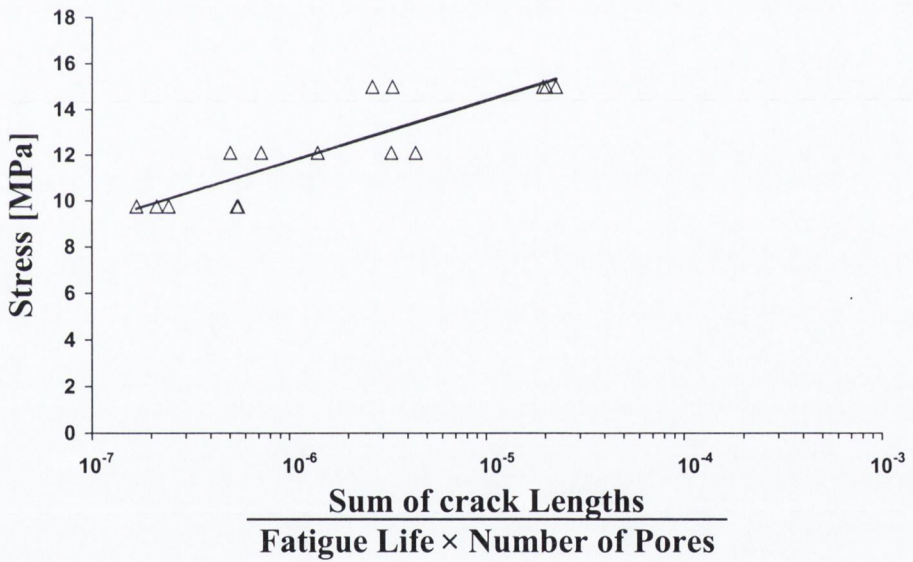
Note: n_c is the number of cracks, n_p is the number of pores, and a_i is an individual crack length.

One method of modelling the damage accumulation rate during the failure process is to assume that damage accumulates at a constant rate until failure—this is called Miner’s Law (Miner, 1945). A plot of damage-per-cycle versus stress, where damage is measured as the sum-of-crack-lengths, shows that the damage accumulation rate increases with stress as would be expected (Fig. 4.13 (a)), although the association of the data is relatively poor with a correlation coefficient of 0.63. However, if the damage-per-cycle is normalised for porosity, an increase in data association is found and the correlation coefficient increases to 0.87, see Fig. 4.13 (b).

* One important point to note is that the number of pores and also the size of individual pores will influence the failure life of each specimen and therefore the damage. Thus, the results presented in this table depend on porosity distributions and the limiting pore (i.e. the pore that causes failure), however for comparison purposes the distribution of pores was assumed to be consistent over the three groups.



(a)



(b)

Figure 4.13 (a) Damage per cycle versus stress. (b) Damage per cycle normalised for porosity versus stress.

Using a student's T-test, or the Mann and Whitney non-parametric significance test, no statistically significant difference ($p < 0.05$) exists between any two adjacent stress levels when the data was normalised for number of cycles to failure; however, when the data was normalised for porosity *and* number of cycles to failure, there was a statistically significant difference between any two adjacent stress levels ($p < 0.05$). This shows the important, perhaps dominant, influence of porosity on the damage accumulation rate.

The number of cracks per specimen varies quite considerably; this can be explained by porosity, as the number of cracks is dependent on the number of pores present. Fig. 4.14 shows that the number of cracks in a specimen increases as porosity increases.

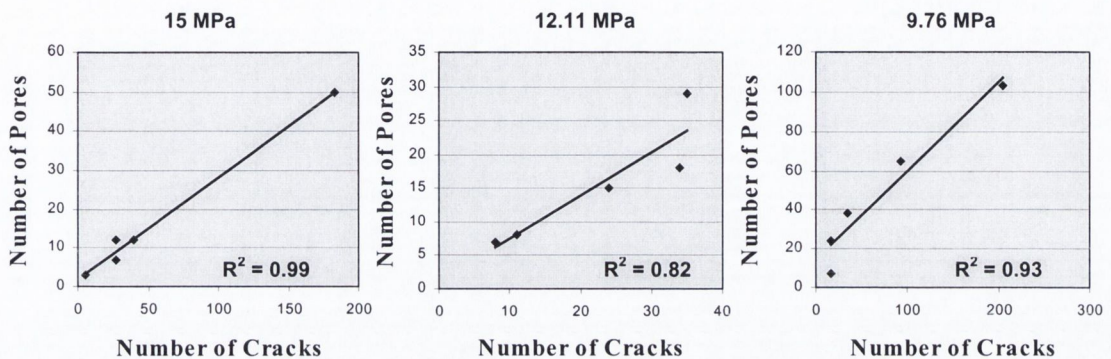
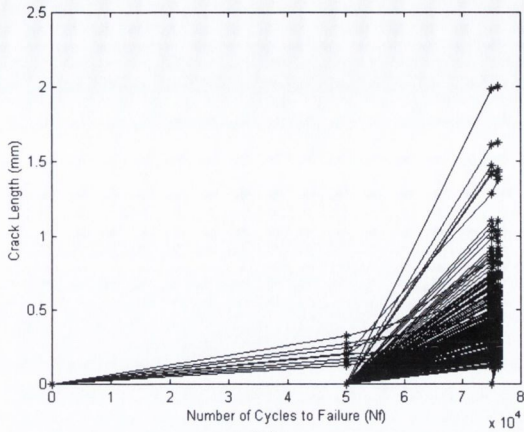


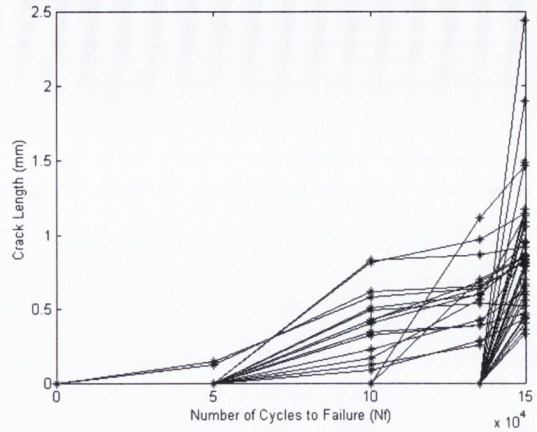
Figure 4.14 Plots of the number of cracks per specimen versus the number of pores for each specimen. It can be seen that the number of cracks is dependent on the number of pores.

Since fatigue damage was measured at specific times throughout a specimen's fatigue life, *individual* cracks could be monitored to observe when they initiated and to discern their propagation pattern. Specimens that were tested at the high stress level (15 MPa) typically accumulated little damage initially but a rapid burst of cracks would occur as the test approached failure (see Fig. 4.15). In the case of the intermediate stress level (12.11 MPa) the number of cracks appearing near to failure reduced; the general trend indicates that cracks forming early on in a specimen's fatigue life tend to grow to a certain length, after reaching this length crack growth seems to become stable (Fig. 4.16). The pattern of cracking at the low stress level (9.76 MPa) further emphasises this trend of non-propagating cracks, see Fig. 4.17.

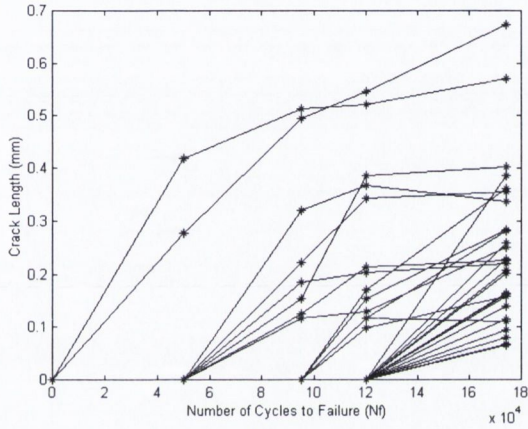
On a number of the crack propagation charts (i.e. Figs. 4.15, 4.16, and 4.17) a number of cracks appear to decrease in length, this was due to dye lying on the surface of the specimen obscuring the correct location of the crack tip, or a blurred specimen where it proved difficult to make out the crack tip precisely.



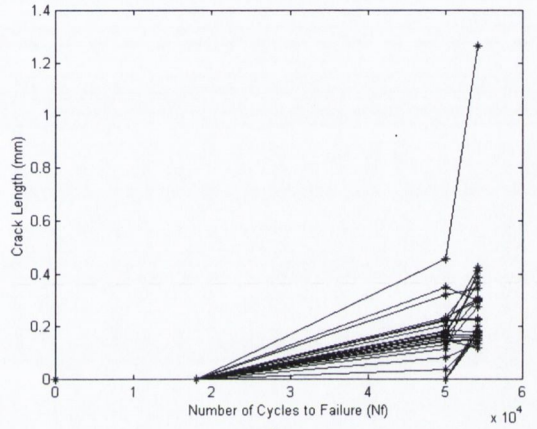
(a)



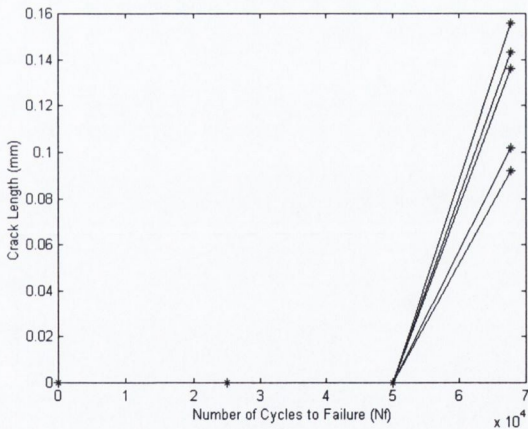
(b)



(c)



(d)



(e)

Figure 4.15 Crack growth graphs for each of the five specimens tested at 15 MPa.

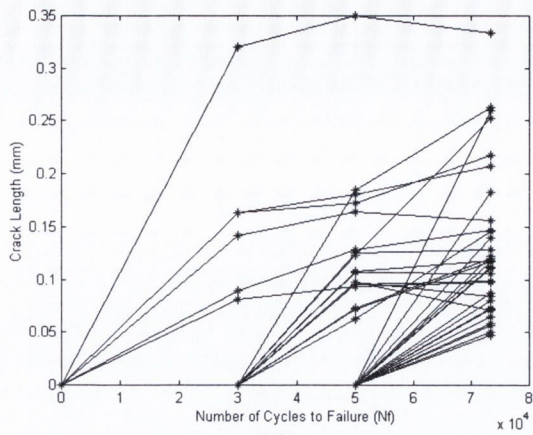
(a) 183 cracks, 73,123 cycles to failure

(b) 40 cracks, 149,592 cycles to failure

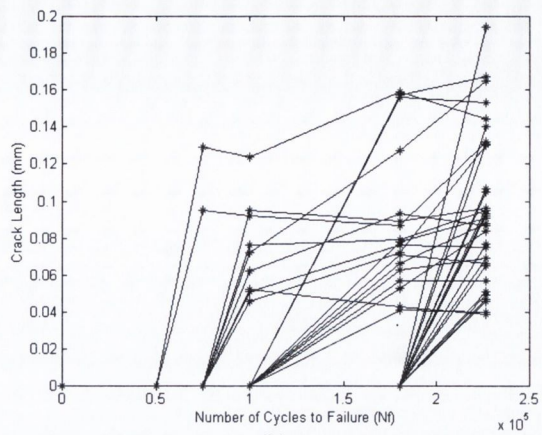
(c) 27 cracks, 174,290 cycles to failure

(d) 27 cracks, 54,236 cycles to failure

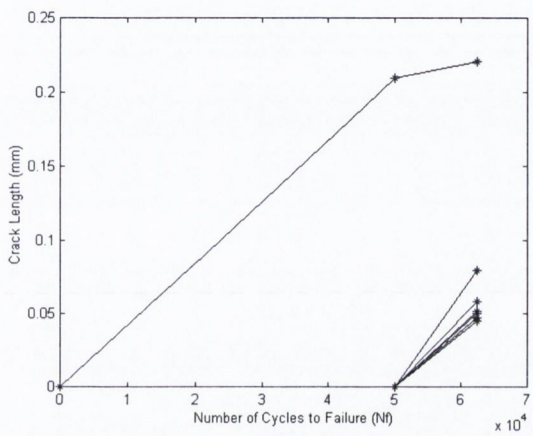
(e) 5 cracks, 67,668 cycles to failure



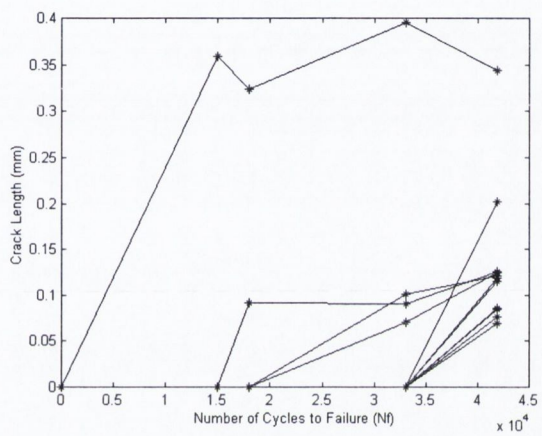
(a)



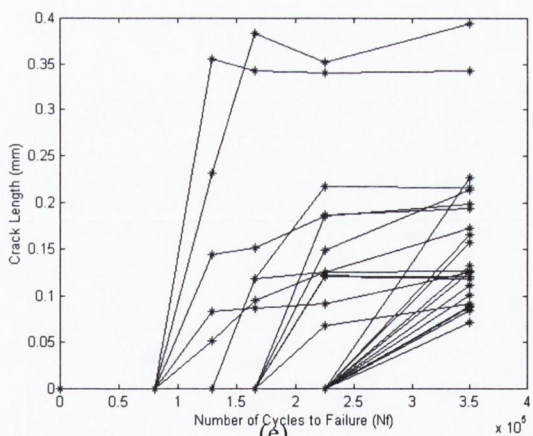
(b)



(c)



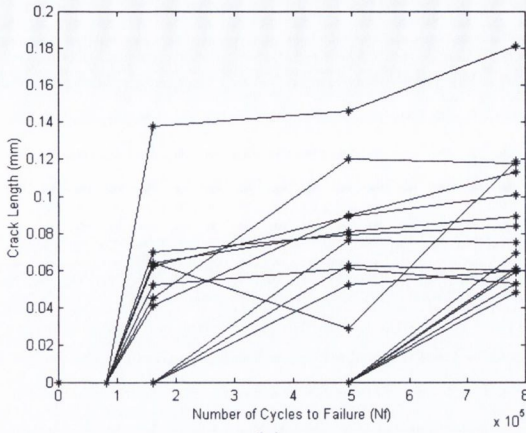
(d)



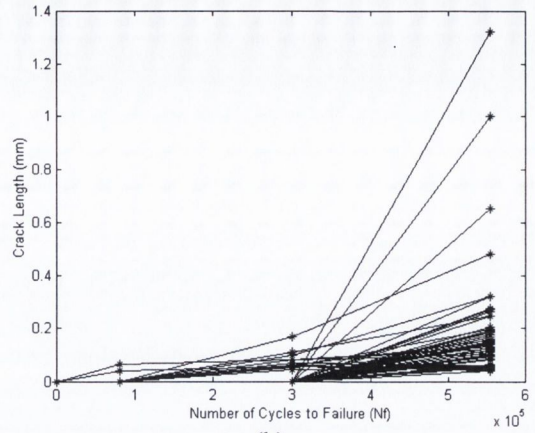
(e)

Figure 4.16 Crack growth graphs for each of the five specimens tested at 12.11 MPa.

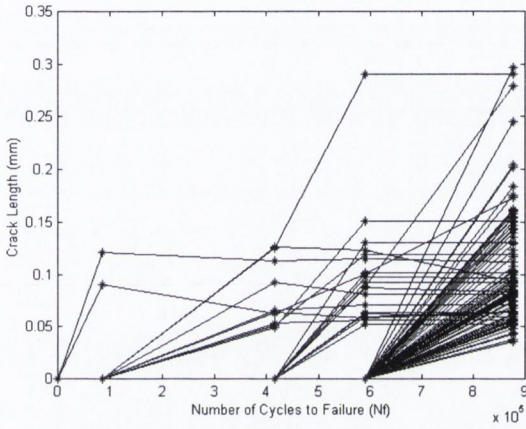
- (a) 34 cracks, 73,260 cycles to failure
- (b) 35 cracks, 226,065 cycles to failure
- (c) 8 cracks, 62,411 cycles to failure
- (d) 14 cracks, 41,895 cycles to failure
- (e) 24 cracks, 350,250 cycles to failure



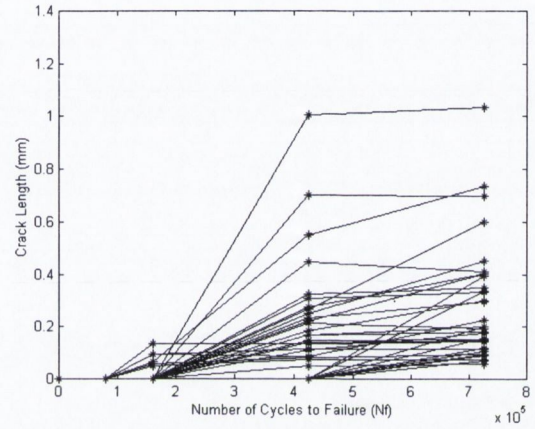
(a)



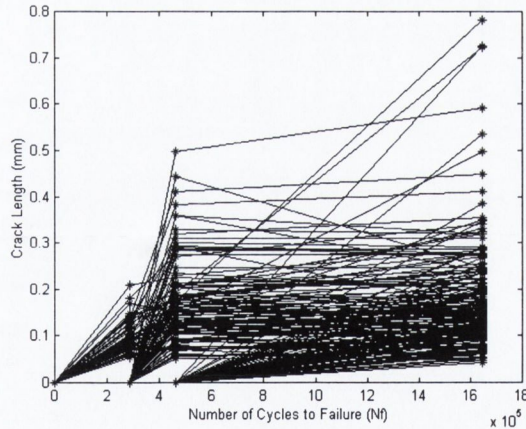
(b)



(c)



(d)



(e)

Figure 4.17 Crack growth graphs for each of the five specimens tested at 9.76 MPa.

- (a) 16 cracks, 783,566 cycles to failure
- (b) 16 cracks, 554,475 cycles to failure
- (c) 92 cracks, 876,250 cycles to failure
- (d) 34 cracks, 725,397 cycles to failure
- (e) 205 cracks, 1,644,158 cycles to failure

4.3.1 The determination of damage evolution curves

Presently computer models which incorporate a damage accumulation mode of failure assume damage evolves according to equation 4.5, where $\gamma = 1$, i.e. Miner's Law. However, the experimental results from this study show that $\gamma \neq 1$ and that damage evolution in acrylic bone cement is non-linear.

$$\frac{\omega}{\omega_f} = \left(\frac{N}{N_f} \right)^\gamma \quad \text{Eqn. 4.5}$$

ω_f is the total damage at failure, N is the number of cycles at a time t , N_f is the number of cycles at failure, and γ is a material constant. ω is the damage at a point in time i.e.,

$$\omega(t) = \sum_{i=1}^{n_c} a_i(t), \quad \text{Eqn. 4.6}$$

where n_c is the total number of cracks in a specimen and a_i is the length of the i^{th} crack.

Graphs of the non-linear damage evolution process were determined from the experimental data of the kind shown in Figs. 4.15, 4.16, and 4.17. The first step in the process is to sum the crack lengths at each measurement point and plot these against the number of cycles at each measurement point. This was done for each specimen at each stress level; these plots are shown in Fig. 4.18 (9.76 MPa), Fig. 4.20 (12.11 MPa), and Fig. 4.22 (15 MPa). This data is normalised as follows: on the x -axis the number of cycles is normalised by the number of cycles to failure and next the y -axis is normalised by the sum of the crack lengths at failure. Power law curves were fitted to these data and the result shows that damage accumulation in acrylic bone cement is non-linear and therefore Miner's law does not apply, see Fig. 4.19 (9.76 MPa), Fig. 4.21 (12.11 MPa), and Fig. 4.23 (15 MPa). Furthermore the non-linearity appears to increase as stress increases. As stress increases, the mean value of γ increases, see Table 4.5. A statistically significant difference exists between the power law constants at the 15 MPa level compared to the 12.11 MPa level. Similarly, a statistically significant difference exists between the 15 MPa and 9.76 MPa stress level; however, there is no statistically significant difference between the 12.11 MPa group and the 9.76 MPa group. These significance values hold for both the student's T-test and the Mann and Whitney test, at a significance level of $p < 0.05$.

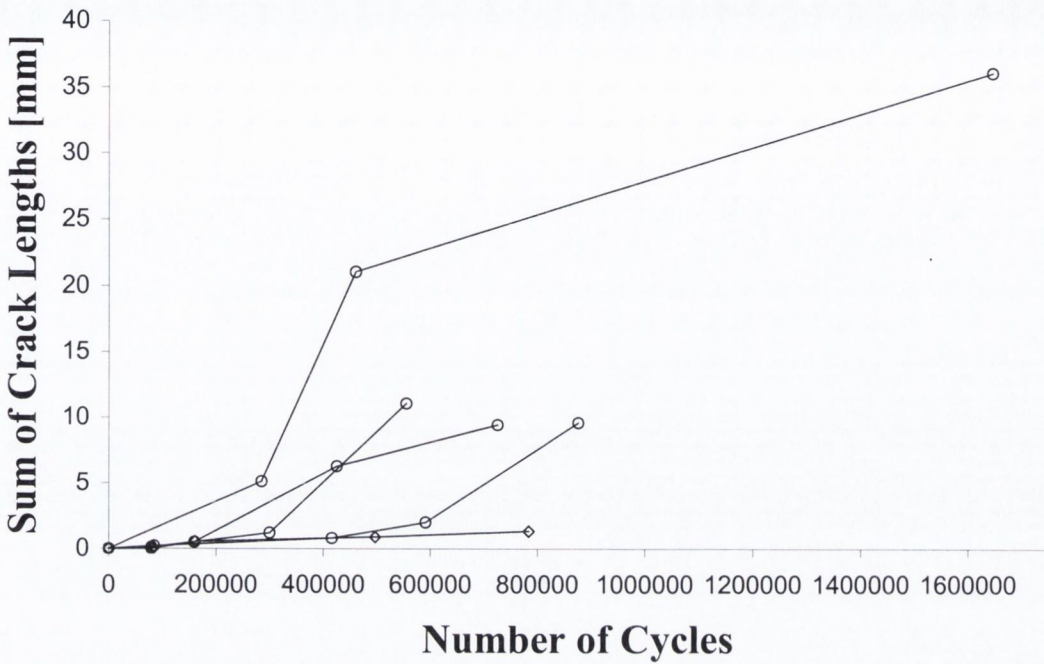


Figure 4.18 The sum of the crack lengths at each measurement point for the specimens tested at 9.76 MPa

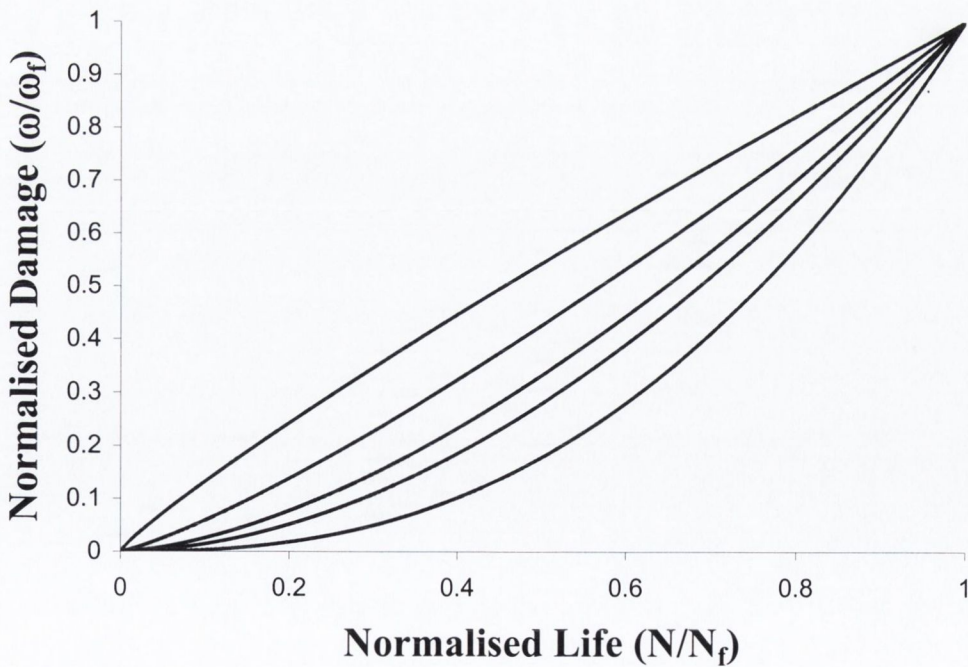


Figure 4.19 Power law curves fitted to the normalised life and normalised damage for each specimen at 9.76 MPa.

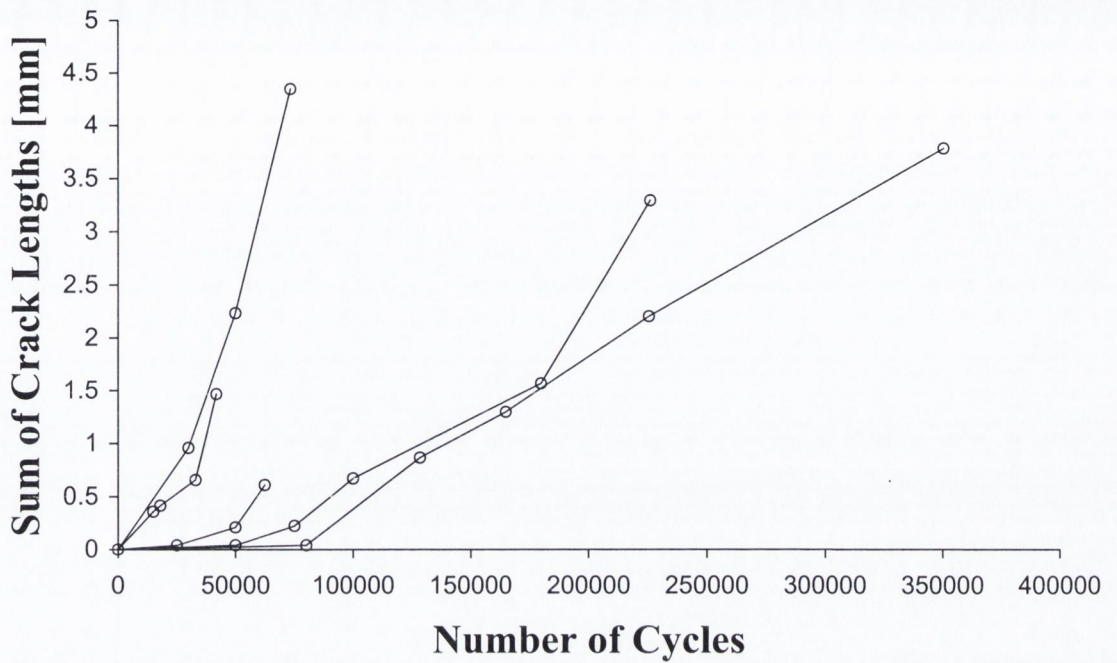


Figure 4.20 The sum of the crack lengths at each measurement point for the specimens tested at 12.11 MPa

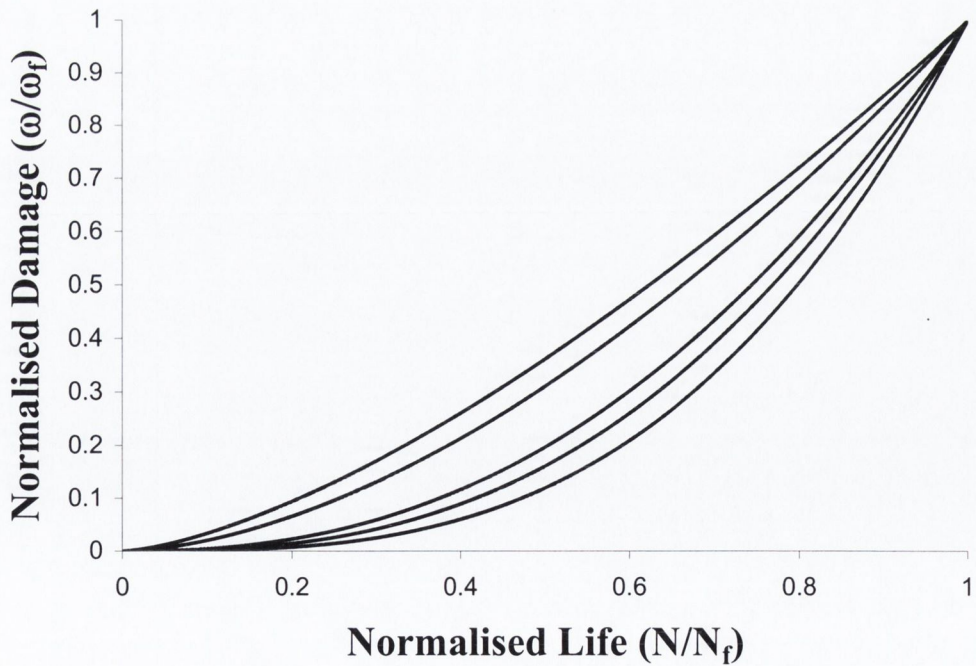


Figure 4.21 Power law curves fitted to the normalised life and normalised damage for each specimen at 12.11 MPa.

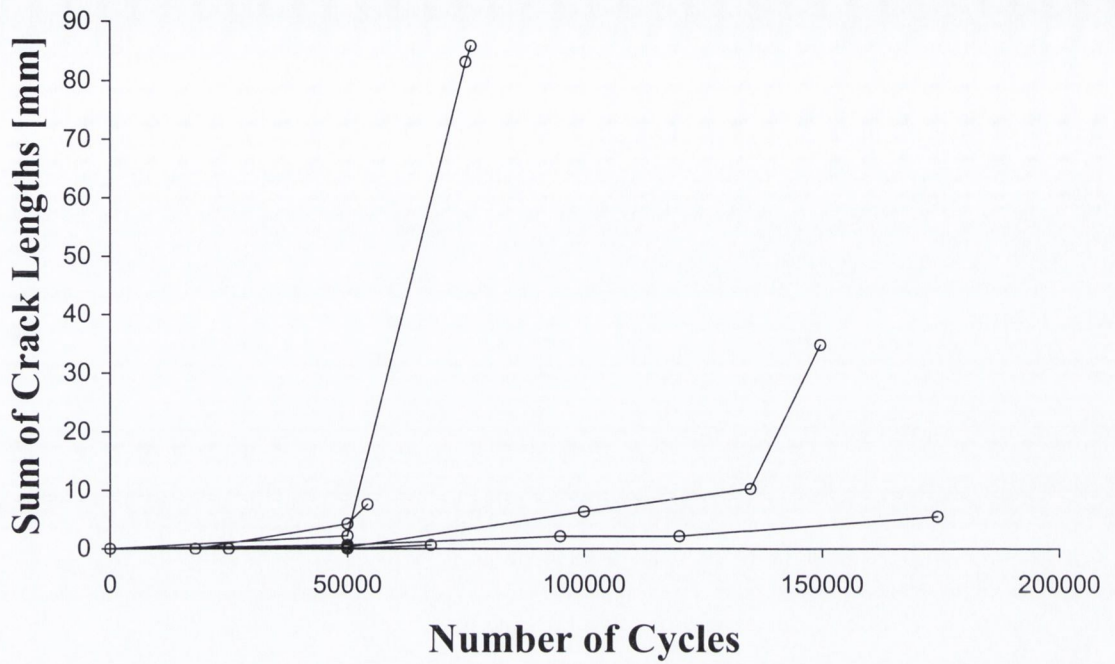


Figure 4.22 The sum of the crack lengths at each measurement point for the specimens tested at 15 MPa.

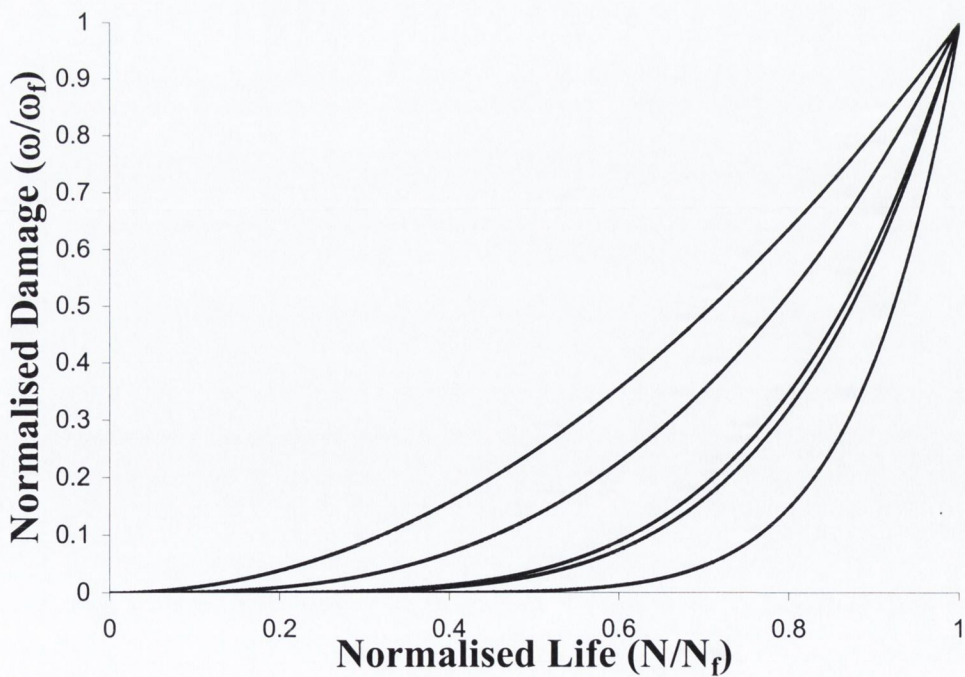


Figure 4.23 Power law curves fitted to the normalised life and normalised damage for each specimen at 15 MPa

Table 4.5 Empirical power law constants

Stress [MPa]	Power law constant, α					Average (α) [SD]
15	2.02	2.91	8.59	5.09	4.73	4.668 [± 2.53]
12.11	1.69	2.35	3.07	2.64	1.47	2.244 [± 0.66]
9.76	1.23	1.84	0.88	1.59	2.49	1.606 [± 0.61]

The average of the power law constants suggests that this value is stress dependent; however, this value was not used to characterise the *most likely* damage evolution curve. Instead the *most likely* value was taken as the power law curve fitted to all the data at each stress level, rather than the mean of a distribution, see Fig 4.24. The equations for each of the curves are as follows:

$$9.76 \text{ MPa} \quad \frac{\omega}{\omega_f} = \left(\frac{N}{N_f} \right)^{1.56} \quad \text{Eqn. 4.7}$$

$$12.11 \text{ MPa} \quad \frac{\omega}{\omega_f} = \left(\frac{N}{N_f} \right)^{2.33} \quad \text{Eqn. 4.8}$$

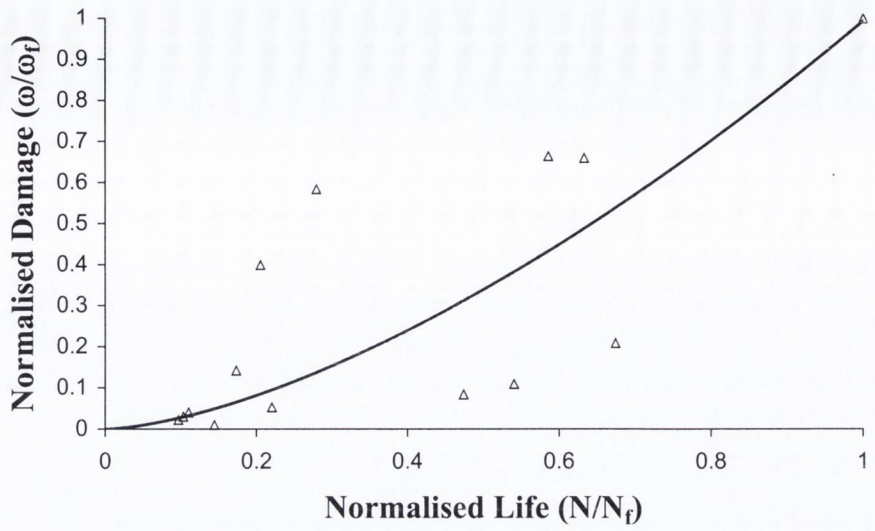
$$15 \text{ MPa} \quad \frac{\omega}{\omega_f} = \left(\frac{N}{N_f} \right)^{3.46} \quad \text{Eqn. 4.9}$$

Plotting the power law constants against the stress level shows that at the stress levels tested the parameter gamma is a function of stress, see Fig. 4.25. The equation fitted to the line in Fig. 4.25 is as follows:

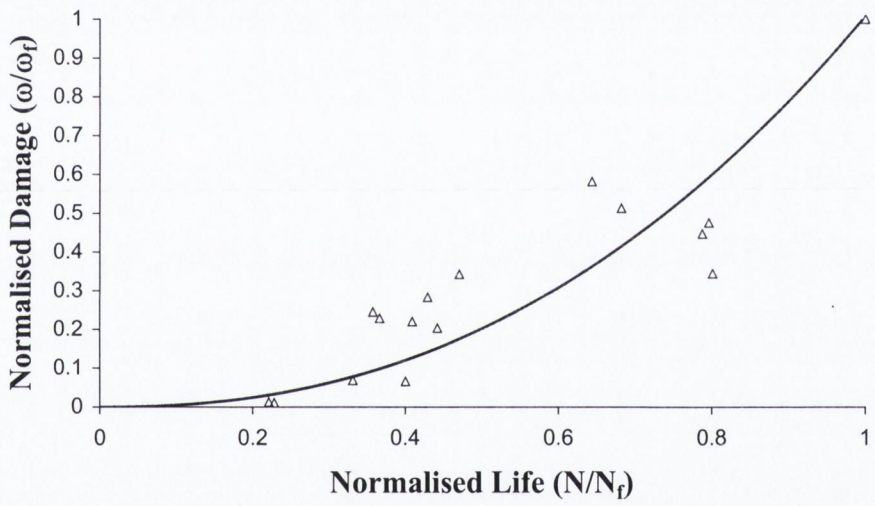
$$\sigma = 2.73\gamma + 5.6 \quad \text{Eqn. 4.10}$$

Damage evolution in acrylic bone cement can therefore be described as:

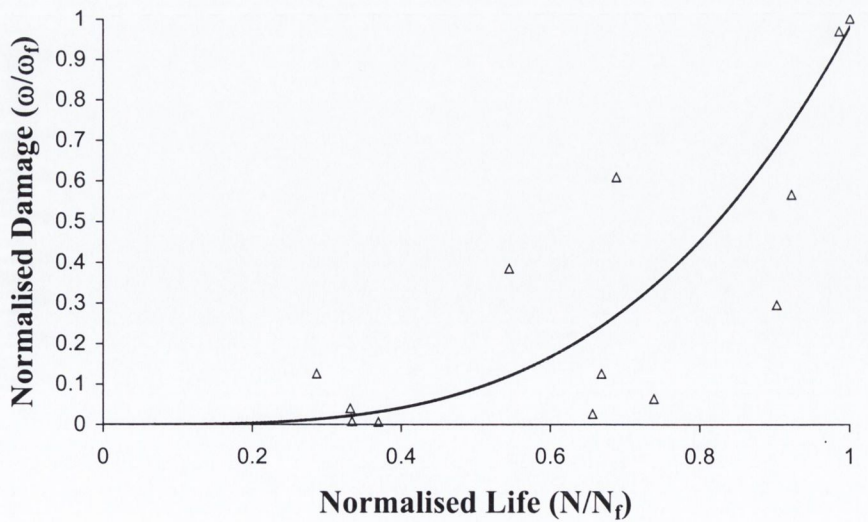
$$\frac{\omega}{\omega_f} = \left(\frac{N}{N_f} \right)^{\frac{\sigma - 5.6}{2.73}} \quad \text{Eqn. 4.11}$$



(a)



(b)



(c)

Figure 4.24 Most Likely damage evolution curves for the stress levels tested at (a) 9.76 MPa (b) 12.11 MPa (c) 15 MPa

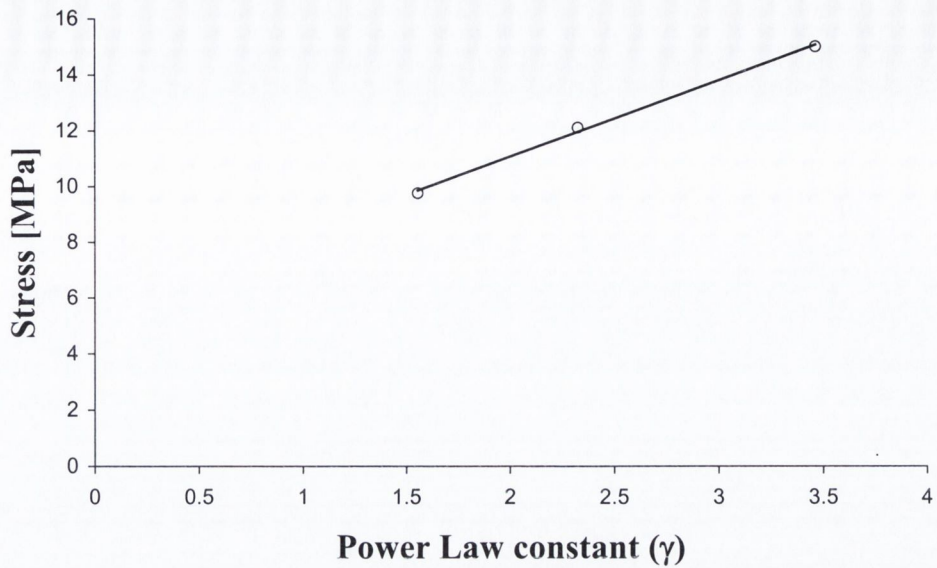


Figure 4.25 Relationship between damage evolution power law constant and cyclic stress level

4.4 Multiaxial fatigue results

The experimental procedure outlined in Chapter 3 Section 3.6 was used to determine the results obtained in this section; the objective was to determine the effect of a multiaxial stress on the fatigue life and the creep properties of acrylic bone cement. The results of this section compare control experiments under uniaxial stress to multiaxial fatigue tests; while the multiaxial tests do not replicate exactly the axial stress of the control specimens (the multiaxial specimens have an increased mean stress and a slightly reduced $\Delta\sigma$). However, it can be assumed that the slight drop in $\Delta\sigma$ and the increase in mean stress will have an insignificant effect on the failure life compared to the presence of multiaxial stresses.

4.4.1 Effect of off-axis stress on fatigue life

At a $\Delta\sigma$ of 15 MPa the average fatigue life reduces to 40% of the uniaxial fatigue life when an equal hoop stress is applied, and similarly, under a change in axial stress of 11 MPa, and a hoop stress of 16.5 MPa the fatigue life is reduced to 30% of the uniaxial value. However an anomalous result is found at 11 MPa axial and hoop

stress whereby a 16% increase in fatigue life occurs compared to 11 MPa axial alone, see Table 4.6 for values.

Table 4.6 Summary fatigue results for the tubular specimens. *p*-values are reported is for the multiaxial stress states versus its corresponding control set.

Axial $\Delta\sigma$	Mean N_f	Standard	<i>p</i> value	<i>p</i> value
15 MPa		Deviation N_f	Mann – Whitney	Student’s t-test
Hoop = 0	68,957	$\pm 89,764$		
Hoop = 15 MPa	28,757	$\pm 53,797$	0.09	0.19

Axial $\Delta\sigma$	Mean N_f	Standard	<i>p</i> value	<i>p</i> value
11 MPa		Deviation N_f	Mann – Whitney	Student’s t-test
Hoop = 0	545,135	$\pm 635,276$		
Hoop = 11 MPa	646,062	$\pm 437,963$	0.41	0.38
Hoop = 16.5 MPa	159,302	$\pm 177,326$	0.06	0.09

Therefore the results clearly indicate the significant effect of the multiaxial nature of the stress, even if considerable variability masks the effect to some degree. The high *p* values show that no significant statistical difference exists between the control data set with a change in axial stress of 11 MPa and the pressurised set with axial and hoop stresses equal to 11 MPa, therefore the two data sets can be assumed to be from the same population. This can be seen clearly when the distribution of fatigue strength is plotted using the two-parameter Weibull distribution, see Fig. 4.26. The distribution of fatigue strength for the higher hoop stress levels is consistently more variable than the control specimens and the group tested at the lower hoop stress level (see Fig 4.26 and Fig. 4.27).

The cumulative Weibull distributions (Fig. 4.26 and Fig. 4.27) confirm the reduction in fatigue strength at the high hoop stress values, whereby a significant decrease in fatigue strength at 50% probability-of-survival exists, and represents a decrease in fatigue life of approximately one order of magnitude. While at the low hoop stress (11 MPa) no such difference in fatigue strength exists, see Fig. 4.26.

One possible reason why no difference in fatigue strength exists at the low hoop stress level may be due to the lower fluctuating pressure resulting in a more consistent hoop stress. The fluctuation in pressure during the fatigue tests was noted

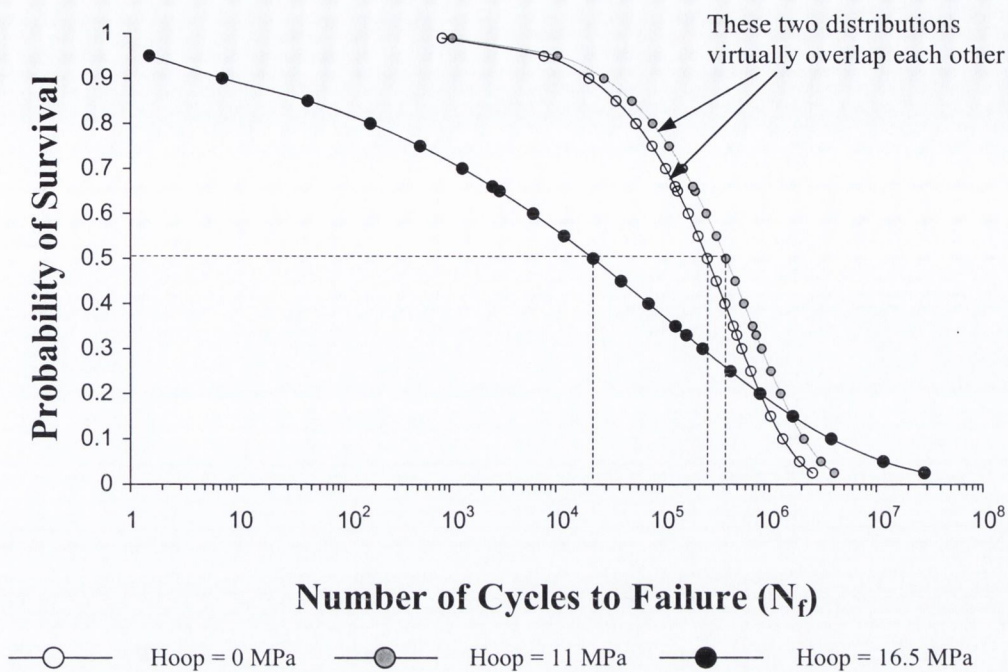


Figure 4.26 Cumulative Weibull distributions for the fatigue tests with an axial stress of 11 MPa. The distribution of fatigue strength of the specimens with no hoop stress is almost identical to the distribution of fatigue strength of the specimens which had a hoop and axial stress of 11 MPa. While the distribution of fatigue strength of the specimens tested at the higher hoop stress (16.5 MPa) is notably different; this distribution spans a wide range of fatigue life (higher variability).

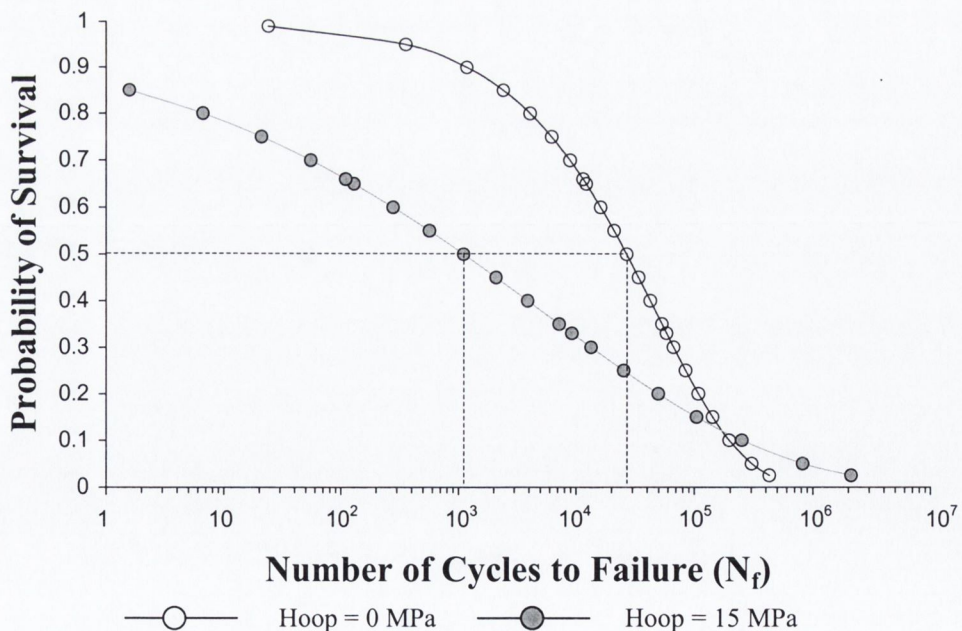


Figure 4.27 Cumulative Weibull distributions for the fatigue tests with an axial stress of 15 MPa. The distribution of fatigue strength of the specimens tested under multiaxial conditions (hoop and axial stress equal to 15 MPa) shows that the fatigue life at 50% probability of survival is reduced significantly; moreover, the variation in fatigue strength is increased, as the distribution spans a wide range.

for each test series. At the higher pressures the fluctuation in internal pressure tended to be greater because a small change in volume resulted in a large pressure change, as the oil was compressed to a greater level. The approximate values for each set-up were noted by checking the fluctuation in pressure on the dial of the pressure gauge, see Table 4.7. The higher hoop stresses caused a greater fluctuation in pressure thus causing the constant stress to fluctuate by more than 10% compared to only 6% at the lower hoop stress values (see Table 4.7 for values).

Table 4.7 Fluctuation in hoop stress caused by specimen expansion and resulting R-ratio. (R-ratio is defined as the minimum cyclic stress value divided by the maximum cyclic stress value).

Axial Stress [MPa]	Hoop Stress [MPa]	Approximate Pressure Fluctuation [Psi]	Minimum Hoop Stress Value [MPa]	Resulting R-ratio
15	15	60	13.1	0.87
11	11	20	10.37	0.94
11	16.5	50	14.9	0.90

4.4.2 Creep induced by cyclic loading

The amount of specimen extension at the first measurement point (400 cycles) showed that the axial deformation was a function of the von Mises equivalent stress, see Fig. 4.28. However, this was not true for the amount of axial deformation at failure (Fig. 4.29), this was due to, firstly, the different failure lives of the specimens, and secondly, the slope of the steady state creep is different for each testing group.

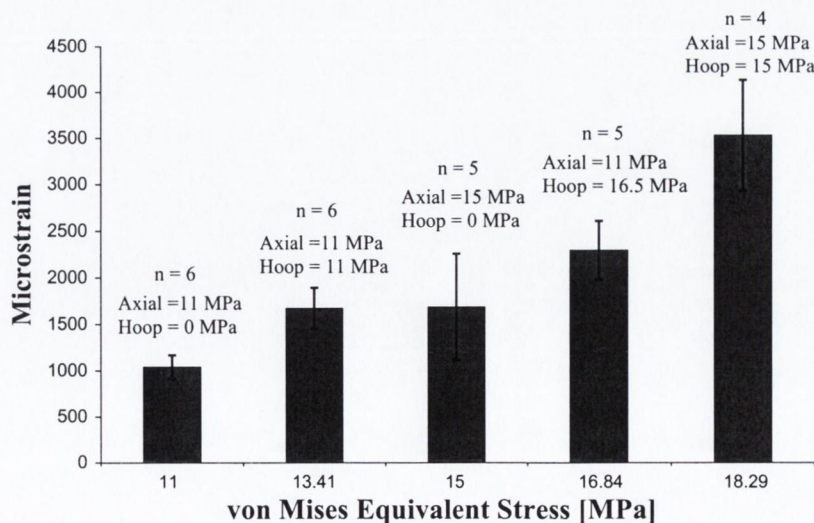


Figure 4.28 Initial deformation measured in the axial direction showing that the axial extension is a function of the von Mises equivalent stress. The values are taken at the first sampling point (i.e. after 400 load cycles).

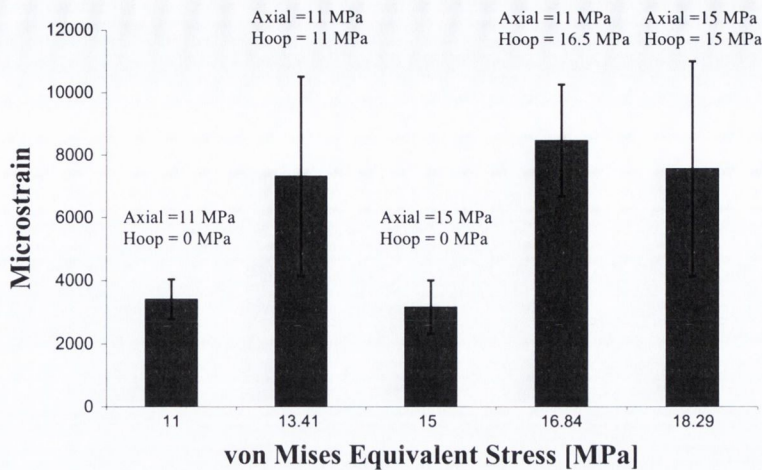


Figure 4.29 *The extension of the specimens at the last sampling point before failure of the specimen occurred. The extension does not conform to the von Mises equivalent because of different failure lives and different extension slopes.*

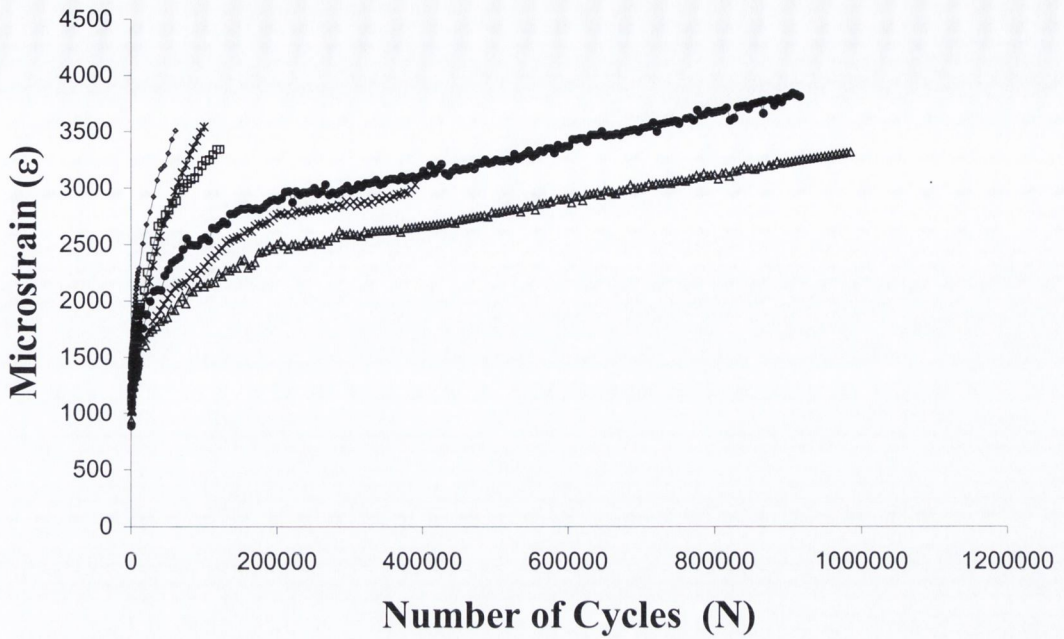
Primary and secondary creep was recorded for each specimen (except for specimens whose failure life was too low to capture any specimen extension); no tertiary creep was recorded for any specimen. Primary creep is clearly visible in Figs. 4.30 (a), 4.31 (a), 4.32 (a) and 4.33 (a). After the primary creep phase steady state creep dominates the remaining life of each specimen. The data was also plotted on a double log scale [Figs. 4.30 (b), 4.31 (b) 4.32 (b) and 4.33 (b)], similar to the analysis of Verdonschot and Huiskes (1994), and a relationship between microstrain and the number of loading cycles was established for each specimen by plotting a regression line of the following form through all the data points:

$$\log(\varepsilon) = A \log(N) + B \quad \text{Eqn. 4.12}$$

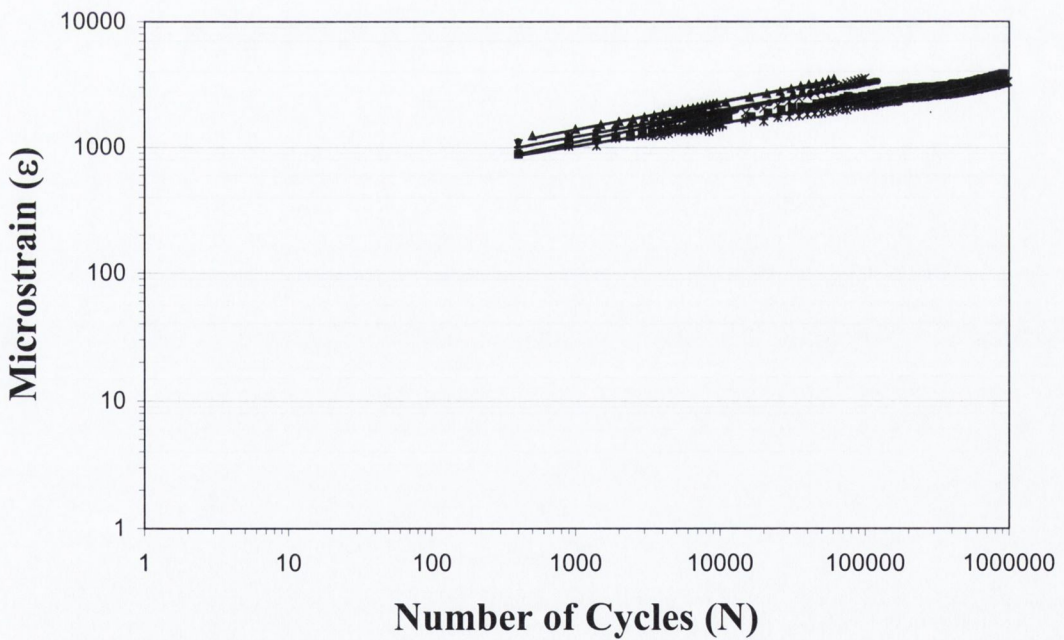
where A and B are constants and ε is the axial strain. The parameter A is the slope of the line, and the parameter B represents the initial displacement after one loading cycle.

The parameter B has the greatest value at the 15 MPa uniaxial stress level (Table 4.8). When a comparison is made between the multiaxial stress states with an axial stress of 11 MPa the parameter B increases as the hoop stress increases from 0 MPa to 16.5 MPa.

The values for the multiaxial stress state of axial and hoop stress equal to 15 MPa were not plotted in the following figures as the failure life was too low to record enough specimen extension data to plot a creep curve.

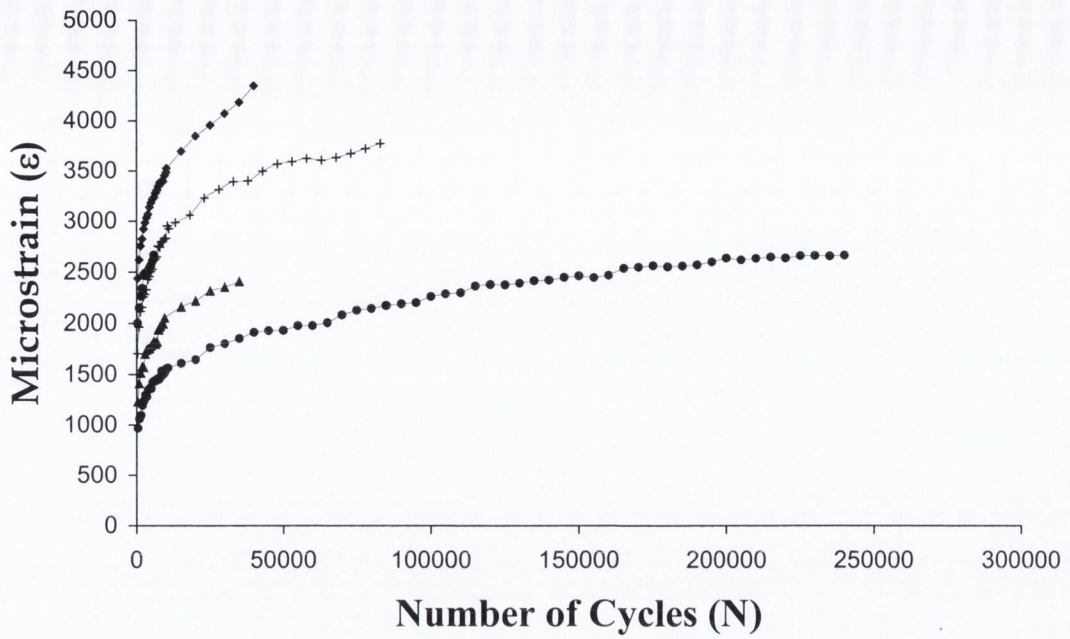


(a)

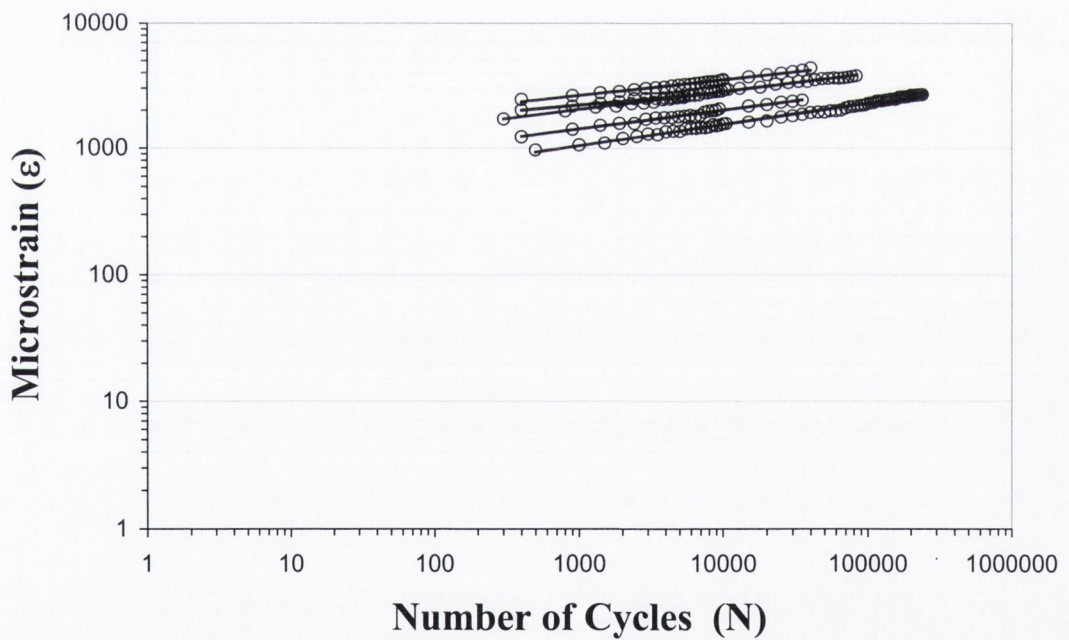


(b)

Figure 4.30 Uniaxial creep data for an axial stress of 11 MPa, graph (a) clearly shows the primary and secondary creep region for each specimen. Regression lines have been fitted to the data on a log-log scale in (b) and their constants are given in Table 4.8.

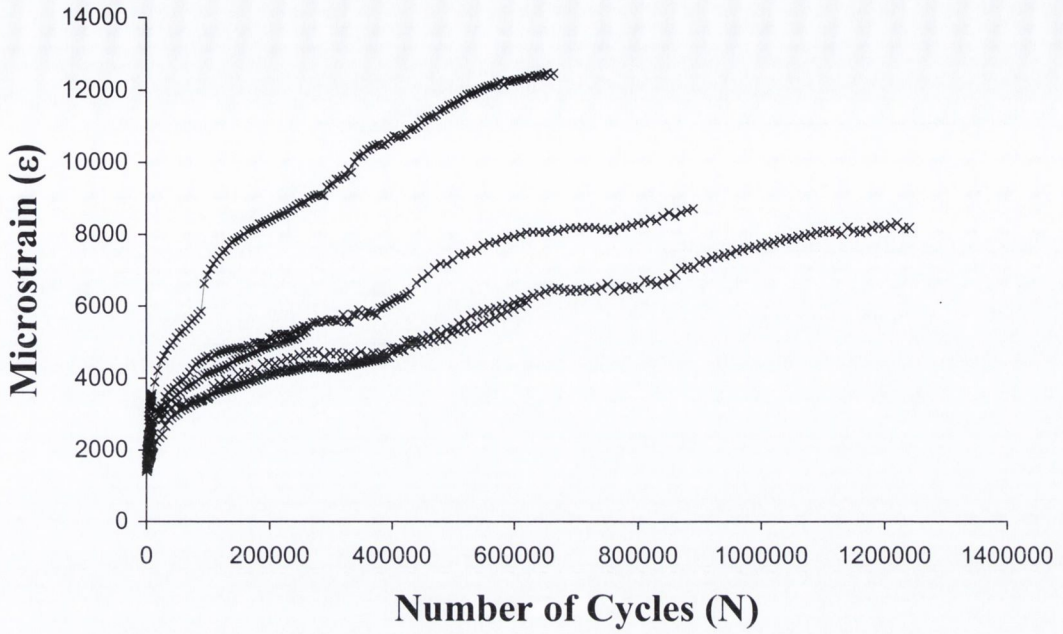


(a)

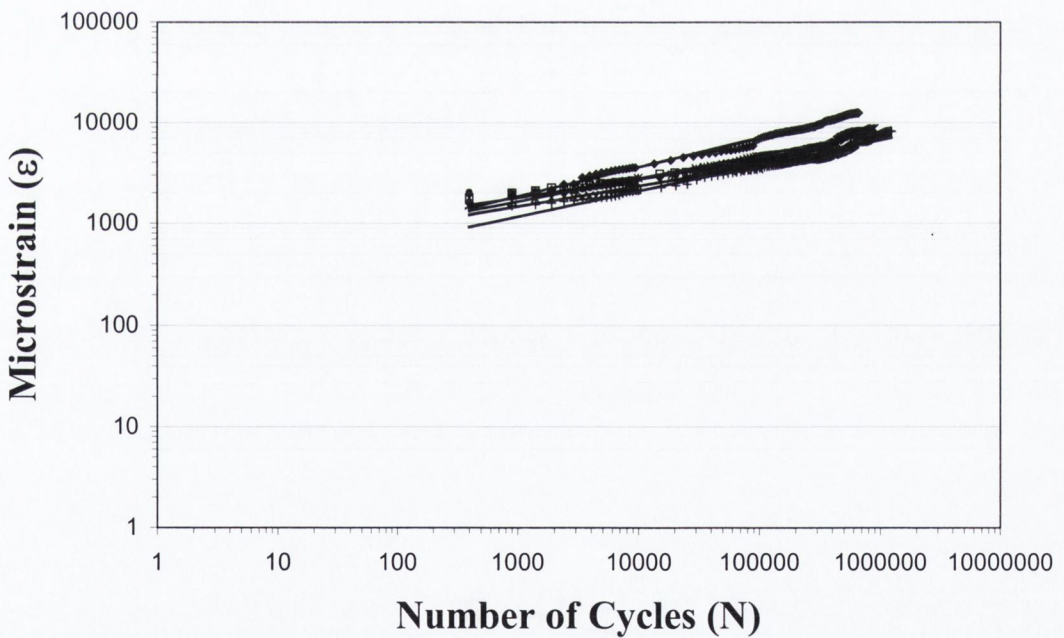


(b)

Figure 4.31 Uniaxial creep data for an axial stress of 15 MPa, graph (a) clearly shows the primary and secondary creep region for each specimen. Regression lines have been fitted to the data on a log-log scale in (b) and their constants are given in Table 4.8.

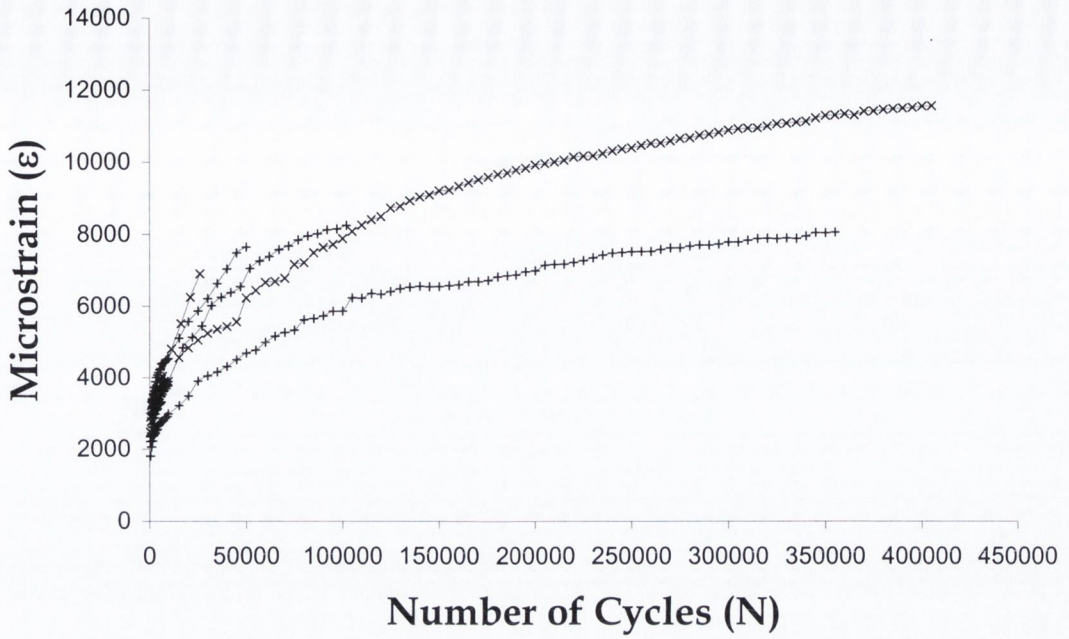


(a)

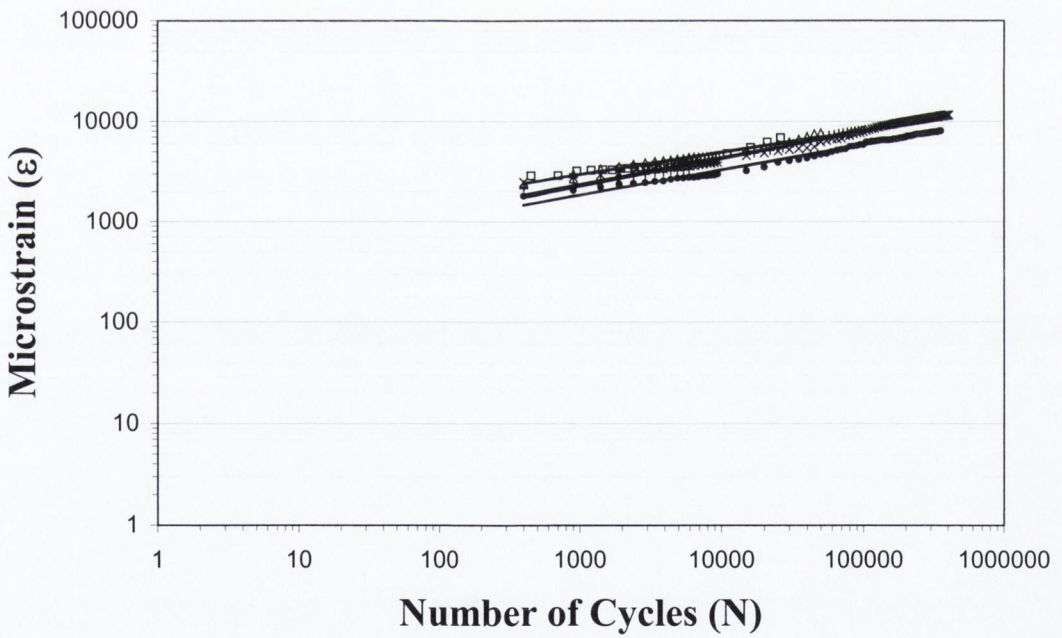


(b)

Figure 4.32 Uniaxial creep data for specimens with a change in axial stress of 11 MPa and a hoop stress of 11 MPa, graph (a) clearly shows the primary and secondary creep region for each specimen. Regression lines have been fitted to the data on a log-log scale in (b) and their constants are given in Table 4.8.



(a)



(b)

Figure 4.33 Uniaxial creep data for specimens with a change in axial stress of 11 MPa and a hoop stress of 16.5 MPa, graph (a) clearly shows the primary and secondary creep region for each specimen. Regression lines have been fitted to the data on a log-log scale in (b) and their constants are given in Table 4.8.

Table 4.8 Table of the regression line constants fitted to the log-log creep data presented in figures 4.30, 4.31, 4.32, and 4.33.

(a) 11 MPa uniaxial regression line constants

Specimen	$\log_{10}(\epsilon_c) = A \log(N) + B$		Microstrain	N_f
	A	B	B^{10}	
1	0.1667	2.503	318.81	1,663,092
2	0.2087	2.458	286.76	126,209
3	0.2355	2.335	216.13	104,453
4	0.1799	2.497	313.9	922,163
5	0.1808	2.466	292.25	392,287
6	0.2087	2.478	300.46	62,604

(b) 15 MPa uniaxial regression line constants

Specimen	$\log_{10}(\epsilon_c) = A \log(N) + B$		Microstrain	N_f
	A	B	B^{10}	
1	0.13	3.039	1095	40,869
2	0.14	2.873	747	82,400
3	0.10	3.030	1072	6,251
4	0.15	2.699	501	38,705
5	0.17	2.510	324	242,514

(c) 11 MPa axial and hoop stress regression line constants

Specimen	$\log_{10}(\epsilon_c) = A \log(N) + B$		Microstrain	N_f
	A	B	B^{10}	
1	0.1451	2.862	727.26	37,701
2	0.2554	2.294	197.00	1,237,259
3	0.2913	2.389	245.39	822,352
4	0.1846	2.698	498.35	261,336
5	0.2299	2.522	332.9	890,964
6	0.2050	2.548	352.9	626,760

(d) 11 MPa axial and 16.5 MPa hoop stress regression line constants

Specimen	$\log_{10}(\epsilon_c) = A \log(N) + B$		Microstrain	N_f
	A	B	B^{10}	
1	0.222	2.805	638.81	50,865
2	0.2508	2.514	326.24	355,938
3	0.2275	2.519	330.91	105,539
4	0.1801	2.943	877.70	33,652
5	0.2643	2.581	381.17	409,801

4.5 Calculation of the Monkman-Grant constant

The Monkman-Grant const (i.e. C in Eqn. 1.1 (page 7)) was calculated from the creep data at three stress levels: uniaxial stress of 11 MPa, and the multiaxial stress states of 11 MPa axial and hoop stress, and 11 MPa axial and 16.5 MPa hoop stress. The Monkman-Grant constant was calculated as follows: linear regression lines were fitted to the creep data for each specimen, see Fig. 4.34 (11 MPa axial).

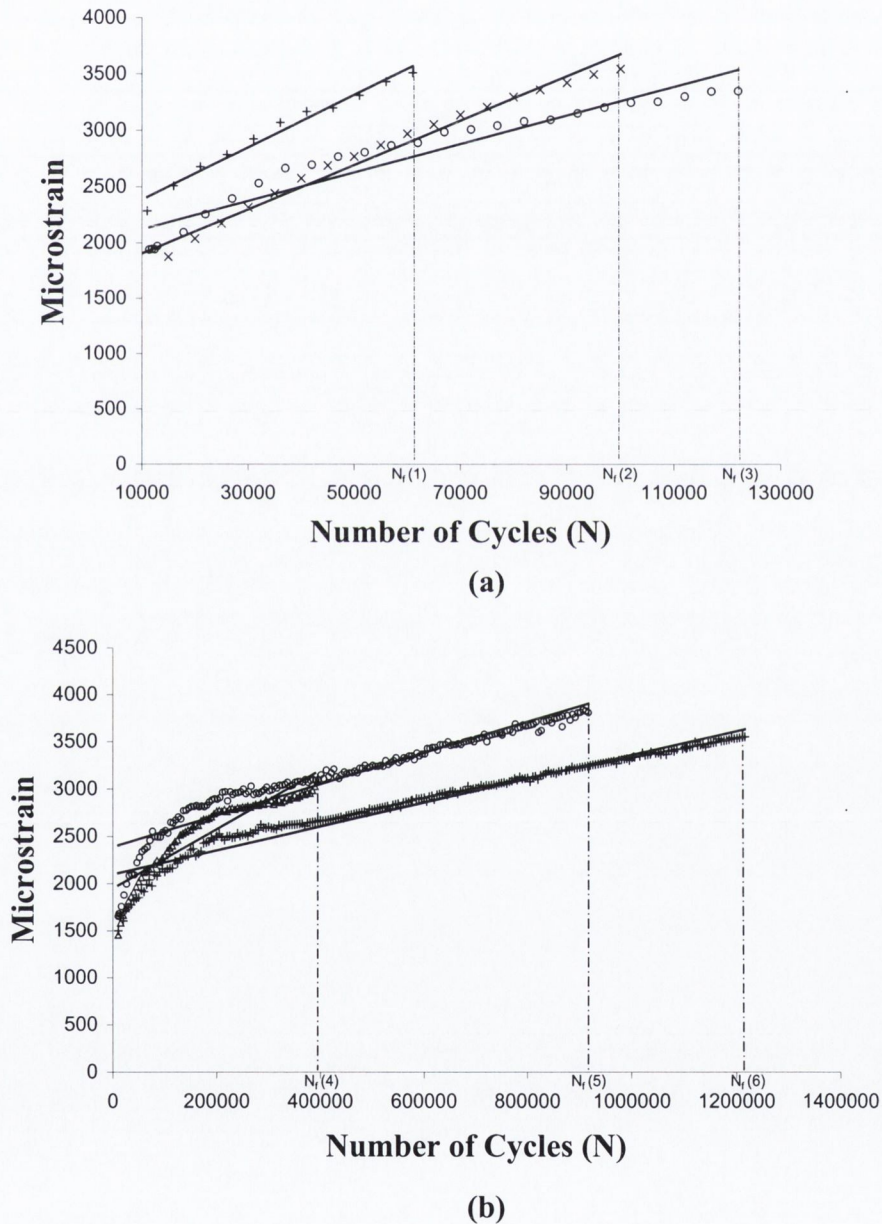


Figure 4.34 The creep curves for the three specimens (axial 11 MPa) with a low fatigue life are plotted in (a) and linear regression lines have been fitted to the creep data from 10,000 cycles to the last sampling point before failure. Similarly the three specimens with a greater fatigue life have been plotted in (b) and linear regression lines have been fitted to the data. The slope of the regression lines is given in Table 4.9.

Table 4.9 The slope of the regression lines plotted in Fig. 4.34 and the corresponding time to failure for each specimen at an axial stress of 11 MPa.

Specimen	Slope ($\dot{\epsilon}_{ss}$)	Number of Cycles to Failure (N_f)	1/Time to Failure ($1/t_f$)
1	0.0232	62,604	7.9×10^{-5}
2	0.0197	104,453	4.8×10^{-5}
3	0.0126	126,209	3.9×10^{-5}
4	0.0031	392,287	1.3×10^{-5}
5	0.0014	922,163	5.4×10^{-6}
6	0.0016	1,663,092	3×10^{-6}

The slope of the regression line plotted in Fig. 4.34 was plotted against the inverse of the time to failure, see Fig. 4.35. A regression line passing through zero was fitted to this data and the constant C was determined (i.e. the slope of the regression line), see Eqn. 4.13. This procedure was repeated for the multiaxial stress states with an axial stress of 11 MPa and a hoop stresses of 11 MPa and 16.5 MPa, see Fig. 4.36 and 4.37.

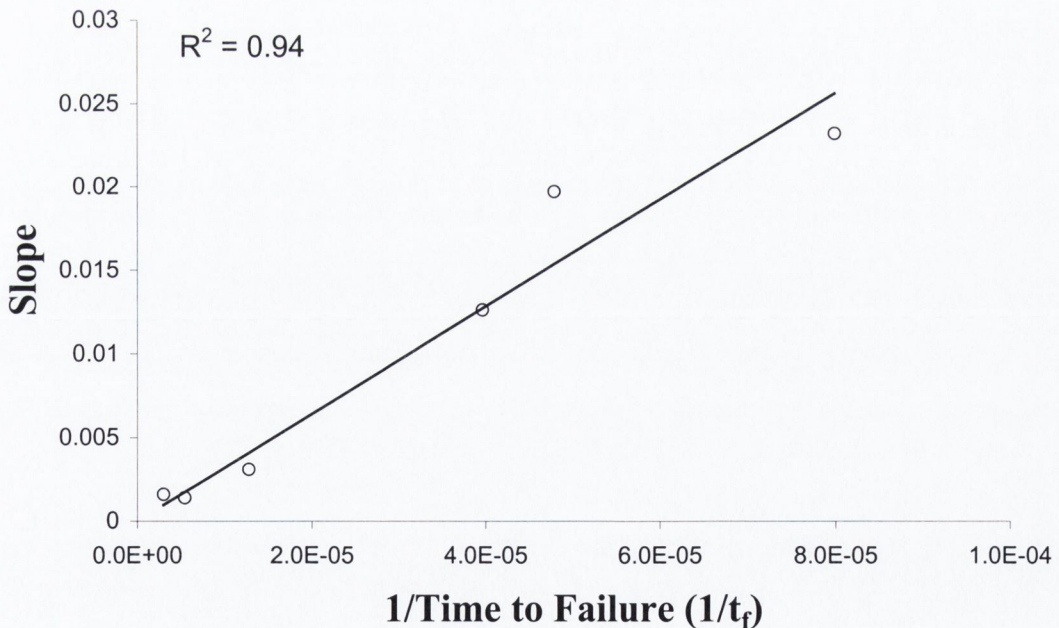


Figure 4.35 The slope of the steady state creep region of each specimen tested at an axial stress of 11 MPa and 0 MPa hoop stress plotted against the inverse of the time to failure.

The equation of the regression line fitted in Fig. 4.35:

$$\dot{\epsilon}_{ss} = 321/t_f \quad \text{Eqn. 4.13}$$

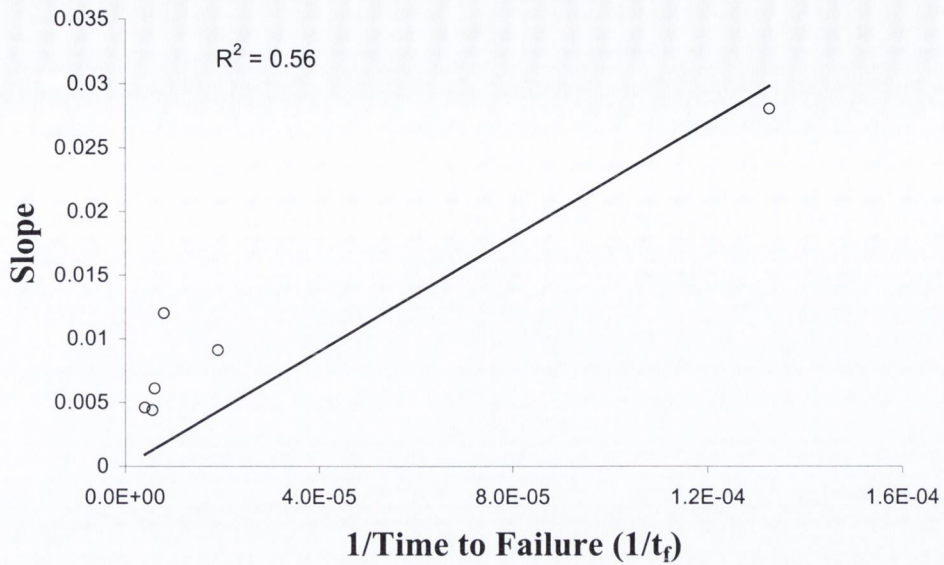


Figure 4.36 The slope of the steady state creep region of each specimen tested at 11 MPa axial and hoop stress plotted against the inverse of the time to failure.

The equation of the regression line fitted in Fig. 4.35:

$$\dot{\epsilon}_{ss} = 225/t_f \quad \text{Eqn. 4.14}$$

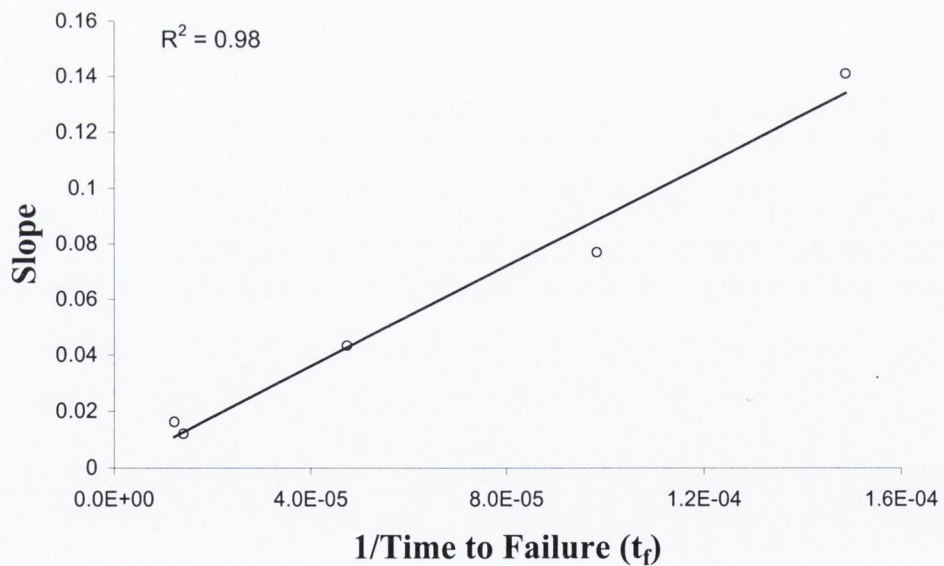


Figure 4.37 The slope of the steady state creep region of each specimen tested at 11 MPa axial and 16.5 MPa hoop stress plotted against the inverse of the time to failure.

The equation of the regression line fitted in Fig. 4.36:

$$\dot{\epsilon}_{ss} = 901/t_f \quad \text{Eqn. 4.15}$$

Chapter 5

Discussion

5.1 Overview	101
5.2 Comparison of hand-mixed and vacuum-mixed cement	101
5.2.1 Magnitude of fatigue strength	101
5.2.2 Reporting of S-N curves	103
5.2.3 Variability of fatigue strength	104
5.2.4 Weibull analysis of strength and variability of strength	105
5.3 Damage accumulation in acrylic bone cement	107
5.4 The choice of S-N curves for finite element analysis	110
5.5 Multiaxial Fatigue: effect on fatigue life	115
5.6 Creep – fatigue interaction	117
5.7 The application of the Monkman-Grant relationship	118

5.1 Overview

In the Introduction chapter of this thesis it was concluded that several aspects of the fatigue behaviour of acrylic bone cement needed further investigation. A list of questions was posed regarding the fatigue strength of acrylic bone cement and it was proposed that the answers to these questions would fundamentally advance our understanding of the fatigue behaviour of this important biomaterial, and, from a practical viewpoint would improve our capacity for pre-clinical evaluation of cemented joint replacements. A series of experimental tests were designed to answer the questions and the results were stated in the previous chapter. This chapter presents an examination of the results with regard to their implications and limitations.

Before the results are discussed certain features of the clinical situation need to be mentioned. First the complex *in vivo* loading cycle is approximated by a sine wave in the tests. Secondly the effect of entrapment of blood and other biological debris is neglected in this study, although it may significantly reduce the strength and increase damage accumulation *in vivo* (Lee *et al.*, 1978). Therefore the experiments simplify the clinical situation to some extent; however both these aspects would serve to reduce the fatigue strength and therefore the results may be seen as a kind of upper-bound to the *in vivo* fatigue performance.

5.2 Comparison of hand-mixed and vacuum-mixed cement

5.2.1 Magnitude of fatigue strength

At the four stress levels tested, the vacuum-mixed cement has a greater mean fatigue life by an order of magnitude in each case. Previous studies also found that vacuum-mixing increases the fatigue strength of acrylic bone cement (Davies *et al.*, 1990, Fritsch, 1996, Lewis, 1999, Launtenschlager *et al.*, 1986). However, several vacuum-mixed specimens have failure lives that lie within the range of the hand-mixed group, and this poses some important questions regarding the variability of fatigue strength in both groups.

The higher fatigue strength of the vacuum-mixed cement can be accounted for by a fracture surface analysis. James *et al.* (1992) made the observation that the presence of two or more pores near each other caused stress concentrations, which initiated several cracks in the form of river patterns. Furthermore the present study found that adjacent pores were associated with the growth of discontinuous crack growth bands. The lower strength of the hand-mixed cement seems to be due to interacting pores which cause stress concentrations. A common observation was that a combination of a large and a small pore formed a crack initiation site, see Figs. 4.4 (page 68), 4.5, 4.6 (page 69). Tsukrov and Kackanov (1994) analysed the interaction of different sized pores in brittle elastic solids, and their study found that the primary interaction site was between large and small pores, rather than between pores of equal size. Therefore the theoretical analysis by Tsukrov and Kackanov (1994) is confirmed by the results of this study (Figs. 4.4 and 4.6, and especially in Fig. 4.5). These stress concentrations cause early fatigue crack growth in the form of discontinuous crack growth bands and therefore early failure. The fatigue crack initiation process in hand-mixed cement is clearly visible in Fig. 5.1.

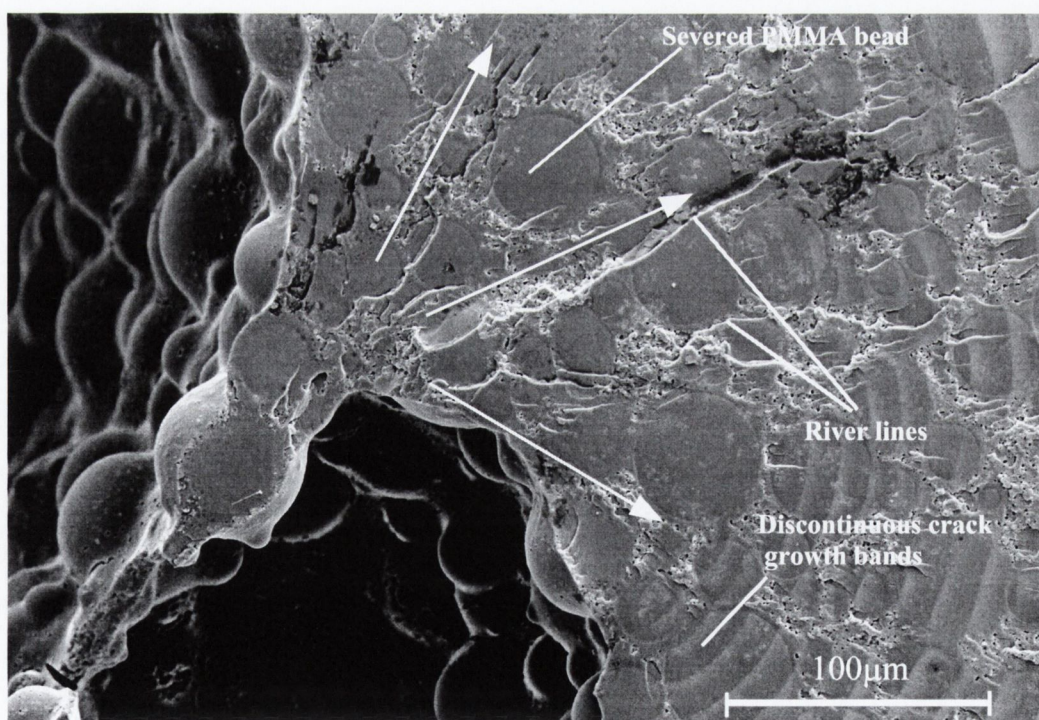


Figure 5.1 Crack initiation process in hand mixed acrylic bone cement. The crack initiates in the lower left-hand corner of the image in the “valley” between two beads on the pore’s interior surface the crack then propagates through the beads. “Discontinuous crack growth bands” are present as the crack grows these become larger, as can be observed in the top right-hand corner. River lines are visible and these indicate the direction of crack growth, as do the arrows.

In contrast with the pore interaction found in the hand-mixed cement, in the vacuum-mixed group, the cement failed from a single pore or defect in all cases. The specimens with a low fatigue life failed from large pores with diameters in the order of 1.5 mm to 3 mm. Fig. 4.10 (page 71) depicts examples of such large pores. Davies and Harris (1990) also made the observation that vacuum-mixing produces a porosity distribution of relatively few pores, consisting of a mixture of generally very small or no pores and the occasional large pore. Moreover, Wang *et al.* (1996) found that vacuum-mixing systems reduced microporosity, but not all the vacuum-mixing systems investigated were effective in eliminating large pores. Therefore the results of this thesis corroborate previous results in respect of vacuum-mixing systems.

5.2.2 Reporting of S-N curves

In this thesis S-N data has been plotted in two ways: regression lines fitted to the complete data set or regression lines fitted to the average values at each stress level. When a regression line is fitted to the complete data set, outliers will have a large influence on the slope of the curve. The problem can be seen clearly when the data is extrapolated to obtain the static strength of bone cement, because, the vacuum-mixed cement is predicted to have a lower static strength than the hand-mixed cement; however, this is not the case as static tests give the opposite result: vacuum-mixed 49.65 MPa (± 4.4 MPa) and hand-mixed 37.66 MPa (± 2.35 MPa), $n = 9$ for both cases. The slope of the lines fitted to the averages avoids this problem, see Eqns. 4.3 and 4.4 (page 64). Moreover, the larger slope of the average lines (see Table 5.1) will provide a more conservative estimate of fatigue life at lower stress levels.

Table 5.1 *The slopes of all the fatigue curves determined in this thesis based on two different regression methods. The slopes of the lines fitted to the averages at each stress level are more consistent compared to regression lines fitted to all the data.*

FATIGUE TEST SERIES	Slope of the lines fitted to the average values	Slopes of lines fitted to the complete data set
S-N vacuum-mixed	-4.82	-2.86
S-N hand-mixed	-4.77	-3.76
S-N tubular	-4.28	-2.28
S-N Damage Accumulation	-4.76	-3.21

The use of a linear relationship between stress and number of cycles to failure (as opposed to an asymptotic curve, such as the Olgive curve), can be justified on a number of fronts. Bone cement can be described as an inconsistent porous material with wildly varying fatigue properties and quoting a fatigue limit for this material could be misleading, since one may not exist due to the porous nature of the material. This point is illustrated in a similar analysis to the one presented in this thesis by Krause *et al.* (1988) who employed an Olgive curve to fit bone cement fatigue data and estimated a mean fatigue limit of 13.43 MPa for Zimmer LVC and 11.72 MPa for Zimmer Regular. It is noteworthy that this “fatigue limit” is higher than some of their fatigue data points suggesting that, even if a fatigue limit does exist for bone cement, asymptotic curves such as the Olgive curve may over estimate it and therefore it may be safer to use a linear relationship.

5.2.3 Variability of fatigue strength

The higher variability of the fatigue strength of the vacuum-mixed cement is confirmed by the correlation coefficients of the S-N regression lines. The correlation coefficient (r) for the vacuum-mixed cement is 0.76 while the correlation coefficient for the hand-mixed cement is 0.89. In a study by Davies *et al.* (1987) the fatigue life of centrifuged cement was compared to hand-mixed cement. They found that the correlation coefficient for the hand-mixed cement ($r = 0.84$) was lower than the centrifuged cement ($r = 0.88$). This was due to the fact that the centrifuged cement produced a more consistent porosity distribution in comparison to the hand-mixed cement. The present thesis shows that the reverse is the case when hand-mixed and vacuum-mixed cement are compared.

To investigate if porosity might explain the higher variability of strength found for vacuum-mixed cement, the pore area was subtracted from the fracture surface area to give a net cross sectional area from which a net section stress could be calculated. The results of this analysis are shown in Fig. 5.2 (a plot of the net section stress versus the number of cycles to failure). There is an improved association of the data ($r = 0.84$) compared to the original vacuum-mixed correlation coefficient ($r = 0.76$). Therefore, by this simple analysis of the fracture surface, we can account for 8% of the variability within the fatigue life of the vacuum-mixed cement. However, this analysis does not account for the stress concentrations caused by pores (see Taylor 1987), either individually or because they are near the edge of the specimen or

another pore; neither does it account for micro-stress concentrations caused by the beads on the inside of the pore. One outlier (the point on the extreme left of the plot) is present in Fig. 5.2; this data point is due to an irregularly shaped large pore located close to the edge of the specimen. If this data point were to be excluded, the correlation coefficient would increase to 0.9, which is almost identical to the correlation coefficient obtained for the hand-mixed cement. This suggests that the greater variability in vacuum-mixed cement found in our study (and in the studies of others [Davies and Harris, 1990]) is due almost entirely to porosity.

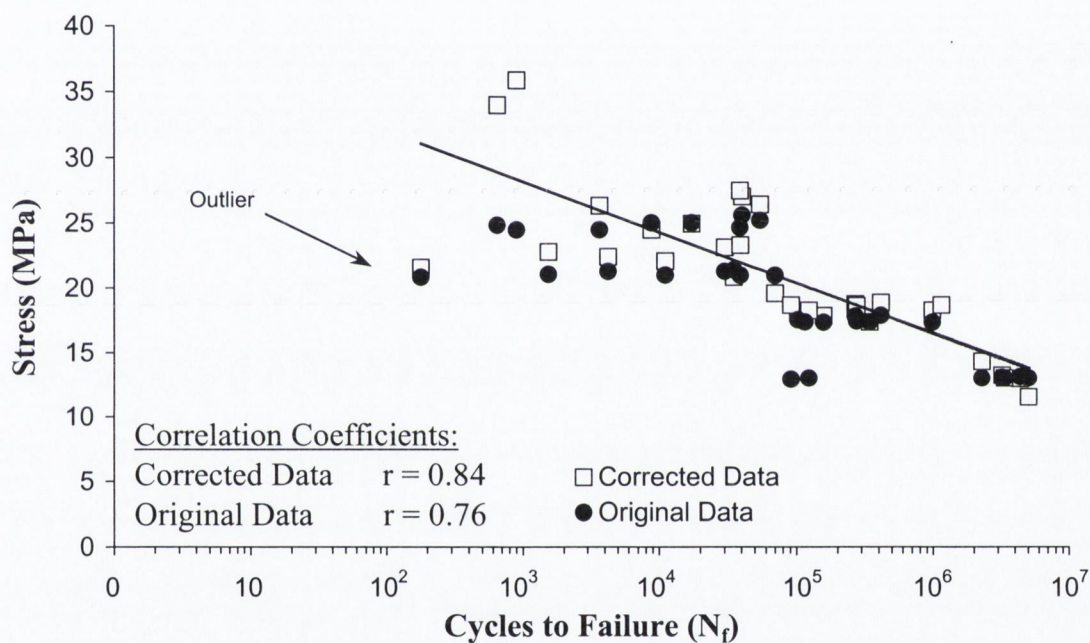


Figure 5.2 A plot of the vacuum-mixed fatigue data, the cross sectional area has been adapted to account for porosity consequently a net section stress could be calculated. The original data has also been plotted for comparison purposes.

5.2.4 Weibull analysis of strength and variability of strength

The two-parameter Weibull distribution was used to determine the probability-of-survival as a function of stress. The plots in Fig. 4.3 (page 67) show that the vacuum-mixed cement has a greater Weibull life at intermediate and low probabilities of survival. However, as you approach a probability-of-survival of 100% (i.e. perfect reliability) the vacuum-mixed cement is predicted to have inferior fatigue properties (it is less reliable) compared to hand-mixed cement. This holds true at all stress levels except 17 MPa where the result is affected by one hand-mixed specimen which failed

at a very low number of cycles because of a large pore located near the edge of the specimen – the outlier on Fig 4.1 (page 65). Johnson *et al.* (1989) also encountered a similar problem with an outlier, which caused a probability distribution to be wildly skewed. If very high reliability is required, it seems that the choice should be for hand-mixed cement.

The clinical results of the Swedish Hip Register (Malchau *et al.*, 2000) indicate that early fatigue failure may occur in vacuum-mixed cement compared to hand-mixed cement, because, in the first five years post-operation, vacuum-mixing has a greater risk associated with it (see Fig. 2.5, page 19). The results of this study show that vacuum-mixing produces a cement that may be less reliable given that “occasional” large pores seem to be a feature of vacuum-mixing systems. The unreliability will be more obvious when a larger cement volume is used, because the probability of a large pore being present is increased with increased cement volume. This could result in an accelerated version of the damage accumulation failure scenario caused by premature fatigue cracking about the stress concentrating large pores; this hypothesis correlates with the clinical results of Malchau *et al.* (2000).

There is a practice when fatigue testing PMMA bone cement to remove specimens with large pores prior to the testing stage (Fritsch, 1996, Lewis, 1999, Lewis and Austin, 1994, Gates *et al.*, 1983). In a recent study (Lewis, 1999) comparing the fatigue strength of different mixing techniques the practice of excluding “unacceptable” specimens was used. Unacceptable specimens were specimens which had large pores (diameter >1mm) within the gauge length or specimens that had visible surface pores. The number of specimens they discarded from the hand-mixed and the vacuum-mixed group was approximately equal and was believed to have no effect on the overall results. In comparative fatigue studies of this nature, this practice should not be undertaken as the true nature of the variability of the fatigue study is missed, as illustrated in this work.

The practice of removing pores has recently taken a turn for the worst, whereby it has been recommended by Cristofolini *et al.* (2000) that any specimen with a pore greater than 1 mm should be removed from the specimen test group. The author of this thesis feels very strongly about such recommendations; as large pores are inevitable in surgical practice and therefore should be assessed in *in vitro* testing.

5.3 Damage accumulation in acrylic bone cement

Cracks observed in this study were similar in nature to the *in vivo* cracks that Jasty *et al.* (1991) reported, indicating that they were not artefacts produced only in *in vitro* testing. In the majority of cases microcracks tended to follow a path through the interbead matrix rather than through the pre-polymerised beads; in some cases cracks were arrested when they encountered a relatively large bead. Thus, the pre-polymerised beads acted as microcrack arrestors. The type of cracking that was observed was mainly of the variety where fibrils spanned the crack surfaces ahead of the main crack; this compares to the “microcraze damage zone” that Topoleski *et al.* (1993) observed where a number of microcracks precede the main crack. The type of cracking found may be due to the slightly higher molecular weight of this bone cement (Kühn, 2000), as it has been shown that PMMA bone cement with a higher molecular weight has a significantly greater fatigue strength (Lewis and Mladi, 1998). The sterilisation method used may account for this, as Cemex[®] cement is ethylene oxide sterilised which has been shown to have less of a negative effect on the molecular weight of the powder than gamma irradiation—which is the most common technique for sterilisation of bone cement (Kühn, 2000). The addition of a crack inhibiting microstructural feature such as titanium fibres to the cement may prevent cracks initiating or propagating, as these have been shown to significantly increase the fracture and fatigue resistance in bone cement (Topoleski *et al.*, 1998), although the workability of the cement may suffer with the addition of these fibres.

It is found in this study that the number of cracks per pore increases dramatically with stress; at the highest stress level (15 MPa) the number of cracks per pore is greater than three, while at the lower stress levels the number of cracks is only approximately one and a half. At the higher stress level it would seem as if all the irregularities on the pore's inner surface act as crack initiation sites. Evidence for this is given in Fig. 4.12 (page 73), as the crack angles at the higher stress are not distributed normally about the direction perpendicular to the normal principal stress. For the 15 MPa cyclic stress, 27% of the cracks lie within the 80-100° range, whereas at 12.11 MPa the corresponding value is 35%, and at 9.76 MPa it is 41%. This trend indicates that, as stress reduces, the majority of cracks propagate perpendicular to the maximum principal stress.

From a fracture mechanics point of view, it is to be expected that *all* cracks would grow perpendicular to the applied load; however this is not observed experimentally. There are a number of explanations for this phenomenon. Firstly, the effect of interacting pores can cause local stress concentrations and complex stress fields. Tsukrov and Kackanov (1997) analysed the stress concentrating effect of interacting holes; they showed that a large hole surrounded by an array of small holes with diverse eccentricities can cause stress concentrations of up to 16 times the original stress, see Fig. 5.3. Moreover, their analysis shows that as porosity increases so too will the value of the maximum stress concentration (Fig. 5.3). Only the

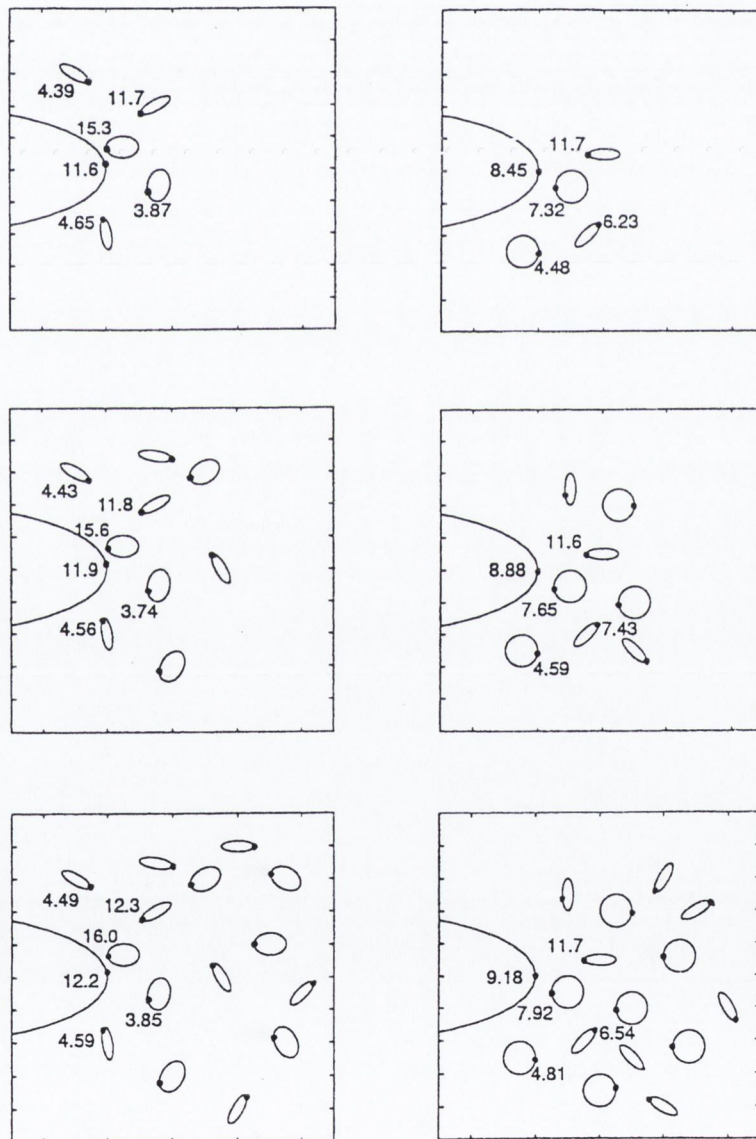


Figure 5.3 Various patterns of porosity in a 2-D case porosity increases down the page similarly the value of the maximum stress concentration increases as porosity increases (Tsukrov and Kachanov, 1997).

maximum values are shown in Fig. 5.3 although the stress field caused by the interacting holes will mean further stress concentrating effects will be present about the entire hole therefore cracks could propagate at any angle from the hole depending on the distribution of pores. This analysis was for *smooth* holes; although the pores in acrylic bone cement are not smooth about their perimeter, which is surrounded by pre-polymerised beads of PMMA, further local stress concentrations will occur in the notch between two beads. Finally, residual stresses formed during the curing stage may initiate microcracks. As bone cement cures shrinkage occurs, tensile hoop stresses are generated around pores; this tensile residual stress may cause microcracks to initiate from the perimeter of the pore – these cracks could have any orientation. Although no cracks were observed in this study prior to mechanical loading; the measurement technique may not have observed these cracks, as it could only account for cracks greater than 30 μm .

When the assumption is made that damage occurs at a linear rate, it can be shown that the crack length per cycle increases with increasing stress [see Fig. 4.13 (a) page 75], although the association of the data is poor. Once the data is normalised for porosity, the data association increases by 24%. This increase in association indicates that porosity is primarily responsible for the variability in damage between the specimens.

This study clearly confirms that damage evolution in acrylic bone cement is non-linear, and may be described by a power law equation as given below:

$$\frac{\omega}{\omega_f} = \left(\frac{N}{N_f} \right)^{\frac{\sigma - 5.6}{2.73}} \quad \text{Eqn. 5.1}$$

Therefore the use of Miner's Law to predict damage accumulation, as done by Verdonschot and Huiskes (1997) and Stolk *et al.* (2000) could be improved and future pre-clinical finite element analysis could use a non-linear stress dependent relationship between damage and fatigue life.

Furthermore at higher stresses damage accumulation is increasingly non-linear and even a small reduction in the stress will succeed in considerably reducing the amount of microcracking present in the bulk cement mantle, see Fig. 5.4. Therefore, if the mechanical integrity of the cement mantle is to be maintained for as long as possible, it would seem that reducing the higher stresses (peak stresses) at the expense of a general increase in the lower stresses would be advantageous; however, if the

stresses are all low, the data obtained in this thesis suggests that reducing the porosity would be of greater benefit than any further reduction in stress.

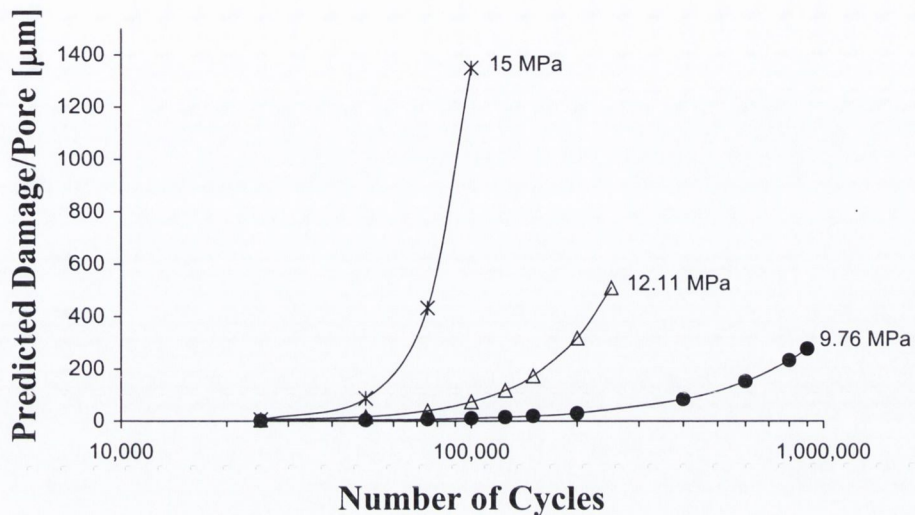


Figure 5.4 Predicted damage versus the number of loading cycles

5.4 The choice of S-N curves for finite element analysis

When modelling the damage accumulation process a dependable relationship between stress and number of cycles to failure is needed for a good predictive model. A number of factors must be considered when choosing an S-N curve for a cement mantle, namely:

- (i) The volume of the cement mantle must be considered, as the probability of a flaw (or large flaw) being present increases as volume increases, therefore the fatigue life will be dependent on the stressed volume.
- (ii) The thickness of the cement mantle. Failure of a cement mantle could be considered as the appearance of a through-mantle crack; consequently the cement mantle thickness would influence the durability of a cement mantle.

In the following analysis the results of this thesis will be used to show how the volume of the cement mantle can be accounted for when choosing a relationship between stress and number of cycles to failure.

In this thesis four different sets of fatigue results were obtained: hand-mixed Cemex Rx dog-bone specimens; vacuum-mixed Cemex Rx dog-bone specimens; vacuum-mixed Cemex translucent large dog-bone specimens; and vacuum-mixed tubular Cemex Rx specimens. The small vacuum-mixed dog-bone shaped specimens can be compared with the control set of tubular specimens because both test series use the same mixing technique and type of bone cement; however, the test conditions vary slightly, a higher loading frequency was used in the dog-bone shaped vacuum-mixed specimens; the work of Cheng *et al.* (1990) and Humpreys *et al.* (1989) indicate that this change in loading frequency should not appreciably affect the failure life of acrylic bone cement.

When the fatigue results are plotted on the same diagram a higher increase in fatigue strength is found for the smaller specimens, see Fig. 5.5.

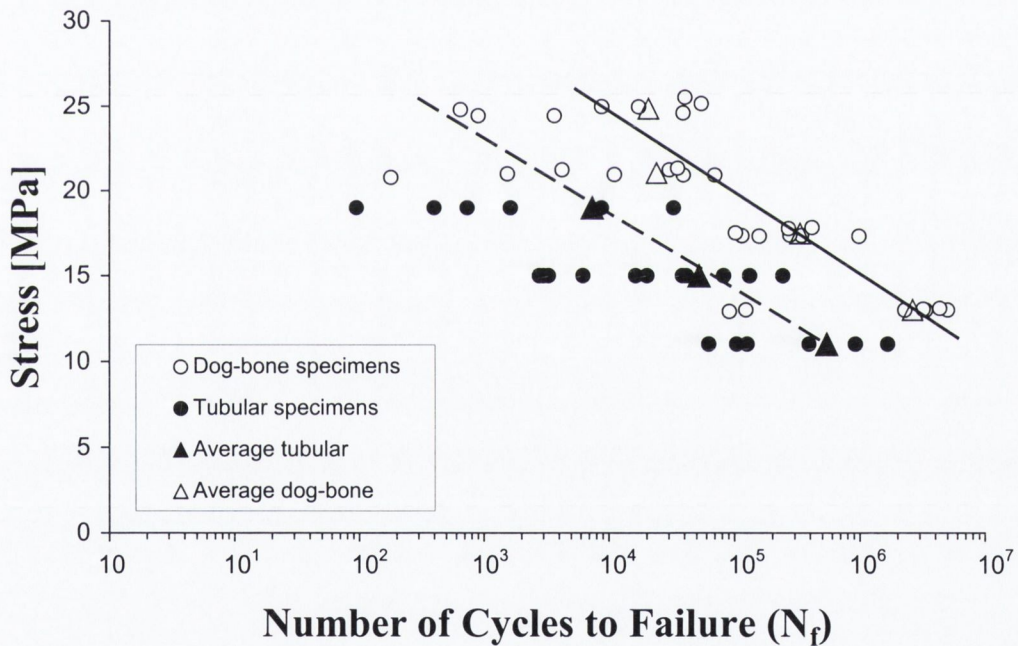


Figure 5.5 *S-N curves for different specimens tested under near-identical conditions (same cement and mixing technique). The lines plotted are regression lines through the averages at each stress level; the equations of these lines are given in Eqn. 5.2 and 5.3.*

Tubular specimens $\sigma = -4.28 \text{Log}_{10}(N_f) + 35.42$ Eqn. 5.2

Dog-bone specimens $\sigma = -4.82 \text{Log}_{10}(N_f) + 43.99$ Eqn. 5.3

The theory of Weibull (1951) describing the probability-of-survival of a set of identically sized specimens (this equation is given in Eqn. 3.1, page 60) can be developed further to show that the probability-of-survival is not only a function of the number of cycles to failure but is also dependent on the stressed volume. The derivation of this function is clearly described by Ashby and Jones (1986); the final design equation showing that probability-of-survival is a function stress and volume is given in Eqn. 5.4. Taylor (1998) showed that this principle could be put to practical use, whereby the difference in fatigue strength of bone was explained based on a stressed volume approach.

$$\ln P_s(V) = -\frac{V_s}{V_{so}} \left(\frac{N_f}{\beta} \right)^\alpha \quad \text{Eqn. 5.4}$$

This equation can be re-written in the form given in Eqn. 5.5, whereby the number of cycles to failure at a specific probability can be predicted.

$$N_f = \beta \left[-\left(\frac{V_{so}}{V_s} \right) \ln(P_s) \right]^{\frac{1}{\alpha}} \quad \text{Eqn. 5.5}$$

where N_f is the number fatigue cycles to failure, P_s is the probability-of-survival and α and β are empirical constants determined from a set of equally sized specimens. The constant α is referred to as the shape parameter of the curve, and β is the location parameter. Given the volume of a specimen V_{so} with parameters α and β the fatigue life of a specimen with volume V_s can be calculated.

Usually α and β are determined from a large sample size (Taylor, 1998); in this study the largest sample size at one stress level is twelve; six fatigue tests are reported at 15 MPa for the vacuum-mixed tubular specimens and there are a further six previously un-reported fatigue results at this stress level; however the temperature control was not as accurate ($\pm 1.5^\circ\text{C}$) so these results were not reported used in the body of the thesis. Although the creep results cannot be used, the number of cycles to failure results can be assumed to be unchanged by the imprecise temperature control. The combination of these data sets was used to determine α ($\alpha = 0.6893$) and β ($\beta = 39,610$). The value of P_s in Eqn. 5.5 is set to the median of the distribution ($P_s = 0.5$). Given the stressed-volume of the tubular specimen (V_{so}) was $7,634 \text{ mm}^3$ and the

stressed-volume of the dog-bone specimen (V_s) was 616 mm^3 the mean number of cycles can be predicted for the smaller dog-bone shaped specimen. Entering the above values into Eqn. 5.5 the fatigue life of the dog-bone shaped specimens was predicted to be approximately 900,000 cycles, while using the S-N curve fitted to the average experimental data, Eqn. 5.2, the fatigue life is approximately 1,000,000 cycles. Therefore the stressed-volume principle results in a reasonably good prediction for the fatigue life of acrylic bone cement.

Based on the above analysis we can assume there is a distribution of fatigue curves for acrylic bone cement (see Fig. 5.6), ranging from a large specimen, for example a complete cement mantle, to a small discrete element of acrylic bone cement, the size of which will depend on some material attribute. The question arises: Which S-N curve should be used in computer simulations?

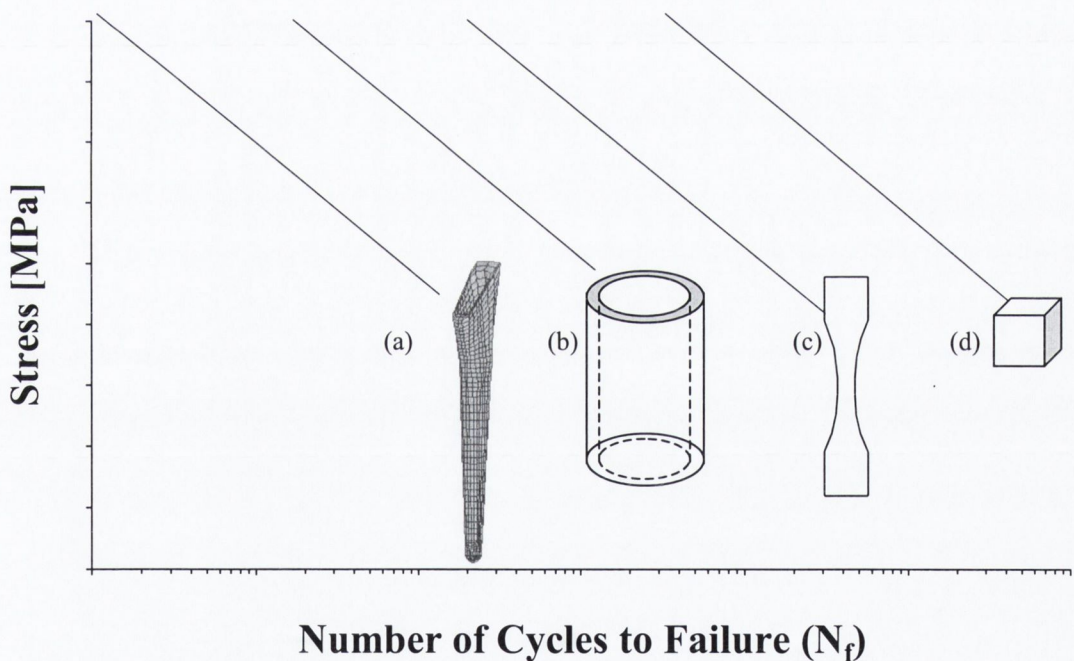


Figure 5.6 Range of S-N curves for acrylic bone cement based on a size effect, with the lowest fatigue strength associated with the large cement mantle and the greatest fatigue strength associated with a small discrete element, with the two different specimens sizes lying within the range.

The work of Stolk *et al.* (2000a) compares two different prosthesis designs and their effect on damage accumulation within the cement mantle. The two different prosthesis designs that are compared are the Lubinus SPII and the Müller curved stem; the volumes of the two different cement mantles are respectively, $12,991 \text{ mm}^3$

and $12,027 \text{ mm}^3$. Using the results of this study the fatigue life of the two cement mantles at a specific stress (15 MPa) can be predicted. The fatigue life is calculated to be 10,763 cycles for the Lubinus SPII cement mantle and 12,036 for the Müller cement mantle at a stress level of 15 MPa. As the Lubinus stem is surrounded by more cement the probability of a flaw (for example a large pore caused by vacuum-mixing) being present is greater than that for the Müller prosthesis, therefore the fatigue life is less for the Lubinus cement mantle based on a stressed volume approach.

If one curve is used in *all* computational models, for example curve *A* in Fig. 5.7, prostheses which have smaller cement mantles will seem less durable in comparison to prostheses which require larger cement mantles because the stressed volume is not accounted for. If curve *A* represented the stress vs. number of cycles to failure relationship for the Lubinus cement mantle, a particular element may have a stress of σ_x and its corresponding fatigue life will be X' . If the same curve is used for the Müller prosthesis the stress will increase, maybe due to a smaller volume of cement available for load transfer—and say the stress now increases to σ_y resulting in a fatigue life of Y' . However, according to the stressed volume approach the true fatigue life for the cement mantle of the Müller prosthesis will be represented by curve *B* resulting in a fatigue life of Y'' , thus, in conclusion using one fatigue curve will negatively weight against prostheses that use smaller cement mantles.

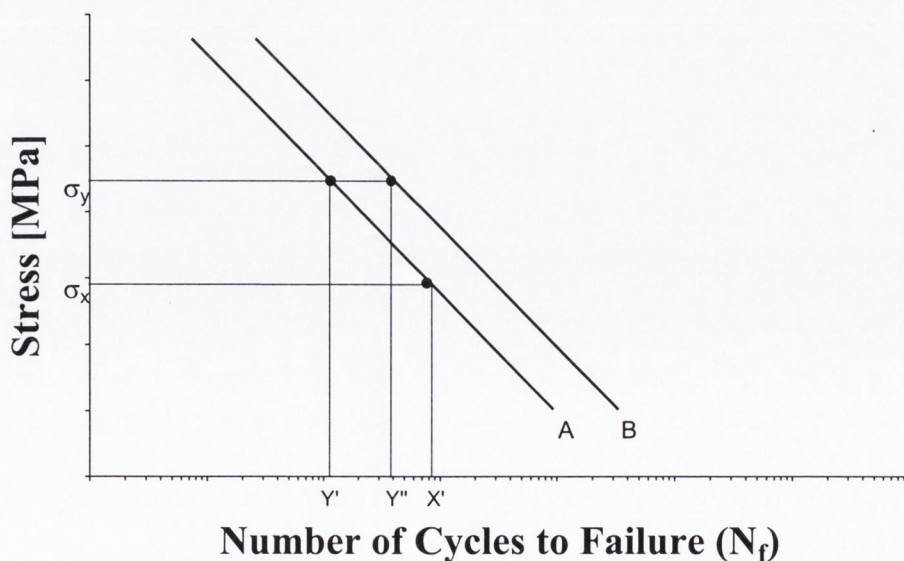


Figure 5.7 The use of one fatigue curve for all cement mantles will weight against a smaller cement mantle by a value of Y'' minus Y' .

It must be noted that this is not the definitive S-N curve for a cement mantle; however, it may be used as a method for accounting for the volume of different cement mantles.

A number points must be noted:

1. This analysis does not account for geometric attributes of different cement mantles (i.e. cement mantle thickness).
2. The curves determined in this analysis assume that the stress in the cement mantle is equal throughout the cement mantle. This is not the case in reality. Finite element models which simulate damage accumulation account for this, as they are subdivided into elements, and the stress at each interpolation point is calculated; similarly the failure life can be determined at each point from the stress–number-of-cycles-to-failure relationship. It must be noted that this is not the fatigue life of a specimen the volume of a finite element, but will be a fatigue life representative of the entire cement mantle based on increased/decreased probability-of-failure according to the size of the cement mantle.

5.5 Multiaxial fatigue: effect on fatigue life

This section of the thesis shows that a tensile stress applied perpendicular to the cyclic stress can reduce the average fatigue life of acrylic bone cement by, on average, a factor of two, and this is statistically significant ($p < 0.1$) for two of the multiaxial stress states studied. Typically, failure occurred by fatigue crack growth perpendicular to the axial stress, although at the higher hoop stresses failure sometimes occurred by cracks growing perpendicular to the hoop stress. Moreover, the *variation* in fatigue strength is greater under multiaxial stresses.

The failure of the specimens was dependent on the orientation of the pore at the failure site. Consider the case illustrated in Fig. 5.8, if the stress in the vertical direction was the only stress present the fatigue life of the specimen shown in Fig. 5.8 (a) would be less than the fatigue life of the specimen shown in Fig. 5.8 (b). However if both stresses σ_1 and σ_2 are present the fatigue life of the specimen shown in Fig. 5.8 (b) would be reduced, as σ_2 would now cause failure, causing a reduction in

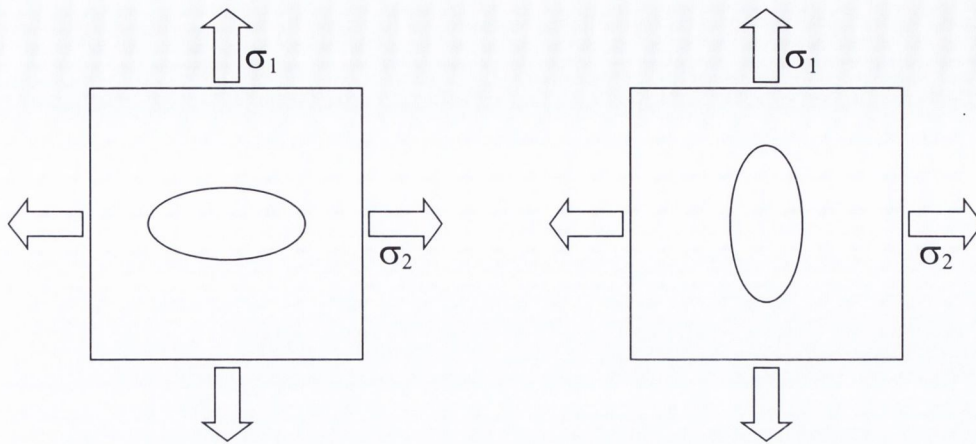


Figure 5.8 *The orientation of pores will effect the orientation of the failure crack (a) σ_1 will cause failure in this case, while in (b) σ_2 will cause failure (if $\sigma_1 = \sigma_2$).*

average fatigue life and if the fatigue life was reduced substantially the *variation* in fatigue life would increase. Failures of this sort were observed at the crack initiation site in the high hoop stress experiments.

The comparison between the experiments at 11 MPa with zero hoop stress and the experiments with a hoop and axial stress of 11 MPa shows that an increase of 16% in average fatigue life results when a tensile hoop stress is applied to the specimen; although when a comparison is made between the entire distribution of fatigue life, rather than just the average life, it can be seen that there is no difference between the two data sets (Fig. 4.26 page 88). This rather strange result requires an explanation one possible reason could be because of the reduced stress amplitude (range) of the hoop stress at this lower hoop stress level. As the specimen extends (due to the axial stress) the hoop stress will fall because of the larger oil cavity; this results in the hoop stress cycling out of phase with the axial stress. When the pressure is relatively low the pressure change will not be as great when the specimen extends, thus the stress amplitude of the hoop stress is lower at low pressures. At higher hoop stress values (15 MPa and 16.5 MPa) the pressure inside the cylinder is greater and any increase in volume of the pressurised cavity will cause the oil in the cavity to have a greater fluctuation in pressure, causing a greater change in hoop stress. At the higher hoop stress values the stress amplitude is greater and the chance that the hoop stress will initiate a fatigue crack is increased, compared to the lower (more constant) hoop stress value (11 MPa). This was observed experimentally; none of the specimens with a

hoop stress of 11 MPa failed from the hoop stress, while some specimens at the higher hoop stress values failed from the hoop stress. In other words, the result is an artefact of the loading mechanism exacerbated by variability of fatigue strength.

In conclusion, the multiaxial behaviour of PMMA is a complicated process and, despite the tests of this thesis, it must be admitted that the effect of off-axis stresses has not been fully quantified; although it has been shown that an off-axis tensile stress definitely affects the failure life and variation in fatigue life. Future work on this problem will have to involve a large series of fatigue tests under very precise loading arrangements.

5.6 Creep – fatigue interaction

Verdonschot and Huiskes (1994 and 1995) have observed creep in bone cement induced under cyclic loading and the results of these experimental studies have been used in finite element analysis to predict subsidence of cemented implants (Verdonschot and Huiskes, 1996a). The results of this study show that Cemex Rx bone cement does creep at 37°C and creeps substantially more than Simplex P, which was the bone cement used in the studies of Verdonschot and Huiskes (1994). The initial creep (parameter *B*, Chapter 4 section 4.4) observed in this study is 30% higher than in the study of Verdonschot and Huiskes (1994), see Fig. 5.9. This result holds true for Cemex Rx bone cement under compressive loads, as a similar result was reported by Verdonschot and Huiskes (2000), which showed Cemex Rx had 30% more creep than Simplex P under compressive dynamic loading. Therefore if subsidence of experiments with Cemex Rx is modelled using creep equations obtained by Verdonschot and Huiskes (1994 and 1995) the equations must be modified to include the 30% increase in creep that Cemex Rx produces.

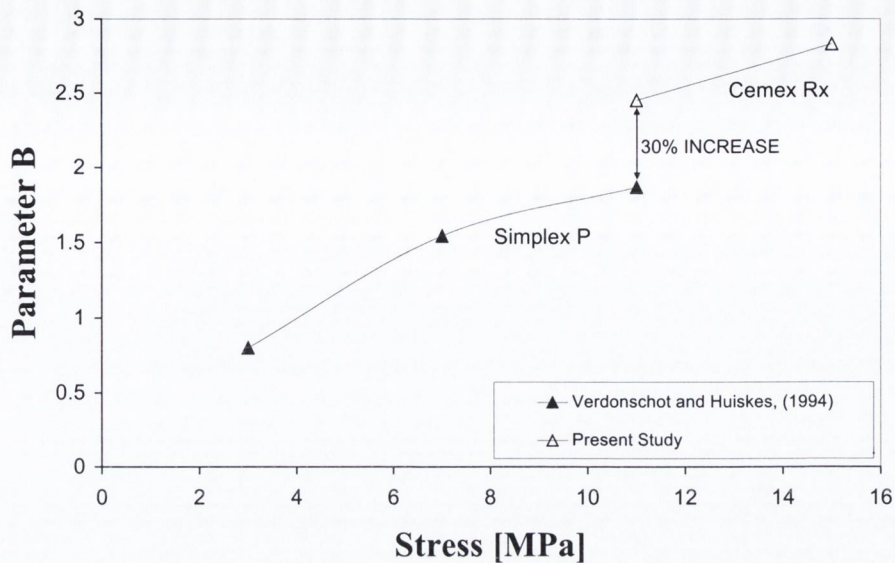


Figure 5.9 Comparison of the parameter B , which relates initial creep, with the work of Verdonschot *et al.* (1994) and the present work, showing that Cemex Rx bone cement exhibits 30% more creep at 11MPa than Simplex P bone cement.

5.7 The application of the Monkman-Grant relationship

The results presented in Chapter 4 section 4.5 certainly indicate that the Monkman-Grant relationship could be a useful tool for predicting early failure of cemented joint replacements. The high R^2 values shown in Figs. 4.35, (page 97) and 4.37 (page 98) indicate that there may be experimental evidence to show that the Monkman-Grant relationship will hold for acrylic bone cement under dynamic loads. Moreover, the Monkman-Grant relationship would seem to be applicable to this type of problem as experimental evidence (Norman *et al.*, 1995) shows that bone cement has a higher creep rate when the % porosity is greater, and generally, when % porosity is higher the fatigue life is reduced. Secondly, the process of damage evolution (cavitation/crazing) may lead to specimen extension. However, the results need further analysis.

On closer inspection of the results the Monkman-Grant relationship does not hold for acrylic bone cement under dynamic loading. The objective of using the Monkman-Grant relationship is to predict failure before it occurs. Therefore, a sensible analysis would be to investigate if the relationship holds for all specimens for the time period between 10,000 cycles and the failure life of the specimen of the

specimen with the lowest fatigue life. When this analysis is conducted the high R^2 values are replaced with low values ranges from 0 to 0.61. Therefore we cannot reliably predict failure before it occurs.

Furthermore, the Monkman-Grant relationship was designed for static creep experiments where the failure mechanism is creep. However, in the present experiments the failure type is brittle failure caused by a single dominant fatigue crack. Therefore it is hard to justify the use of the Monkman-Grant relationship under the testing conditions described in this thesis or in any other testing set-up where the failure mechanism is caused by fatigue.

Chapter 6

Conclusions

6.1 Conclusions	121
6.2 Future work	122

6.1 Conclusions

The conclusions reached in this thesis are:

Vacuum-mixed vs. Hand-mixed

1. The mean fatigue strength of vacuum-mixed cement is greater than that of hand-mixed cement. However the variability in fatigue strength of vacuum-mixed cement is greater.
2. The difference in fatigue strength, and variability of fatigue strength, for both mixing techniques is accounted for by the different porosity distributions.
3. The experimental results of this thesis agree with the clinical results of the Swedish Hip Register, showing that vacuum-mixing does not produce a reliable cement.
4. The practice of removing specimens with large pores from a specimen test group significantly affects the variability and magnitude of fatigue results and is a practice of very dubious merit.

Damage accumulation in acrylic bone cement

5. Damage evolution in acrylic bone cement is non-linear and the degree of non-linearity is stress dependent.
6. Crack propagation directions at lower stress levels are normally distributed about the direction perpendicular to the applied load whereas at a higher stress a wider distribution exists.
7. At higher stresses more cracks are produced per pore.
8. At lower stress, porosity may tend to dominate over stress in controlling the damage accumulation failure scenario.

General conclusions

9. An off-axis tensile stress superimposed on a tensile cyclic load can reduce the fatigue life of acrylic bone cement by up to 50%.
10. The volume of the cement mantle affects the probability of survival of cemented joint replacements and different S-N curves should be considered in FE analysis of cemented joint replacements to account for different volumes of cement.
11. The Monkman-Grant relationship does not hold for acrylic bone cement under cyclic loading.

6.2 Future work

There are a number of possible directions future work can focus on:

1. Porosity was found to be the key feature involved in fatigue failure and damage accumulation. The author believes that cement mixing systems are not fully optimised and further porosity reduction can be achieved by further research on mixing methods.
2. Stress analysis in combination with experimental results may be used to predict likely crack initiation sites; this analysis could then be used to ascertain an acceptable level of porosity at which a minimal amount of damage will exist.
3. In this thesis, the multiaxial stress state involved a fatigue loading in one direction and a constant loading in a perpendicular direction. However two cyclic loads may result in a further decrease in fatigue strength, as pores that have a larger stress concentration in the opposite direction will be more likely to cause early failure. The production of a function relating number of cycles to failure to the two principle stresses could be generated from such a series of tests.
4. Computer models incorporating non-linear stress dependent damage accumulation empirical laws and stress vs. number of cycles to failure relationships which account for the stressed volume of the cement mantle can now be used to evaluate cemented joint replacements.

References

- Ashby, M.F., Jones, D.R., (1998) *Engineering Materials 2, An introduction to microstructures, processing and design*, Butterworth-Heinemann, Oxford, p178-82
- Askew, M.J., Kufel, M.F., Fleissner P.R., Gradisar, I.A., Salstrom, S.-J., (1990), Effect of vacuum mixing on the mechanical properties of antibiotic-impregnated polymethymethacrylate bone cement, *Journal of Biomedical Materials Research*, Vol.24, 573-580
- Beckenbaugh, R.D., Ilstrup, D.M., (1978), Total hip arthroplasty, *Journal of Bone and Joint Surgery*, 60 –A: 306-13
- Beim, G.M., Lavernia, C., Convey, F.R., (1989), Intramedullary plugs in cemented hip arthroplasty, *Journal of Arthroplasty*, 4:139-141
- Bergmann, G., Gracichen, F., Rohlmann, A., (1993), Hip joint loading during walking and running measured in two patients, *Journal of Biomechanics*, vol 26, 969-990
- Bhambri, S.K., Gilbertson, L.N., (1995), Micromechanisms of fatigue crack initiation and propagation in bone cements, *Journal of Biomedical Materials Research*, Vol. 29, 233-237
- Biomet 2000 Annual Report, *The Story Behind the numbers*
- Bovey, F.A., Winslow, F.H., (1979), *Macromolecules An Introduction to Polymer Science*, Academic Press, New York
- Burke, D.W., Gates, M.D., Harris, W.H., (1984), Centrifugation as a method of improving tensile and fatigue properties of acrylic bone cement, *The Journal of Bone and Joint Surgery*, Vol. 66A, No. 8, 1265-1273
- Carter, D.R., Gates, E.I., Harris, W.H., (1982), Strain controlled fatigue of acrylic bone cement, *Journal of Biomedical Materials Research*, Vol. 16, 647-657
- Charnley, J., (1970), *Acrylic Cement in Orthopaedic Surgery*, E. S. Livingstone, Edinburgh
- Cheng, W.M., Miller, G.A., Manson, J.A., Hertsberg, R.W., Sperling, L.H., (1990), Mechanical behaviour of poly (methyl methacrylate) Part 2 the temperature and frequency effects on the fatigue crack propagation behaviour, *Journal of Materials Science*, 25: 1924-1930
- Chwirut, D.J., (1984), Long-term compressive creep deformation and damage in acrylic bone cements, *Journal of Biomedical Materials Research*, Vol. 18, 25-37

- Cristofolini, L., Minari, C., Viceconti, M., (2000),** A methodology for acrylic bone cement fatigue tests, *Fatigue Fract Engng Mater Struct*, 23: 953-957
- Culleton, T.P., Prendergast, P.J., Taylor, D., (1993),** Fatigue failure in the cement mantle of an artificial hip joint. *Clinical Materials*, 12: 95-102
- Daniels, C.A., (1989),** *Polymers: Structure and Properties*, Technomic Pub Co, New York
- Davies, J.P., Burke, D.W., O'Connor, D.O., Harris, W.H., (1987),** Comparison of the fatigue characteristics of centrifuged and uncentrifuged Simplex P Bone Cement, *Journal of Orthopaedic Research*, 5: 366-371
- Davies, J.P., Harris, W.H., (1990),** Optimization and comparison of three vacuum mixing systems for porosity reduction of Simplex P cement, *Clinical Orthopaedics and Related Research*, No. 254, 261-269
- Davies, J.P., Harris, W.H., (1992),** The effect of the addition of methylene blue on the fatigue strength of Simplex p bone-cement, *Journal of Applied Biomaterials*, Vol. 3, 81-85
- Davies, J.P., Harris, W.H., (1993),** In vitro and in vivo studies of pressurization of femoral cement in total hip arthroplasty, *Journal of Arthroplasty*, 8: 585-91
- Davies, J.P., O'Connor, D.O., Burke, D.W., Harris W.H., (1989),** Influence of antibiotic impregnation on the fatigue life of Simplex P and Palacos R acrylic bone cements, with and without centrifugation, *Journal of Biomedical Matials Research*, Vol. 23, 379-397
- Demarest, V.A., Lautensclager, E.P., Wixson R.L., (1983),** Vacuum mixing of acrylic bone cement, *9th Annual Meeting of the Society for Biomaterials Birmingham, Alabama, April 27-May 1, 1983*, p 37
- Fritsch, E., Rupp, S., Kaltenkirchen, N., (1996a),** Does vacuum mixing improve the fatigue properties of high-viscosity poly(methyl-methacrylate) (PMMA) bone cement?, *Arch Orthop Trauma Surg*, 115: 131-135
- Fritsch, E.W., (1996),** Static and Fatigue properties of two new low-viscosity PMMA bone cements improved by vacuum mixing, *Journal of Biomedical Materials Research*, Vol. 32, 451-456
- Gates, E.I., Carter, D.R., Harris, W.H., (1983),** Tensile fatigue failure of acrylic bone cement, *Journal of Biomechanical Engineering*, 105 (4) 393-7
- Gelb, H., Schumacher, H.R., Cuckler, J., Baker, D.G., (1994),** In vivo Inflammatory response to polymethylmethacrylate particulate debris: Effect of size, morphology, and surface area, *Journal of orthopaedic Research*, 12: 83-92

- Gilbert, J.L., Menis, D.W., Smith, S.M., Lautenschlager, E.P., Wixson, S.M., (1990)**, Effect of pore size and morphology on fatigue crack initiation in acrylic bone cements, *The 16th Annual Meeting of the Society for Biomaterials, May 20-23, 1990, Charlstown, SC, USA*, p103
- Gruen, T.A., McNeice, G.M., Amstutz, H.C., (1979)**, “Modes of failure” of cemented stem-type femoral components, *Clinical Orthopaedics and Related Research*, 141: 17-27
- Hardinge, K., (1983)**, *Hip Replacement. The facts*, Published by Oxford University Press
- Harper, E.J., Bonfield, W., (2000)**, Tensile characteristics of ten commercial acrylic bone cements, *Journal of Biomedical Materials Research (Applied Biomaterials)*, 53: 605-616
- Harrigan, T.P., Kareh, J.A., O'Connor, D.O., Burke, D.W., Harris, W.H., (1992)**, A finite element study of the initiation of failure of fixation in cemented femoral total hip replacements, *Journal of Orthopaedic Research*, 10: 134-144
- Hertzberg, R.W., Manson, J.A., (1980)**, *Fatigue of Engineering Plastics*. London, Academic Press, London
- Huiskes, R., (1993)**, Failed innovation in total hip replacement: Diagnosis and proposals for cure, *Acta Orthop Scand*, 64 (6): 699-716
- Huiskes, R., (1993a)**, Mechanical failure in total hip arthroplasty with cement, *Current Orthopaedics*, 7, 239-247
- Humphreys, P.K., Orr, J.F., Bahrani, A.S., (1989)**, An investigation into the effect of cyclic loading and frequency on the temperature of PMMA bone cement hip prostheses, *Proc. Instn Mech Engrs*, Vol. 203, 167-170
- James, S.P., Jasty, M., Davies, J., Piehler, H., Harris, W.H., (1992)**, A fractographic investigation of PMMA bone cement focusing on the relationship between porosity reduction and increased fatigue life, *Journal of Biomedical Materials Research*, Vol. 26, 651-662
- James, S.P., Schmalzried, T.P., McGarry, F.J., Harris, W.H., (1993)**, Extensive porosity at the cement-femoral prosthesis interface: A preliminary study, *Journal of Biomedical Materials Research*, Vol. 27, 71-78
- Jasty, M., Davies, J.P., O'Connor, D.O., Burke, D.W., Harrigan, T.P., Harris, W.H., (1990)**, Porosity of various preparations of acrylic bone cements, *Clinical Orthopaedics and Related Research*, No. 259, 122-129
- Jasty, M., Maloney, W.J., Bragdon, C.R., O'Connor, D.O., Haire, T., Harris, W.H., (1991)**, The initiation of failure in cemented femoral components of hip arthroplasties, *Journal of Bone and Joint Surgery*, 73-B: 551-558

- Johnson, J.A., Provan, J.W., Krygier, J.J., Chan, K.H., Miller, J., (1989),** Fatigue of acrylic bone cement-effect of frequency and environment, *Journal of Biomedical Materials Research*, Vol. 23, 819-831
- Kadakia, N., Noble, P., Beardsley, C., Aberman, H., Paravic, V., (2000),** Do cement voids cause premature failure of cement mantles in total hip arthroplasty, 46th Annual meeting, Orthopaedic Research Society, March 12-15, 2000, Orlando, Florida p221
- Kärrholm, J., Borssen, B., Lowenhielm, G., Snorrason, F., (1994),** Does early micromotion of femoral stem prostheses matter? 4-7 year follow-up of 84 cemented prostheses, *Journal of Bone and Joint Surgery*, 76B: 912-916
- Klekamp, J., Dawson, J.M., Haas, D.W., DeBoer, D., Christie, M., (1998),** The use of vancomycin and tobramycin in acrylic bone cement, *The Journal of Anatomy*, vol. 14 No. 3, 339-346
- Krause, W., Mathis, R.S., Grimes, L.W., (1988),** Fatigue properties of acrylic bone cement: S-N, P-N, and P-S-N data, *Journal of Biomedical Materials Research (Applied Biomaterials)*, Vol, 22, No. A3, 221-244
- Krause, W.R., Grimes, L.W., Mathis, R.S., (1988a),** Fatigue testing of acrylic bone cements: Statistical concepts and proposed methodology, *Journal of Biomedical Materials Research*, Vol. 22, 179-190
- Kühn, K.-D., (2000),** *Bone Cements: Up-to-date comparison of physical and mechanical properties of commercial materials*, Springer Verlag New York
- Lautenschlager, E.P., Wixson, R.L., (1986),** Fatigue and fracture toughness of Simplex-P, 32nd Annual ORS, New Orleans, Louisiana, p118
- Lee, A.J., Ling, R.S., Vangala, S.S., (1978),** Some clinically relevant variables affecting the mechanical behaviour of bone cement, *Arch Orthop Trauma Scand*, 92; 1-18
- Leevers, P.S., Culver, L.E., Radon, J.C., (1979),** Fatigue crack growth in PMMA and rigid PVC under biaxial stress, *Engineering Fracture Mechanics*, vol. 11, 487-498
- Lewis G., (1999),** Effect of mixing method and storage temperature of cement constituents on the fatigue and porosity of acrylic bone cement, *Journal of Biomedical materials Research (Applied Biomaterials)*, 48:143-149
- Lewis G., (1999a),** Effect of two variables on the fatigue performance of acrylic bone cement: mixing method and viscosity, *Bio-Medical Materials and Engineering*, 9, 197-207
- Lewis, G., (1997),** Properties of acrylic bone cement: state of the art review, *Journal of Biomedical Materials Research*, 38: 155-182

- Lewis, G., Austin, G.E., (1994)**, Mechanical properties of vacuum mixed acrylic bone cement, *Journal of Applied Biomaterials*, Vol. 5, 307-314
- Lewis, G., Mladi, S., (1998)**, Effect of sterilization method on properties of Palacos P acrylic bone cement, *Biomaterials*, 19: 117-124
- Lidgren, L., (2000)** Annual report of the Swedish hip register, www.ort.lu.se/knee/pdf/report2000.pdf.
- Lindén, U., (1989a)**, Fatigue properties of bone cement; Comparison of mixing techniques, *Acta Orthop Scand*, 60(4), 431-433
- Lindén, U., Gillquist, J., (1989)**, Air inclusion in bone cement, *Clinical Orthopaedics and Related Research*, No. 247, 148-151
- Maher, S.A., (2000)**, *Design and development of a pre-clinical test for cemented femoral hip replacements*, University of Dublin, PhD. Thesis
- Maher, S.A., Prendergast, P.J., (2001)**, Discriminating between cemented hip prostheses in an *in vitro* test, *Journal of Biomechanics*, (In Press)
- Malchau, H., Herberts, P., (1996)**, Prognosis of total hip replacement. Surgical and cementing technique in THR: A revision-risk study of 134,359 primary operations, *Scientific Exhibition presented at the 63rd Annual Meeting of the AAOS*
- Malchau, H., Herberts, P., (1998)**, Prognosis of total hip replacement. Revision and re-revision rate in THR: A revision-risk study of 148,359 primary operations, *Scientific Exhibition presented at the 65th Annual Meeting of the AAOS*
- Malchau, H., Herberts, P., Ahnfelt, L., (1993)**, Prognosis of total hip replacement in Sweden: Follow-up of 92,675 operations performed 1978-1990, *Acta Orthopaedica Scandinavia*, 64(5), 497-506.
- Malchau, H., Herberts, P., Söderman, P., Odén, A., (2000)**, Prognosis of total hip replacement, update and validation of results from the Swedish hip arthroplasty registry 1979-1998, *Scientific Exhibition presented at the 67th Annual Meeting of the AAOS*
- Maloney, W.J., Jasty, M., Rosenberg, A., Harris, W.H., (1990)**, Bone lysis in well-fixed cemented femoral components, *Journal of Bone and Joint Surgery*, 72-B: 966-70
- McCormack, B.A.O., Prendergast, P.J., (1996)**, An analysis of crack propagation paths at implant/bone-cement interfaces, *Journal of Biomechanical Engineering*, Vol. 118, p579-585
- McCormack, B.A.O., Prendergast, P.J., (1999)**, Microdamage accumulation in the cement layer of hip replacements under flexural loading, *Journal of Biomechanics*, 32: 467-475

- McCormack, B.A.O., (1997),** *On damage accumulation in cemented hip replacements*, NUI PhD. Thesis
- McCormack, B.A.O., Prendergast, P.J., O'Dwyer, B., (1999a),** Fatigue of cemented hip replacements under torsional loads, *Fatigue Fract Engng Mater Struct*, 22, 33-40
- Miner, M.A., (1945),** Cumulative damage in fatigue, *Journal of Applied Mechanics*, p159-164
- Molino, L.N., Topoleski, L.D.T., (1996),** Effect of BaSO₄ on the fatigue crack propagation rate of PMMA bone cement, *Journal of Biomedical Materials Research*, Vol. 31, 131-137
- Müller, R.T., Heger, I., Oldenburg, M., (1997),** The mechanism of loosening in cemented hip prostheses determined from long term results, *Arch Orthopaedic trauma Surgery*, 116: 41-45
- Mulroy, R.D., Harris, W.H., (1990),** The effect of improved cementing techniques on component loosening in total hip replacement, *Journal of Bone and Joint Surgery*, 72-B, 757-60
- Noble, P.C., Jay, J.L., Lindahl, C.J., Maltry, J., Dreeben, S.M., Tullos, H.S., (1987),** Methods for enhancing acrylic bone cement. In: Transactions of the society for Biomaterials 13th Annual Meeting, New York, New York, June 3-7.
- Norman, T.L., Kish, V., Blaha, J.D., Gruen, T.A., Hustosky, K., (1995),** Creep characteristics of hand- and vacuum-mixed acrylic bone cement at elevated stress levels, *Journal of Biomedical Materials Research*, Vol. 29, 495-501
- Oshi, C.S., Walker, R.H., Colwell, C.W., (1994),** The femoral component in total hip arthroplasty, *Journal of Bone and Joint Surgery*, 76-A; 8; 1130-1136
- Pal, S., Saha, S., (1982),** Stress Relaxation and creep behaviour of normal and carbon fibre reinforced acrylic bone cement, *Biomaterials*, Vol. 3, 93-96
- Perkins, R.D., Lee A.J.C., Ling, R.S.M., (1989),** Creep of methylmethacrylate cement, *Journal of Bone and Joint Surgery*, 71-B; 722
- Petty, W., (1991),** *Total joint replacement*, W.B. Saunders Company, Philadelphia
- Pilliar, R.M., Blackwell, R., Macnab, I., Cameron, H.U., (1976),** Carbon fibre-reinforced bone cement in orthopaedic surgery, *Journal of Biomedical Materials Research*, Vol. 10, 893-906
- Prendergast, P.J., (2000),** *Bone Mechanics Handbook*, Bone prostheses and implants, CRC Press, New York

- Prendergast, P.J., Maher, S.A., (2001)**, Issues in pre-clinical testing of human implants, *Journal of Materials Processing Technology*, (In Press)
- Prendergast, P.J., Monaghan, J., Taylor, D., (1989)**, Materials selection in the artificial hip joint using finite element stress analysis, *Clinical Materials*, 4: 361-376
- Rimnac, C.M., Wright, T.M., McGill, D.L., (1986)**, The effect of centrifugation on the fracture properties of acrylic bone cements, *Journal of Bone and Joint Surgery*, 68-A: 281-287
- Schmalzried, T.P., Kwong, L.M., Jasty, M., Sedlacek, R.C., Haire, T.C., O'Connor, D.O., Bragdon, C.R., Kabo, J.M., Malcolm, A.J., Harris, W.H., (1992)**, The Mechanism of loosening of cemented acetabular components in total hip arthroplasty, *Clin Orthop.* 274: 60-77
- Silvestre, A., Raya, A., Fernández-Fairén, M., Anglada, M., Planell, J.A., (1990)**, Failure of acrylic bone cements under triaxial stresses, *Journal of Materials Science*, 25: 1050-1057
- Sitwell, W.T., (1987)**, *The art of total hip arthroplasty*, Grune and Stratton, Inc. London
- Soltész, U., (1994)**, The Influence of loading conditions on the life-times in fatigue testing of bone cements, *The Journal of Materials Science: Materials in Medicine*, 5, 654-656
- Stauffer, R.N., (1982)**, Ten year follow-up study of total hip replacement: with particular reference to roentgenographic loosening of the components, *Journal of Bone and Joint Surgery*, 64-A: 983-90
- Stolk, J., Verdonschot, N., Hiskes, R., (2000a)**, Preclinical testing of cemented hip replacement implants: pre-normative research for a European standard, Annual report 2000
- Stolk, J., Verdonschot, N., Huiskes, R., (2000)**, FE simulation of damage accumulation in cement around a prosthetic hip stem, Proceedings of the 12th Conference of the European Society of Biomechanics, p112
- Taylor, D., (1998)**, Fatigue of bone and bones: An analysis based on stressed volume, *Journal of Orthopaedic Research*, 16: 163-169
- Taylor, D., (1987)**, Fatigue failure in bone cements for hip joint implants, *Fatigue '87*, vol. 3, edited by Ritchie, R.O., and Starke Jr., E.A., EMAS Ltd., West Midlands, UK, 1353-1362
- Taylor, D., Clarke, F., McCormack, B., Sheehan, J., (1989)**, Reinforcement of bone cement using metal meshes, *Proc Instn Mech Engrs*, 203: 49-53

- Topoleski, L.D.T., Ducheyne, P., Cuckler, J.M., (1990),** A Fractographic analysis of *in vivo* poly(methyl methacrylate) bone cement failure mechanisms, *Journal of Biomedical Materials Research*, Vol. 24, 135-154
- Topoleski, L.D.T., Ducheyne, P., Cuckler, J.M., (1993),** Microstructural pathway of fracture in poly(methyl methacrylate) bone cement, *Biomaterials*, Vol. 14, No. 15, 1165-1172
- Topoleski, L.D.T., Ducheyne, P., Cuckler, J.M., (1995),** The effects of Centrifugation and titanium fiber reinforcement on fatigue failure mechanisms in poly(methyl methacrylate) bone cement, *Journal of Biomedical Materials Research*, Vol. 29, 299-307
- Topoleski, L.D.T., Ducheyne, P., Cuckler, J.M., (1998),** Flow intrusion characteristics and fracture properties of titanium-fibre reinforced bone cement, *Biomaterials*, 19: 1569-1577
- Tsukrov, I., Kachanov, M., (1997),** Stress concentrations and microfracturing patterns in a brittle-elastic solid with interacting pores of diverse shapes, *International Journal of Solids and Structures*, Vol. 34, p2887-2904
- Verdonschot, N., (1995),** *Biomechanical failure scenarios for cemented hip replacement*, Ponsen & Looijen bv, Wageningen
- Verdonschot, N., Huiskes, (1997),** The effects of cement-stem debonding in THA on the long term failure probability of cement, *J Biomech*, 30(8), 795-802
- Verdonschot, N., Huiskes, R. (1996a),** Mechanical effects of stem cement interface characteristics in total hip replacement. *Clin Orthop*. 329:326-36
- Verdonschot, N., Huiskes, R., (1994),** Creep Behaviour of hand-mixed Simplex P bone cement under cyclic tensile loading, *Journal of Applied Biomaterials*, Vol. 5, 235-243
- Verdonschot, N., Huiskes, R., (1995),** Dynamic creep behaviour of acrylic bone cement, *Journal of Biomedical Materials Research*, Vol. 29, 575-581
- Verdonschot, N., Huiskes, R., (2000),** Creep properties of three low temperature-curing bone cements: A preclinical assessment. *Journal of Biomedical Materials Research (Applied Biomaterials)*, 53: 498-504
- Wang, J.-S., Toksvig-Larson, S., Müller-Willie, P., Franzén, H., (1996),** Is there any difference between vacuum mixing systems in reducing bone cement porosity?, *Journal of Biomedical Materials Research (Applied Biomaterials)*, Vol. 33, 115-119
- Weibull, W., (1951),** A statistical distribution function of wide applicability. *Journal of Applied Mechanics*, 18: 293-297

Wirth, M.A., Rockwood, C.A., (1996), Current concepts review: complications of total shoulder-replacement arthroplasty. *Journal of Bone and joint Surgery*, 78A: 603-616

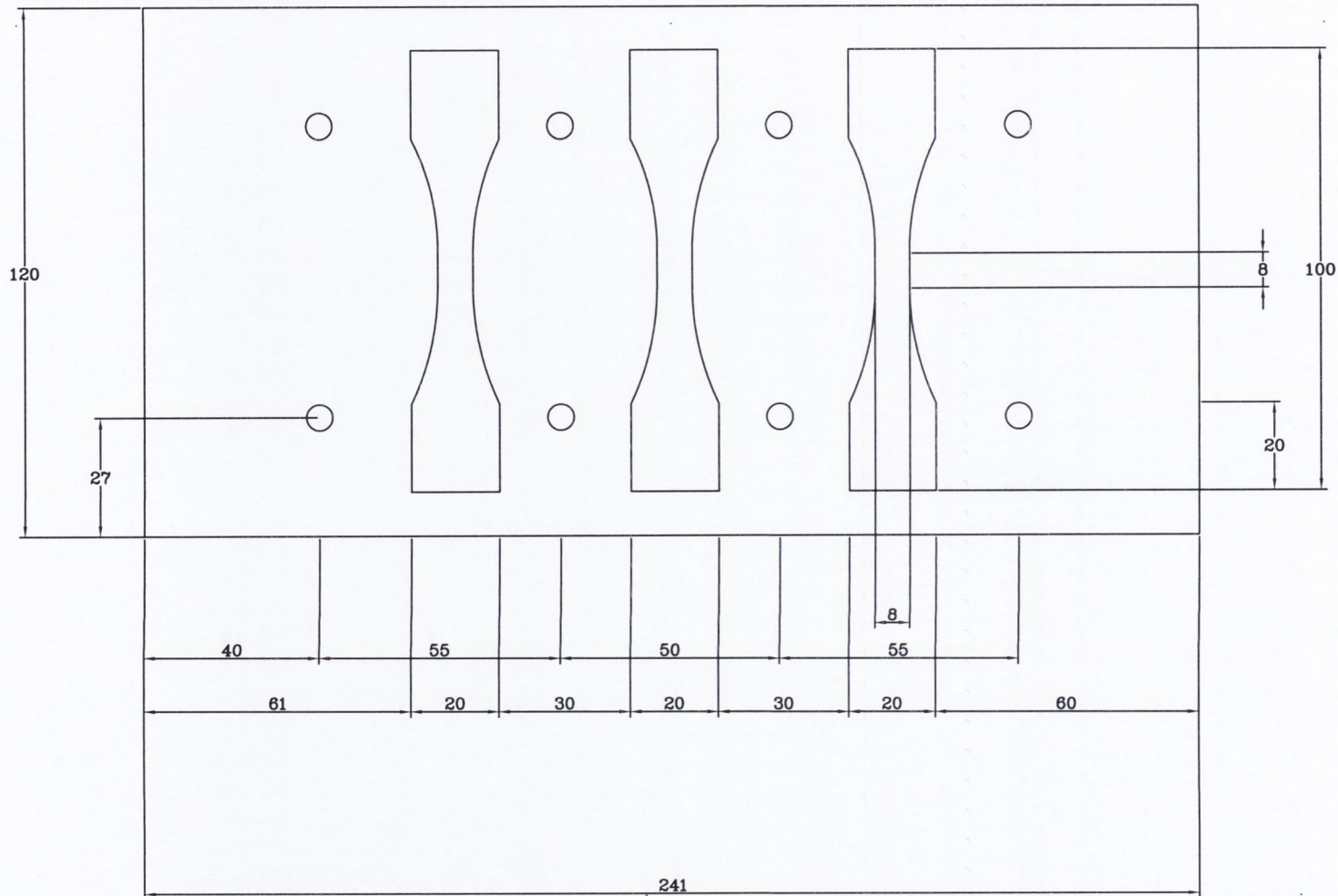
Wixson, R.L., Lautenschlager, E.P., Novak, M.A., (1987), Vacuum mixing of acrylic bone cement, *The Journal of Arthroplasty*, Vol. 2, no. 2,141-149

www.howmedica.com/simplex/pages/intro.htm.

APPENDIX I

Drawings

S-N Curves specimen mould	133
Damage analysis specimen mould	134
Lower plate dog bone specimens	135
Top plate dog bone specimens	136
Uniaxial specimen grip (part I)	137
Uniaxial specimen grip (part II)	138
Multiaxial specimen mould	139
Multiaxial specimen grips	140
Multiaxial specimen grips upper and lower sections	141



133

CODE No.

DRAWING TITLE

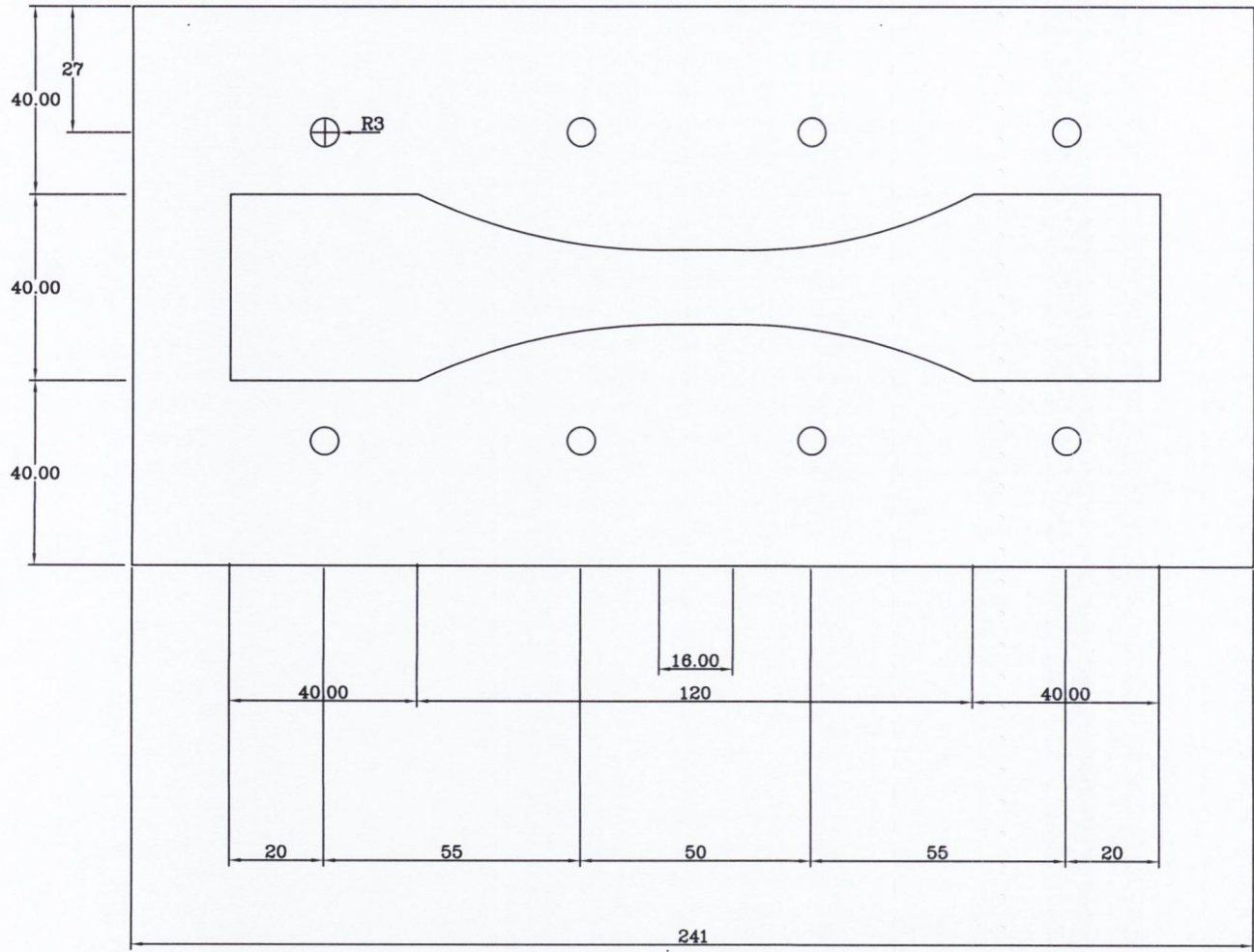
NAME BRUCE MURPHY

S-N Curves, Specimen Mould

DATE 19/11/97 SCALE



DEPT. of MECHANICAL & MANUFACTURING ENGINEERING

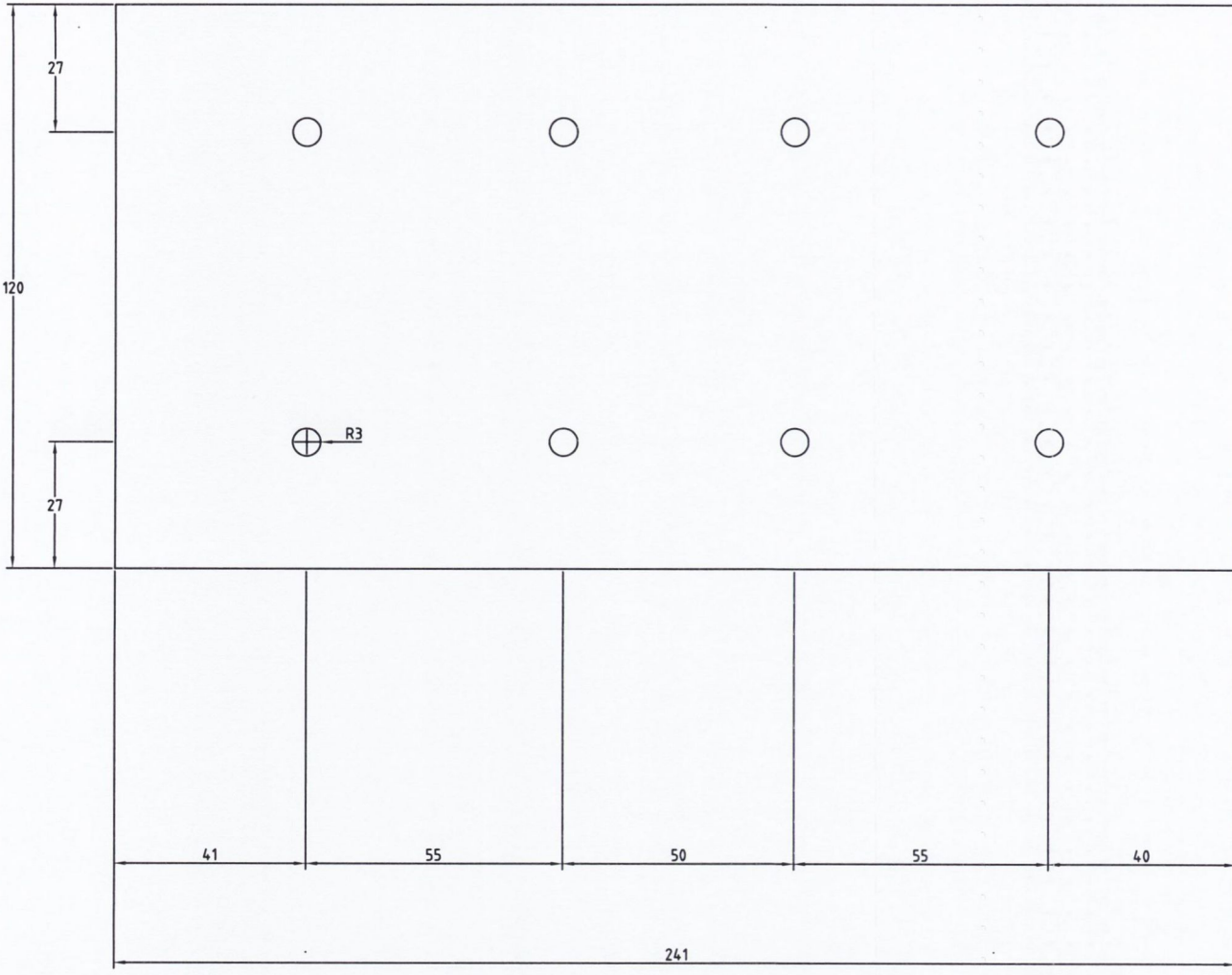


134

CODE No.	DRAWING TITLE Damage Analysis, Specimen Mould	NAME BRUCE MURPHY	
		DATE 11/11/97	SCALE



DEPT. of MECHANICAL & MANUFACTURING ENGINEERING

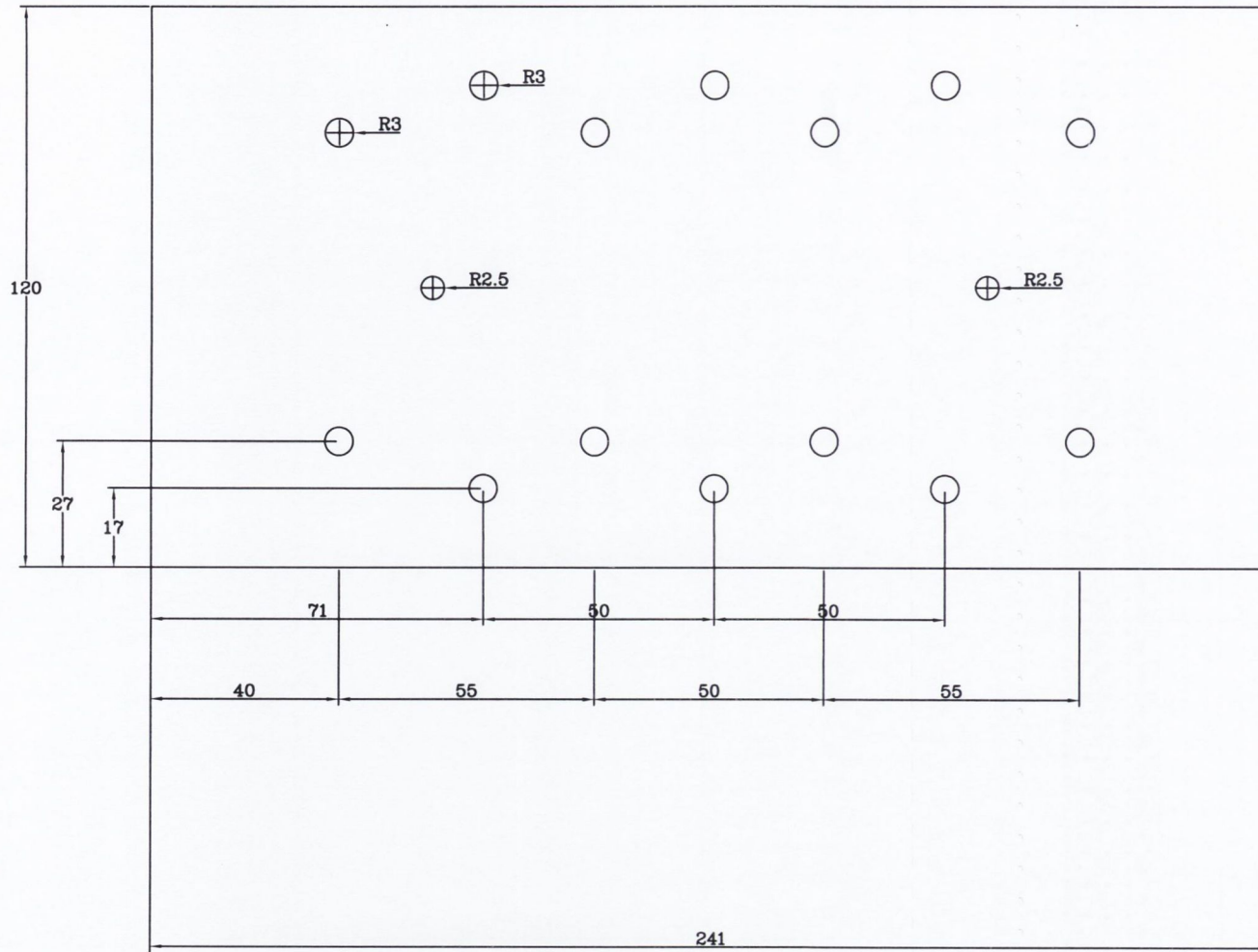


135

CODE No. DWG	DRAWING TITLE	NAME	
		DATE DATE	SCALE SCALE



DEPT. of MECHANICAL & MANUFACTURING ENGINEERING



136

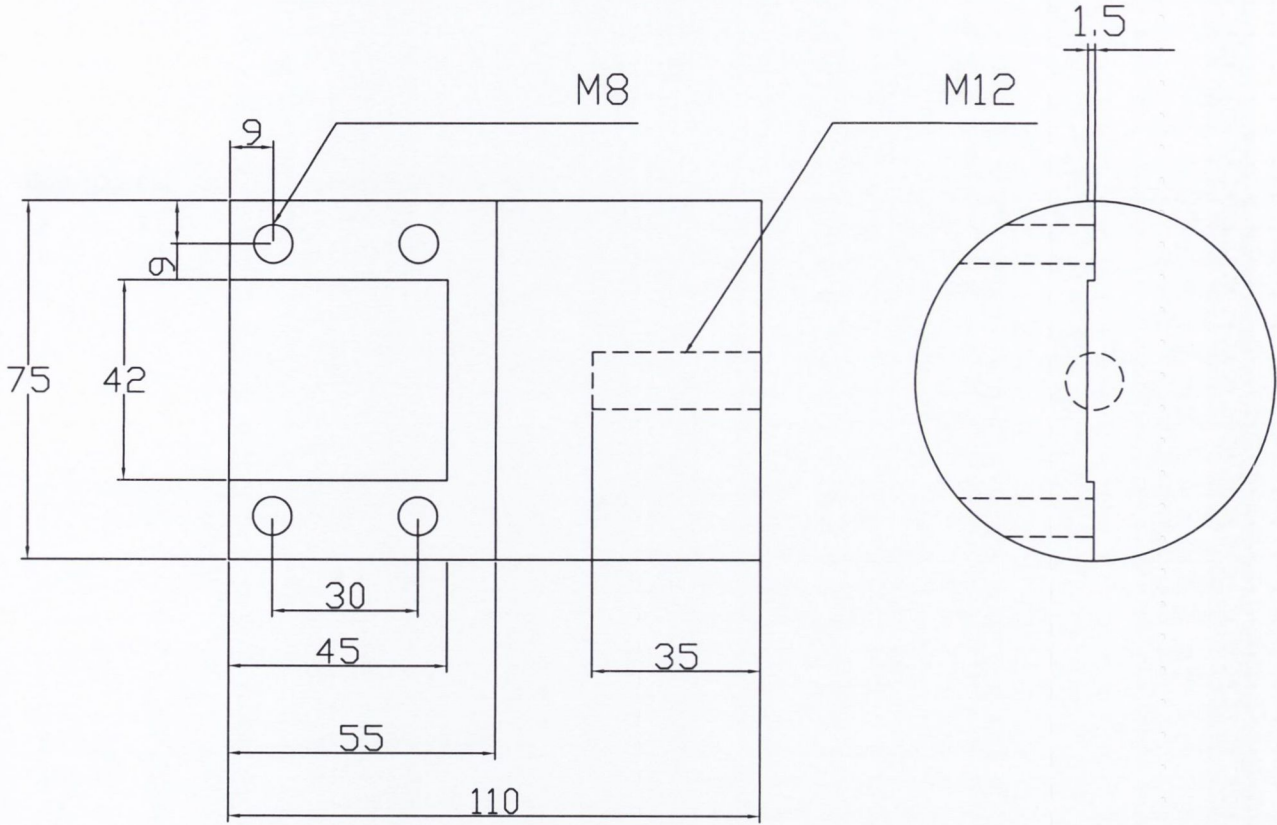
CODE No.

DRAWING TITLE

NAME BRUCE MURPHY

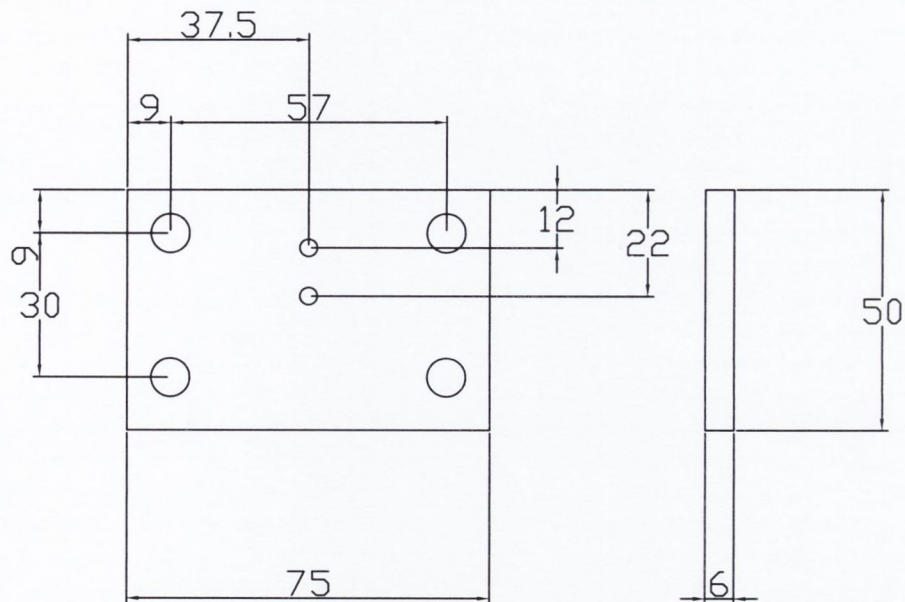
Top Plate – aluminium/polyethelene

DATE 19/11/97 SCALE



137

CODE No. DWG	DRAWING TITLE SAMPLE GRIP (STAINLESS STEEL)	NAME BRUCE MURPHY	
		DATE 13/2/98	SCALE



138

CODE No.

DRAWING TITLE

NAME BRUCE MURPHY

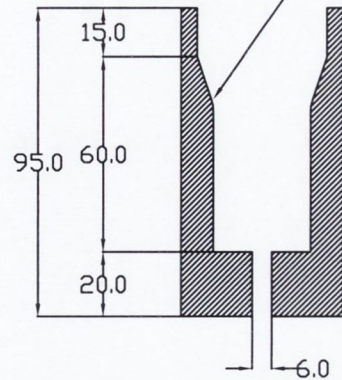
DWG

STAINLESS STEEL PLATES × 2.

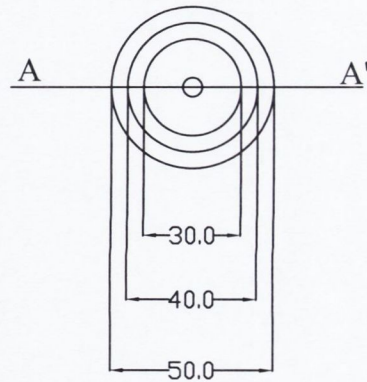
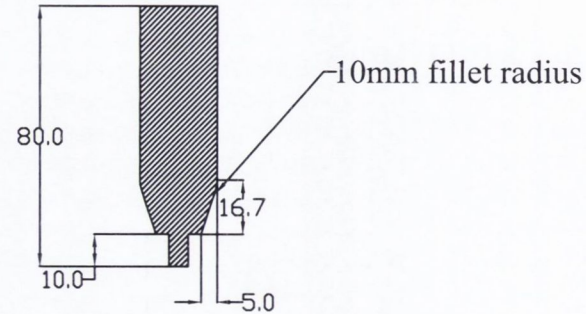
DATE 27/2/98

SCALE

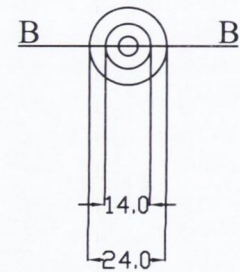
Section through A-A' 10mm fillet radius



Section through B-B'

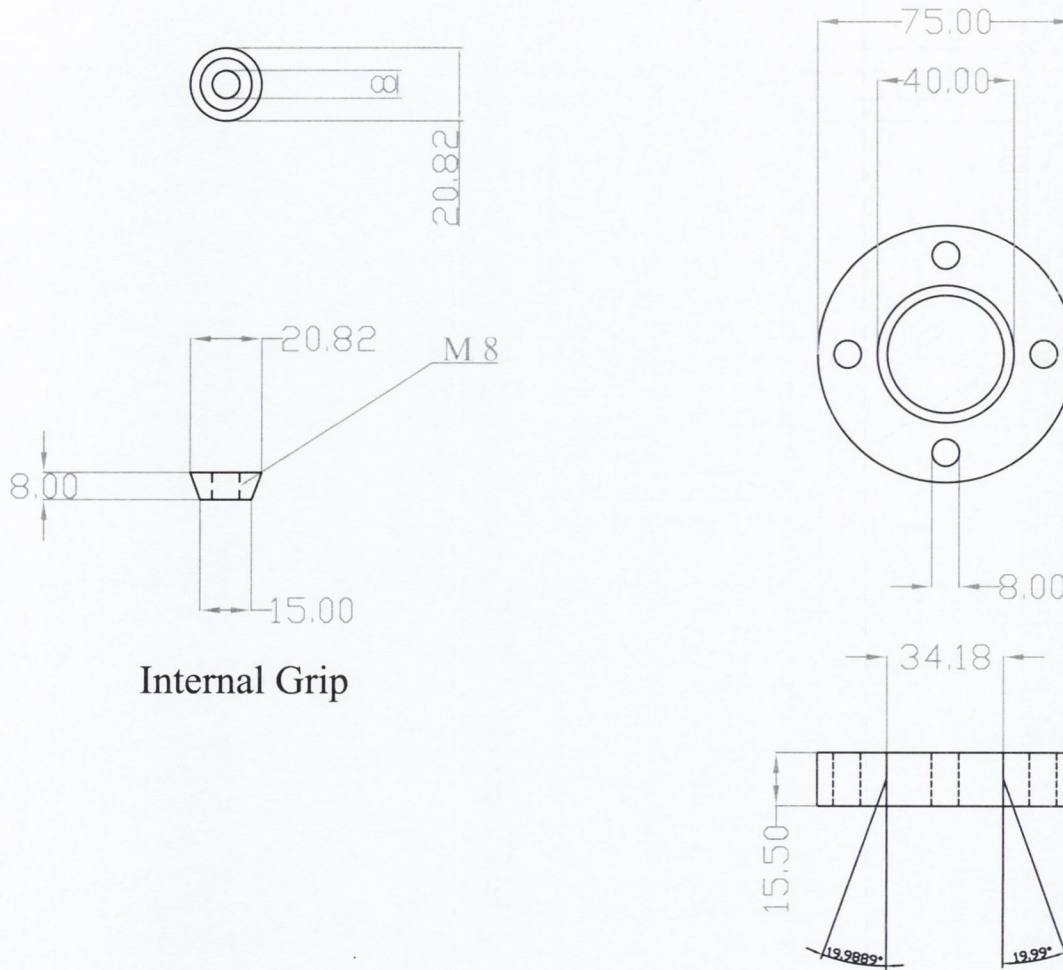


Outer Body of Mould



Inner Body of Mould

CODE No.	DRAWING TITLE	Multiaxial Mould MATERIAL: POLYETHYLENE	NAME BRUCE MURPHY	
			DATE 25 02 99	SCALE



Internal Grip

CODE No.

DRAWING TITLE

Multiaxial tensile cement grips
MATERIAL: STAINLESS STEEL

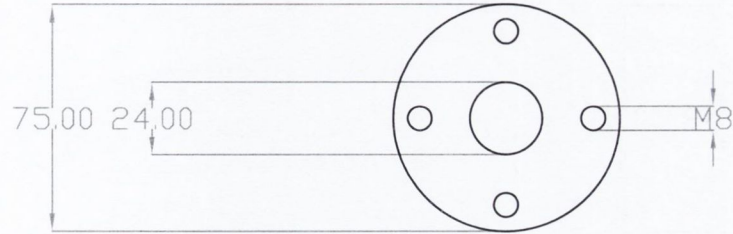
NAME

BRUCE MURPHY

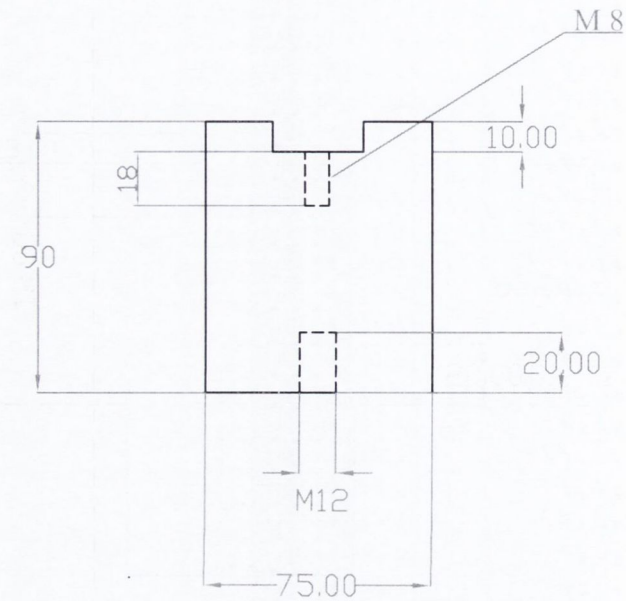
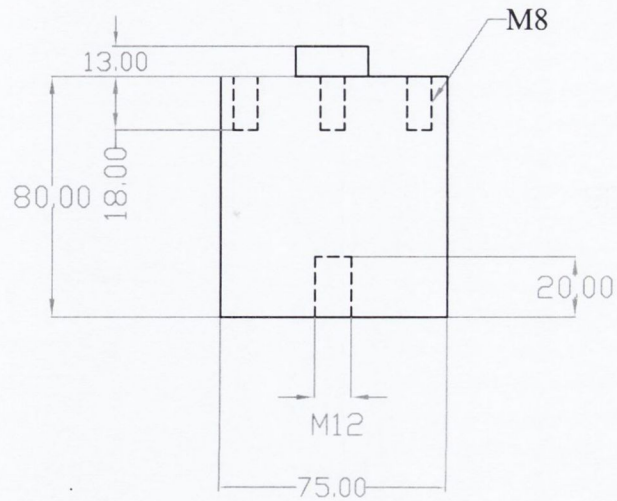
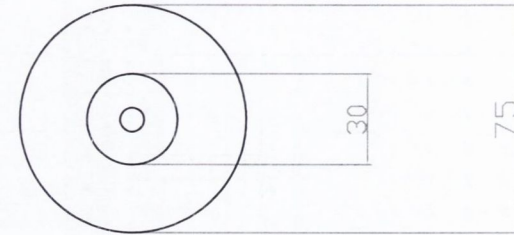
DATE 25 02 99

SCALE

Upper Grip



Lower Grip



141

CODE No.

DRAWING TITLE

Multiaxial grips upper\lower

MATERIAL: STAINLESS STEEL

NAME

BRUCE MURPHY

DATE 25 02 99

SCALE

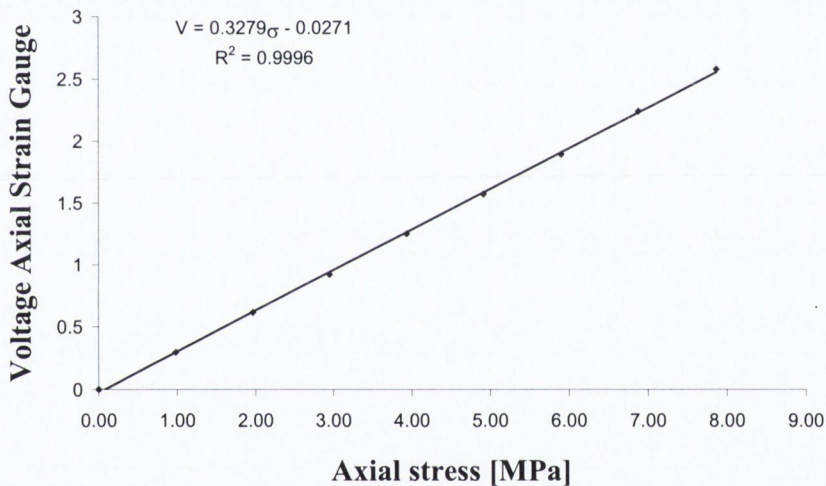
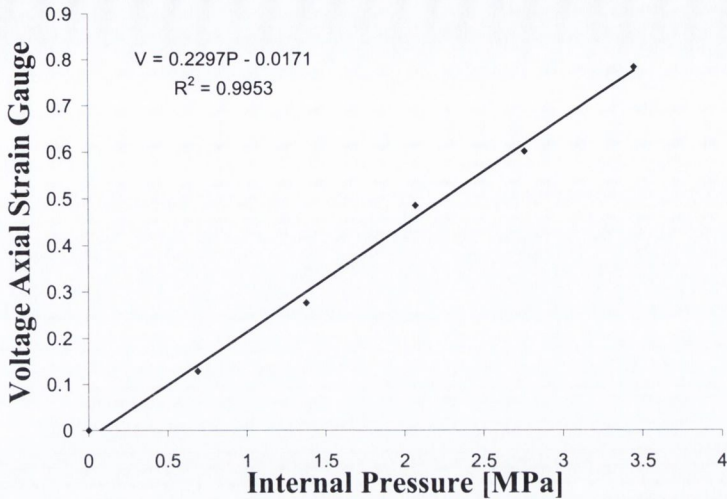
APPENDIX II

Pressure measurements

Strain Gauge measurements

143

Strain gauge results



Graph one shows the strain gauge results when an internal pressure is applied to the specimen and graph two shows the strain gauge results when a load is applied to the specimen with the materials test machine.

Combining the two equations from the graphs gives:

$$\sigma = \frac{0.2297P + 0.01}{0.3279} \quad \text{Eqn. A3.1}$$

Entering the experimental values for P into eqn. A3.1

Corresponding values Table 3.2

$P = 525 \text{ psi} = 3.62 \text{ MPa}$	$\sigma = 2.57$	2.88
$P = 475 \text{ psi} = 3.275 \text{ MPa}$	$\sigma = 2.32$	2.61
$P = 350 \text{ psi} = 2.41 \text{ MPa}$	$\sigma = 1.72$	1.92

The strain gauge measurements are approximately 10% off the values read from the Instron thus corroborating the results of the Instron load cell as a 10% error with strain gauges is a reasonable error.

APPENDIX III

Experimental protocols

Moulding procedure uniaxial specimens	145
Moulding procedure multiaxial specimens	146
Pre-test procedure	147
Experimental procedure	148

Moulding procedure uniaxial specimens

Moulding a uniaxial specimen	
1.	Clean all polyethylene mould parts with alcohol and allow the mould to dry before starting.
2.	Assemble the three lower plates by placing the bolts through the eight holes.
3.	Check the temperature of the room
4.	Mix the cement in the appropriate manner
5.	Apply the cement to one end of the mould; filling one of the tab ends of the central plate and proceed to fill the remainder of the cavity by working your way to the other end of the specimen by filling the gauge length.
6.	Place the top polyethylene plate over the mould and then place the top aluminium plate over the polyethylene plate.
7.	Screw on the nuts onto the eight alignment bolts
8.	Remove the excess cement from the pressure relief holes before it hardens.
9.	Leave the mould for 24hrs at room temperature
Removing a uniaxial specimen	
1.	Remove the eight bolts and the two aluminium plates
2.	Remove the lower polyethylene plate and then gently remove the top polyethylene plate.
3.	Push out each specimen by pushing from the side the lower polyethylene was in contact with.

Moulding procedure multiaxial specimen

Moulding a Multiaxial specimen	
1.	Clean all parts of the mould.
2.	Place a 6 mm cylindrical bar vertical in a vice and then place the outer part of the mould over the 6 mm bar.
3.	Vacuum-mix the cement.
4.	Allow the cement to settle.
5.	Add the cement to the mould in a retrograde fashion.
6.	Place the central piece into the mould and align it centrally by placing it in the 6 mm hole of the outer piece. Push down on the central piece so it is correctly in place.
7.	Add the plunger and push down until the plunger has reached a pre-determined point (specified by the line on the side of the plunger).
8.	Remove the excess cement from the pressure relief holes.
9.	Remove the excess cement from the centraliser hole.
10.	Allow to cure in the mould for 24 Hrs
Removing a multiaxial specimen	
1.	Place the complete assembly in a lathe with the plunger fitting loosely in the chuck, and the main body of the mould pressing against the chuck.
2.	Attach a 6 mm cylindrical bar to the drill chuck and tighten in place. Force the cement, plunger, and central piece out of the mould by advancing the 6 mm bar into the centraliser hole in the bottom of the mould.
3.	Place a 10 mm hollow bar in the drill chuck
4.	Place the remainder of the mould against the main chuck, the plunger must push against the chuck leaving enough room for the central piece to pass into the chuck when it is extruded out.
5.	Advance the 10 mm bar against the central piece of the mould thus pushing it out of the cement specimen and through the plunger.
6.	Using a hack-saw saw through the cement that is stuck in the pressure relief holes
7.	The specimen will then come away from the plunger with ease.

Pre-test procedure

1.	Rough specimen edges are removed from the uniaxial specimens by sanding the edges of the gauge length with 320 grit silicon carbide grinding paper. A further light sanding smoothed the area where the cement extruded via the pressure relief holes.
2.	The rough end of the multiaxial specimens was grinded flat using 320 SiC grinding paper on a grinding wheel (Struers, Knuth-rotor, Denmark).
3.	The specimens were then numbered and stored in a water bath at 37°C for 14 days.

Experimental procedure uniaxial specimens

1.	Attach the lower section of the testing rig to the Instron (model) 8501.
2.	Attach the upper section of the rig to the testing machine align the rig by placing a dummy specimen in the grips, tighten the top section into place once the dummy specimen was locked and aligned in the rig.
3.	Place the lower end of a specimen in the lower grip and place an alignment pin through the grip and specimen.
4.	Move the actuator up and place the upper end of the specimen in the upper grip and insert the alignment pin.
5.	Apply a tensile load to the specimen (50N)
6.	Tighten upper and lower grips and remove the alignment pins
7.	Pour water into test rig so it completely immerses the specimen.
8.	Place a polyamide cover on the top of the test rig to prevent any evaporation.
9.	Turn on the heating element and allow the water to reach equilibrium temperature while the specimen is in an unloaded state.
10.	Set the load and position limits
11.	Ramp to the mean value
12.	Input the desired wave form
13.	Start the fatigue test and run till failure or till a set number of cycles (damage accumulation tests).

Experimental procedure multiaxial specimens

1.	Attach the lower section of the rig to the Instron.
2.	Place the o-ring in the cavity of the lower grip.
3.	Place the outer grip ring on the lower grip making sure it is the correct orientation for final assembly.
4.	Take a prepared sample from the water bath and place it in the lower grip
5.	Place interior taper grip in the specimen and tighten into place with a 6 mm allen key.
6.	Attach the upper grip to the Instron but do not tighten into place.
7.	Place an o-ring on the upper grip
8.	Lower crosshead and move actuator up so the specimen is now sitting over the upper grip
9.	Tighten upper grip into place once the specimen is aligned correctly
10.	Attach the pressure gauge to the rig.
11.	Balance the load cell once the upper grip has been tightened in place.
12.	Partially fill a balloon with oil and attach it to the upper grip
13.	Drop the crosshead and raise the actuator until the balloon is inside the specimen.
14.	Attach the outer ring to the upper grip and tighten it locking the specimen in place.
15.	Fill the tank and pumping tank full of water.
16.	Set the position and load limits
17.	Switch on the tank and allow the system to reach equilibrium temperature while the specimen is under zero load
18.	Set the data logging system up and turn it on
19.	Apply the set pressure to the specimen
20.	Ramp to the mean load and input the desired wave parameters.
21.	Start the fatigue test and run till failure or till a set number of cycles